Identification of phosphate adsorption mechanisms on Fe- and Al-hydroxides and the influence of inorganic and organic compounds to reduce long-term phosphorus fixation on mineral surfaces

Von der Fakultät für Umwelt und Naturwissenschaften
der Brandenburgischen Technischen Universität Cottbus-Senftenberg
zur Erlangung des akademischen Grades eines
Doktors der Naturwissenschaften

genehmigte Dissertation
vorgelegt von

M. Sc. Landnutzung und Wasserbewirtschaftung

Stella Gypser

aus Cottbus

Gutachter: apl. Prof. Dr. agr. habil. Dirk Freese
Gutachter: Prof. Dr. Sjoerd E. A. T. M. van der Zee
Tag der mündlichen Prüfung: 03.02.2020

Abstract

With regard to the depletion of global phosphorus reserves and with the aim of ensuring sustainable soil fertility on agricultural soils, a fundamental understanding of mechanisms of fixation and mobilization of inorganic phosphorus in soils is required. Amongst others, phosphorus availability is affected by ad- and desorption reactions on pedogenic Fe- and Al-hydroxide surfaces. The characterization of phosphate binding on those contrasting mineral surfaces can help to find solutions for enhancing the mobilization of fertilized but not available soil inorganic phosphate. Fourier-transform infrared spectroscopic experiments were carried out during phosphorus adsorption on crystalline gibbsite, poorly crystalline 2-line-ferrihydrite and amorphous Fe:Al-hydroxide mixtures. Desorption experiments with $CaCl_2$, $CaSO_4$, citric acid ($C_6H_8O_7$), and humic acid ($C_9H_9NO_6$) were conducted to determine the capacity of phosphate fixation and mobilization in short- and long-term. Additionally, phosphorus release from the Fe- and Ca-phosphates vivianite and hydroxyapatite were analyzed.

For gibbsite, the formation of $AlHPO_4$ and Al_2HPO_4 can be assumed, while for ferrihydrite, a $FeHPO_4$ or Fe_2PO_4 complex and the precipitation of $FePO_4$ with longer equilibration time were observed. Fe_2HPO_4 or a Fe_2PO_4 surface complex was deduced for amorphous Fe-hydroxides, an AlH_2PO_4 surface complex was identified for Al-hydroxides. The weakly associated amorphous FeO(OH) molecules enhance the precipitation of $FePO_4$. With high Al content, a weaker phosphate binding of both inner- and outer-sphere complexes and either no or minor quantities of precipitate were formed. Ferrihydrite showed a more rigid structure and a lower extent of precipitation compared to amorphous Fe-hydroxide. The cumulative phosphorus desorption followed the order $CaCl_2$ < $CaSO_4$ < humic acid < citric acid for crystalline and amorphous Fe-

and Al-hydroxides as well for vivianite and hydroxyapatite. While inorganic anion exchange took part at easily available binding sites and fast exchangeable phosphorus, organic acids additionally affect the more heavily available binding sites and slow exchangeable phosphorus. For humic acid, the accumulation of metal-organic complexes in the desorption solution was suggested, whereas for citric acid the dissolution of the minerals was maintained. The cumulative release rates of the Flow-Through-Reactor setup were higher compared to batch due to a short residence time and a continuous concentration gradient. This could lead either to an over- or underestimation of the available phosphorus pools and influenced the comparability of both methods.

Keywords: Phosphorus, Adsorption/Desorption kinetics, FT-IR, Hydroxides, Phosphates, FTR

Zusammenfassung

Im Hinblick auf die Verknappung der globalen Phosphorreserven und mit dem Ziel, eine nachhaltige Bodenfruchtbarkeit auf landwirtschaftlichen Böden zu gewährleisten, ist ein grundlegendes Verständnis der Mechanismen der Fixierung und Mobilisierung von anorganischem Phosphor in Böden erforderlich. Die Phosphorverfügbarkeit wird unter anderem durch Ad- und Desorptionsreaktionen an pedogenen Fe- und Al-Hydroxidoberflächen beeinflusst. Die Charakterisierung der Phosphatbindung an diesen kontrastierenden mineralischen Oberflächen kann helfen, Lösungen zu finden, um die Mobilisierung von gedüngtem, aber nicht verfügbarem anorganischem Phosphat im Boden zu verbessern. Untersuchungen mittels Fourier-Transformations-Infrarot-Spektroskopie wurden während der Phosphoradsorption an kristallinem Gibbsit, schlecht kristallinem Ferrihydrit sowie an amorphen Fe:Al-Hydroxidgemischen durchgeführt. Desorptionsversuche mit $CaCl_2$, $CaSO_4$, Zitronensäure ($C_6H_8O_7$) und Huminsäure ($C_9H_9NO_6$) wurde durchgeführt, um die Kapazität der kurz- und langfristigen Phosphorfixierung und -mobilisierung zu bestimmen. Zusätzlich wurde die Phosphorfreisetzung der Fe- und Ca-Phosphate Vivianit und Hydroxylapatit analysiert.

An Gibbsit konnte die Bildung von $AlHPO_4$ und Al_2HPO_4 beobachtet werden, während an Ferrihydrit $FeHPO_4$- oder Fe_2PO_4-Komplexe identifiziert wurden. Bei anhaltender Reaktionszeit konnte die Ausfällung von $FePO_4$ erfasst werden. An amorphen Fe- und Al-Hydroxiden wurde die Bildung von Fe_2HPO_4- oder Fe_2PO_4- sowie AlH_2PO_4-Oberflächenkomplexen identifiziert. Die schwach assoziierten FeO(OH)-Moleküle begünstigten die Ausfällung von $FePO_4$, wohingegen bei steigendem Al-Gehalt eine schwächere Phosphatbindung durch Inner- und Outer-Sphere-Komplexe ohne oder nur geringer Ausfällung festgestellt werden konnte. Durch die

starrere Struktur von Ferrihydrit fiel der Gehalt an ausgefallenem $FePO_4$ im Vergleich zu den amorphen Fe-Hydroxiden niedriger aus. Für die kumulative Phosphatdesorption konnte die Reihenfolge $CaCl_2$ < $CaSO_4$ < $C_9H_9NO_6$ < $C_6H_8O_7$ für kristalline und amorphe Fe- und Al-Hydroxide sowie Vivianit und Hydroxylapatit ermittelt werden. Während der Austausch anorganischer Ionen an leicht zugänglichen Bindungsstellen und somit leicht austauschbarem Phosphor stattfand, beeinflussen die organischen Säuren auch schwer zugängliche Bindungsstellen mit schwer und langsam austauschbarem Phosphor. Für $C_9H_9NO_6$ wurde die Akkumulation von metall-organischen Komplexen in der Desorptionslösung in Betracht gezogen, während $C_6H_8O_7$ zur Auflösung der Minerale beiträgt. Die kumulierten Freisetzungsraten mittels Flow-Through-Reactor fielen aufgrund einer kurzen Verweilzeit und eines kontinuierlichen Konzentrationsgradienten höher aus als im Batch-Versuch. Dies könnte entweder zu einer Über- oder Unterschätzung der verfügbaren Phosphorpools führen und die Vergleichbarkeit beider Verfahren beeinflussen.

Stichworte: Phosphor, Adsorptions-/Desorptionskinetik, FT-IR, Hydroxide, Phosphate, FTR

Table of contents

Abstract 1

Zusammenfassung 3

Table of contents 5

Tables 8

Figures 9

Abbreviations 11

Thesis at a glance 13

1 Introduction 14

2 Impact of crystalline and amorphous iron- and aluminum hydroxides on mechanisms of phosphate adsorption and desorption 23

2.1 Abstract 23

2.2 Introduction 24

2.3 Materials and methods 26

2.3.1 Adsorbents 26

2.3.2 Adsorption and desorption experiments 28

2.3.3 Fourier transform infrared spectroscopy 29

2.4 Results 30

2.4.1 Characterization of minerals 30

2.4.2 Kinetics of phosphate adsorption 32

2.4.3 FT-IR spectroscopic investigation of phosphate adsorption 36

2.4.3.1 Gibbsite 39

2.4.3.2 Ferrihydrite 41

2.4.3.3 Amorphous Fe: Al-hydroxide 44

2.4.4 Phosphate desorption 49

2.5 Discussion 50

2.5.1 FT-IR spectroscopic experiments during phosphate adsorption 50

2.5.1.1 Gibbsite 50

2.5.1.2 Ferrihydrite 53

2.5.1.3 Amorphous Fe: Al-hydroxide mixtures 54

2.5.2 Kinetics of adsorption and desorption 58

2.5.3 Crystallinity 60

2.6 Conclusions 61

3 Crystallization of single and binary iron- and aluminum hydroxides affect phosphorus desorption 63

3.1 Abstract 63

3.2 Introduction 64

3.3 Materials and methods 66

3.3.1 Fe- and Al-hydroxides 66

3.3.2 Desorption experiments 67

3.3.3 Equations and mechanisms of desorption kinetics 69

3.4 Results 70

3.4.1 Characterization of hydroxides 70

3.4.2 Efficiency of desorption 71

3.4.3 Kinetics of phosphorus desorption 73

3.4.4 Desorption mechanism of humic and citric acid 78

3.5 Discussion 79

3.5.1 Efficiency of desorption 79

3.5.2 Kinetics of phosphorus desorption 80

3.5.3 Desorption mechanism of inorganic and organic solutions 82

3.6 Conclusion 84

4 Phosphorus release from vivianite and hydroxyapatite by organic and inorganic compounds 86

4.1 Abstract 86

4.2 Introduction 87

4.3 Materials and methods 91

4.3.1 Phosphate minerals 91

4.3.2 Phosphorus release experiments 92

4.3.2.1 Preparation of coated silica sand *92*

4.3.2.2 Batch experiment *93*

4.3.2.3 FTR-experiment *93*

4.3.2.4 Microbial activity and carbon content *95*

4.3.3 Kinetics of phosphorus release 95

4.4 Results 96

4.4.1 Characterization of phosphate minerals 96

4.4.2 Efficiency of phosphorus release 97

4.4.3 Kinetics of phosphorus release 98

4.4.4 C_{Total} during humic and citric acid treatment 101

4.5 Discussion 102

4.5.1 Efficiency of phosphorus release 102

4.5.2 Kinetics of phosphorus release 105

4.5.3 Comparison of batch and FTR 107

4.6 Conclusion 109

5 General discussion 111

5.1 Phosphate adsorption mechanisms on iron- and aluminum hydroxides and its implications on desorption 111

5.2 Influence of organic and inorganic compounds on phosphorus desorption 116

5.3 Recovery of immobilized phosphorus from secondary resources 120

6 Conclusions 124

References 127

Acknowledgements 148

Tables

Tab. 1. Specific surface of the crystalline and amorphous Fe- and Al-hydroxides and the content of Fe and Al coated on silica sand. 32

Tab. 2. P adsorption rates of gibbsite, ferrihydrite and amorphous Fe:Al-hydroxide mixtures after 2688 h and initial P concentrations of 150, 1000, 2000 and 5000 µmol l^{-1}. 34

Tab. 3. Described frequencies and symmetry of dissolved phosphate species. 37

Tab. 4. Observed frequencies of OH vibrations of gibbsite, ferrihydrite and Fe:Al-hydroxides. ..38

Tab. 5. Elemental composition (SEM-EDX) of the pure minerals and amount of Fe, Al and P of the used Fe-Al-hydroxides coated on silica sand. 71

Tab. 6. Total P desorption after eight weeks of desorption time by using desorption solutions $CaCl_2$, $CaSO_4$, humic acid and citric acid at pH 6. 72

Tab. 7. Coefficients of determination (R^2) and standard errors (S.E.) for the kinetic equations used to describe the kinetic release of P after 1344 h desorption time and the kinetic parameters of the selected Elovich and Exponential function equations for P desorption from $CaCl_2$, $CaSO_4$, humic acid and citric acid. 77

Tab. 8. Amount of Fe, Ca and P of the used phosphate minerals and the infinite sink coated on silica sand. 97

Tab. 9. Total P release after 1344 h as well as extent of desorbed P related to the amount of total desorbed P after 48 h and 1344 h desorption time by using desorption solutions $CaCl_2$, $CaSO_4$, humic acid and citric acid at pH 6. 98

Tab. 10. Coefficients of determination (R^2) and standard errors (S.E.) for the kinetic equations used to describe the kinetic release of P after 1344 h desorption time, and kinetic parameters of the selected Elovich and Exponential function equations for P release. 100

Figures

Fig. 1. Scheme of P cycling in the plant-soil system. 15

Fig. 2. Scale levels of the BMBF-project "InnoSoilPhos" (2015-2018). 17

Fig. 3. X-ray diffraction patterns of gibbsite, ferrihydrite and amorphous Fe:Al-hydroxide mixtures in the ratio 1 Fe:0 Al, 10 Fe:1 Al, 1 Fe:1 Al, 1 Fe:10 Al and 0 Fe:1 Al. 31

Fig. 4. P adsorption kinetics of gibbsite (P_{150}, P_{1000}, P_{2000}) and ferrihydrite (P_{1000}, P_{2000}, P_{5000}). ..33

Fig. 5. P adsorption kinetic of amorphous Fe:Al-hydroxide mixtures at P_{1000}, P_{2000} and P_{5000}. ...35

Fig. 6. Correlation of the amount of adsorbed P and the Fe- and Al-content of the mineral samples for initial P concentrations of 1000 µmol l^{-1}, 2000 µmol l^{-1} and 5000 µmol l^{-1}.....36

Fig. 7. Edited FT-IR spectra of gibbsite during P adsorption. 40

Fig. 8. FT-IR spectra of ferrihydrite and amorphous Fe:Al-hydroxide mixtures 1 Fe:0 Al, 10 Fe:1 Al, 5 Fe:1 Al and 1 Fe:1 Al, 1 Fe:5 Al, 1 Fe:10 Al and 0 F e:1 Al in the OH stretching region from 3800 to 2500 cm^{-1} (A, B) and in the OH stretching region from 1800 to 500 cm^{-1} (C, D) during phosphate adsorption. Please notice the different scaling of the Kubelka-Munk units in (A) and (B). 43

Fig. 9. FT-IR spectra of amorphous Fe:Al-hydroxide mixtures in the OH stretching region.....44

Fig. 10. Comparison of FT-IR spectra of pure amorphous Fe:Al-hydroxides, ferrihydrite and gibbsite in the wavelength range from 1900 cm^{-1} to 500 cm^{-1}.....46

Fig. 11. P desorption kinetics of gibbsite, ferrihydrite and goethite (A), and amorphous Fe:Al-hydroxide mixtures in 0.01 M $CaCl_2$ at pH 6 (B). 50

Fig. 12. Desorption kinetics of (A) goethite, (B) gibbsite, (C) ferrihydrite, (D) 1 Fe:0 Al, (E) 10 Fe:1 Al, (F) 5 Fe:1 Al, (G) 1 Fe:1 Al, (H) 1 Fe:5 Al, (I) 1 Fe:10 Al and (J) 0 Fe:1 Al by using desorption solutions $CaCl_2$, $CaSO_4$, humic acid and citric acid at pH 6. 74

Fig. 13. Extent of desorbed P related to the extent of total desorbed P (= 100 %) after 48 h and 1344 h desorption time for (A) $CaCl_2$ and $CaSO_4$ and (B) humic acid and citric acid. 75

Fig. 14. C_{Total} in mg l^{-1} in the desorption solutions humic acid and citric acid after eight weeks of desorption time (n = 2). 79

Fig. 15. Setup of the Flow-Through-Reactor desorption experiments with (1) top of the reactor chamber, (2) intermediate, (3) desorption solution, (4) phosphate-coated silica sand, (5) bottom of the reactor chamber with filter holder, membrane filter and silicon gasket, (6) peristaltic pump and (7) infinite sink. 94

Fig. 16. XRD patterns of (A) hydroxyapatite and (B) vivianite. 96

Fig. 17. P release kinetics of (A) vivianite and (B) hydroxyapatite by using $CaCl_2$, $CaSO_4$, humic acid and citric acid at pH 6. 99

Fig. 18. C_{Total} in mg l^{-1} in humic acid and citric acid after eight weeks of reaction time (n = 2). 101

Fig. 19. Possible chemical reactions of vivianite and hydroxyapatite during desorption with $CaCl_2$, $CaSO_4$, citric acid and humic acid at pH 6. 104

Fig. 20. Scheme of P adsorption on gibbsite and ferrihydrite (adapted from Antelo *et al.* 2010). 113

Fig. 21. Scheme of P adsorption on amorphous Fe- and Al-hydroxides (adapted from Antelo *et al.* 2010). 114

Fig. 22. Scheme of P desorption processes using the example of a monoprotonated monodentate inner-sphere surface complex. 119

Fig. 23. Unit cells of vivianite and hydroxyapatite (RRUFF project (Lafuente *et al.,* 2015), according to Mori and Ito (1950) and Hughes *et al.* (1989)). 121

Abbreviations

Al	Aluminum
$Al(NO_3)_3 \cdot 9\ H_2O$	Aluminum nitrate nonahydrate
$Al(OH)_3$	Aluminum hydroxide
BET	Brunauer-Emmett-Teller
BMBF	German Federal Ministry of Education and Research
BonaRes	"Soil as a sustainable resource for the bioeconomy"
C	Carbon
$C_6H_8O_7$	Citric acid
$C_9H_9NO_6$	Humic acid
Ca	Calcium
$CaCl_2$	Calcium chloride
$CaSO_4$	Calcium sulfate
Cl	Chlorine
C_{Total}	Total carbon
Cu	Copper
DRIFT	Diffuse reflection (Fourier-transform infrared spectroscopy)
Fe	Iron
$Fe(NO_3)_3 \cdot 9\ H_2O$	Iron(III) nitrate nonahydrate
FeO(OH)	Iron(III) oxide hydroxide
FT-IR	Fourier-transform infrared spectroscopy
FTR	Flow-Through-Reactor
H	Hydrogen
H_2O	Hydrogen oxide
$H_2PO_4^-$	Dihydrogen phosphate
H_2SO_4	Sulfuric acid
H_3PO_4	Phosphoric acid
HNO_3	Nitric acid
HPO_4^{2-}	Hydrogen phosphate
ICP-AES	Inductively coupled plasma - Atomic emission spectrometry

IR	Infrared
K	Potassium
KCl	Potassium chloride
KH_2PO4	Potassium dihydrogenphosphate
KNO_3	Potassium nitrate
KOH	Potassium hydroxide
N	Nitrogen
Na	Sodium
$NaNO_3$	Sodium nitrate
O	Oxygen
P	Phosphorus
PO_4^{3-}	Phosphate
R^2	Coefficient of determination
S	Sulfur
S.E.	Standard error
SEM-EDX	Scanning electron microscopy
Si	Silicon
SO_4^{2-}	Sulfate
TOC	Total organic carbon
XRD	X-ray diffraction

Thesis at a glance

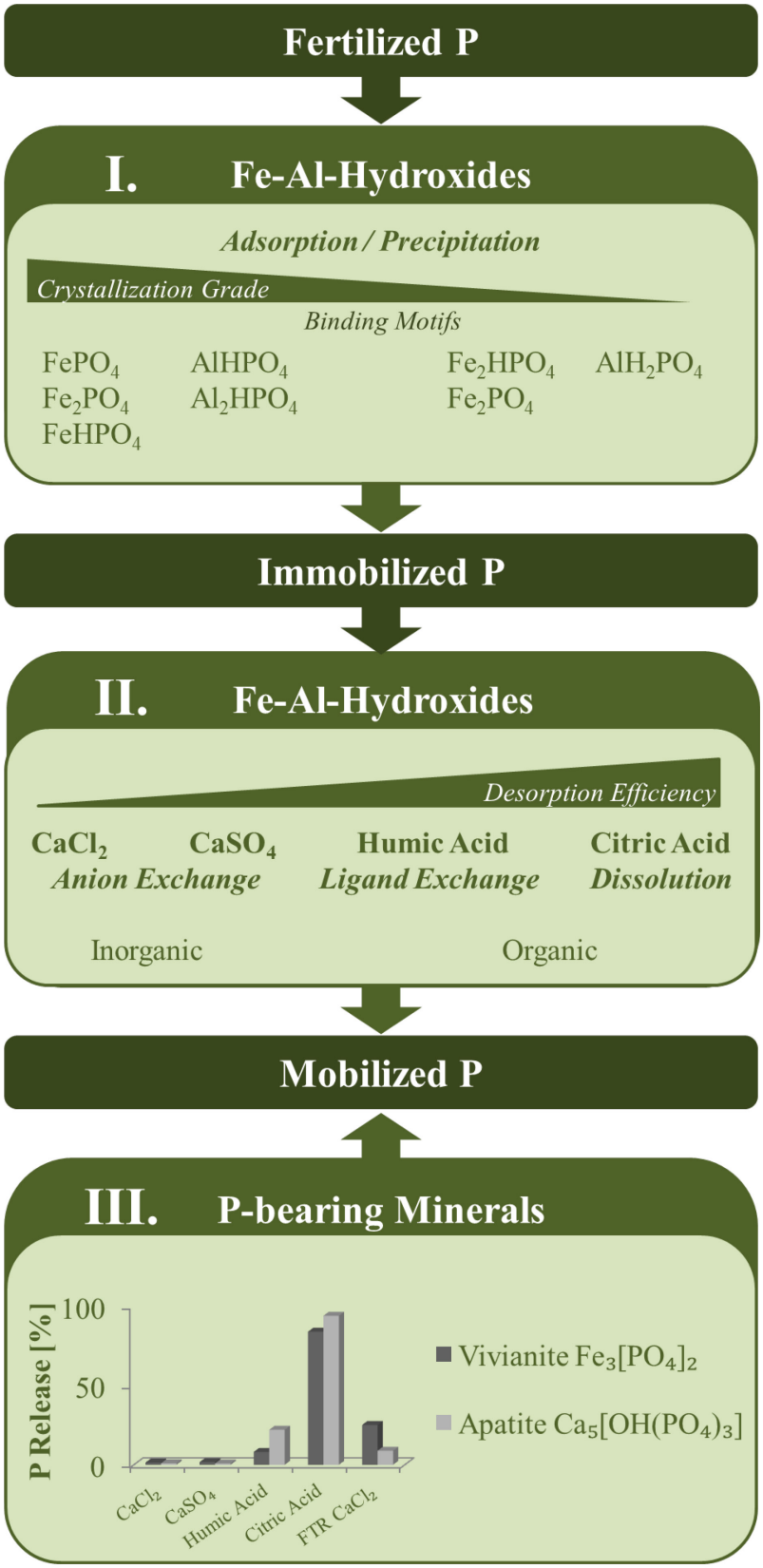

1 Introduction

After carbon and nitrogen, phosphorus is an essential element for all living organisms and indispensable for physiological structures and processes, e.g. as a component of DNA and RNA molecules, ATP molecules during energy metabolism or as phospholipids for membrane formation (Brennicke and Schopfer, 2010). In many ecosystems, phosphorus is a main limiting nutrient and its availability affects the growth and development of plants (Simpson *et al.,* 2011; Wyngaard *et al.,* 2016; Zhu *et al.,* 2018). In contrast to nitrogen, phosphorus cannot be synthesized from other elements or chemical compounds, and the demand for mineral phosphorus fertilizers is covered by mineable fossil rock phosphates. This fossil phosphorus resources can be divided in *reserves*, which are resources that exist currently and can be mined with current technology and actual costs, the *reserve base*, referring to known resources that can be mined with future technology and future costs, as well as the *additional resources*, which are currently undiscovered and might be exploitable in the future, but with uncertain estimations e.g. continental low-grade or sub-marine phosphate rocks and deposits (Reijnders, 2014; Scholz and Wellmer, 2013). Reijnders (2014) summarized studies, estimating the remaining fossil phosphorus resources in the range from 2.4×10^{15} to 38.8×10^{15} Gt (gigatons) and 80 to 8900 years based on estimated current fossil phosphorus mining. Certainly, limitations in prospecting and accessibility, as well as insecurity regarding future technology and costs, contribute to an uncertain evaluation of remaining fossil phosphorus resources (Edixhoven *et al.,* 2014; Reijnders, 2014; Scholz and Wellmer, 2013; van Vuuren *et al.,* 2010). The availability and the uptake of P by plants are limited by processes of surface runoff, particulate transport, conversion to organic

compounds and phosphorus sequestration (Dungait *et al.,* 2012; Javid and Rowell, 2002; Sattari *et al.,* 2012; Syers *et al.,* 2008) (Fig. 1).

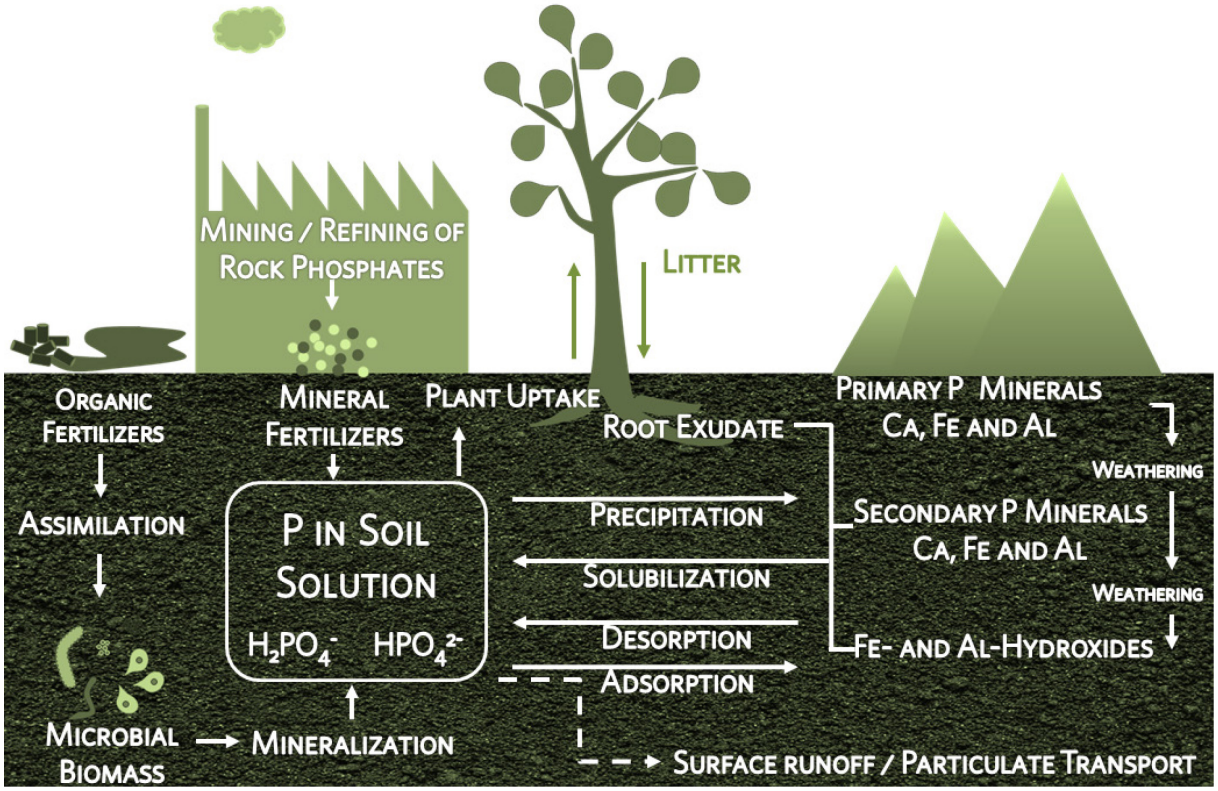

Fig. 1. Scheme of P cycling in the plant-soil system.

Several factors such as pH, redox potential, phosphorus ionic strength, competitive anions, solubility product or organic matter affect the mobility and availability of phosphorus in soils. The processes of phosphorus adsorption, desorption and precipitation on pedogenic mineral surfaces are of particular interest in the context of plant nutrition and its important role as a limiting nutrient, but also with regard to leaching into water bodies. Surface runoff from agricultural soils caused by excess fertilization is the main-polluter to causing eutrophication of rivers, lakes, and seas by over-enrichment and still a widespread environmental problem (Carpenter *et al.,* 1998; Sims and Pierzynski, 2005).

Due to their major role in the environmental phosphorus cycle, the reactions of phosphorus with pedogenic hydroxides have been thoroughly studied (Arai and Sparks, 2001; Barrow, 1983; Chitrakar *et al.,* 2006; Khare *et al.,* 2007; Krumina *et al.,* 2016; Lookman, 1995; Tejedor-Tejedor and Anderson, 1990; Torrent *et al.,* 1992). In recent years, more and more investigations have been carried out on phosphorus binding on mineral iron- and aluminum-hydroxide (Fe- and Al-hydroxide) surfaces, but these have mainly been limited to the model minerals goethite, ferrihydrite or gibbsite. Though two- or multi-component hydroxide systems are more common in soils, they were given less attention. Also, the mineral crystallinity and porosity were only little considerated in the investigations, although these are important aspects for phosphorus ad- and desorption processes. Soils contain hydroxides with different degrees of crystallinity such as completely crystallized minerals or fine crystalline minerals with an amorphous basic structure, offering varying properties such as reactive surface area during pedogenesis (Scheffer *et al.,* 2010). Therefore, this work is intended to achieve a more detailed and fundamental understanding of phosphate binding motifs on those contrasting mineral surfaces. Great importance was also given to the detection of possible binding changes over time, and their implications on phosphorus desorption behavior. There is a huge challenge to ensure sustainable soil fertility and productivity of agricultural soils by minimizing losses of phosphorus and, hence, recovery of naturally bound phosphorus was one aspect which has been examined in more detail.

The investigation of these issues was part of the BMBF project "**Inno**vative solutions to sustainable **Soil Phos**phorus management - InnoSoilPhos", where the research was carried out on the following scale levels: I. the atomic and molecular scale, II. the plot to field scale, III. the field to catchment scale, and IV. the societal scale (Fig. 2).

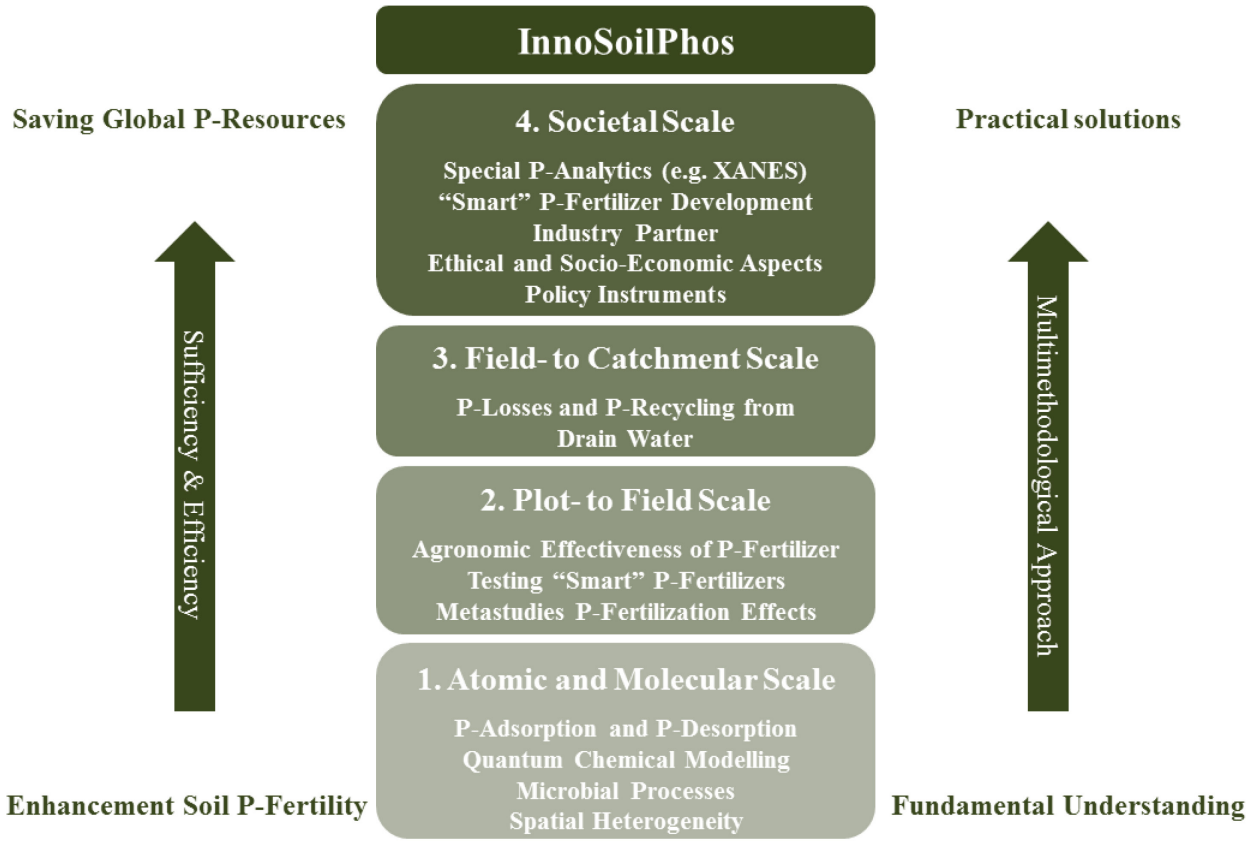

Fig. 2. Scale levels of the BMBF-project "InnoSoilPhos" (2015-2018).

Objectives

Within the "atomic and molecular scale" the contribution of this work is to create and extend basic knowledge in the subjects: I) identification of phosphorus binding forms on synthetic Fe- and Al-hydroxides including combinations with altering Fe and Al content, II) determination of medium- and long-term phosphorus desorption kinetics of synthetic Fe- and Al-hydroxides as well as Fe- and Ca-phosphates, and III) investigation of the influence of organic compounds on phosphorus availability. According to this, the following questions have arisen: I) Which phosphorus bindings are formed on the various mineral Fe- and Al-hydroxide surfaces and how do they influence phosphorus desorption? II) To what extent affect inorganic and organic

compounds the identified phosphorus bindings on the Fe- and Al-hydroxide surfaces, and positively influence phosphorus mobilization? III) How do inorganic and organic compounds contribute to the availability of naturally bound phosphorus from Fe- and Ca-phosphates?

I) Therefore, the aim of the first part of this work was to investigate and detect changes in phosphorus adsorption kinetics on the crystalline Al-hydroxide gibbsite, the poorly crystalline Fe-hydroxide ferrihydrite and on amorphous single and binary Fe:Al-hydroxide mixtures during short- and long-term equilibration times with varying phosphorus concentrations. On the basis of these investigations, Diffuse reflection (DRIFT) Fourier-transform infrared (FT-IR) spectroscopy was used to identify and compare phosphate binding motifs on the hydroxide surfaces and assess their contribution to desorption. Besides the symmetric and asymmetric P-O stretching vibrations, which have been widely used for phosphate species symmetry analyses (Arai and Sparks, 2001; Krumina *et al.,* 2016; Tejedor-Tejedor and Anderson, 1990), the OH stretching bands and their changes during adsorption were included for speciation of the adsorbed phosphate surface complexes.

II) The aim of the second part of this work was to characterize kinetics and mechanism of phosphorus desorption of the crystalline and amorphous Fe- and Al-hydroxides. Fast (easily bound) and slow (strongly bound) releasable phosphorus over time should be detected by applying long-term desorption kinetic experiments. Despite the aspect that mineral crystallinity is an important factor influencing the characteristic phosphorus behavior in soil systems, the influence of the degree of mineral crystallinity on soil desorption behavior is not well understood until now. Goethite and gibbsite represented model substances of crystalline Fe- and Al-hydroxides, whereas synthesized Fe- and Al-hydroxide mixtures were model substances of the amorphous fraction appearing in soils. Ferrihydrite was used as a transitional Fe-hydroxide with a

predominant amorphous character, bridging between the initial amorphous hydroxide structure and crystalline goethite during pedogenesis. In addition, the influence of inorganic and organic components on phosphorus mobilization was investigated.

One aspect of this investigation was mechanisms that influence soil phosphorus resources. One the one hand, plants had developed a range of adaptive strategies to enhance the availability of phosphorus from soils. This includes symbiotic root-microbe associations, root- mycorrhiza interactions and the secretion of root exudates (Bais *et al.,* 2006). The exudation of low-molecular-weight organic acids (Chen *et al.,* 2004; Jones, 1998) such as citric acid, which was often detected at a higher concentration in the rhizosphere, was described as highly effective in mobilizing inorganic phosphorus (Johnson and Loeppert, 2006; Kpomblekou-A and Tabatabai, 2003). One the other hand, substance conversion processes take place in the soil system. High-molecular-weight organic compounds such as humic acid, formed during humification and mineralization, play an important role in soil environment and phosphorus mobilization (Hua *et al.,* 2008; Jones, 1998). Therefore, $CaCl_2$ and $CaSO_4$ were chosen as inorganic desorption solutions to represent the main constituents of the soil solution, and citric acid, as well as humic acid, were chosen as model organic ligands for the determination of the influence of humification compared to plant exudate in the rhizosphere.

III) In the third part of this work, the inorganic $CaCl_2$ and $CaSO_4$ as well as the organic citric and humic acid were used again as desorption solutions, but long-term kinetic experiments were carried out on the synthetic Fe-phosphate vivianite and the Ca-phosphate hydroxyapatite. Apatite is a lithogenic mineral in soils worldwide and the primary source of phosphorus in terrestrial ecosystems. Many physical, chemical and biological processes affect the release of phosphorus from the lithosphere into the soil (Heindel *et al.,* 2018). By weathering and

dissolution of apatite in sediments and soils, secondary precipitated phosphorus will be released, differing in stability (Mehmood *et al.,* 2018). During the early stages of soil development, the majority of phosphorus is embedded within minerals. Since apatite is relatively insoluble at a near neutral pH, but a rather soft mineral, it was suggested that physical weathering could be a precondition for biogeochemical weathering (Föllmi *et al.,* 2009). However, both solubility and dissolution increase strongly with increasing acidity (Dorozhkin, 2012; Harouiya *et al.,* 2007). With continuing pedogenesis, the total content of soil phosphorus decreases and the recovery of organic matter replace the mineral weathering as the dominant process in the soil phosphorus cycle (Walker and Syers, 1976).

Vivianite is one of the most common stable iron phosphates and has been found in many anthropogenically influenced sediment worldwide. It occurs preferentially in sediments of lakes, rivers, canals, moors, swamps or water-saturated soils. It is also found in sewage sludges as a weathering product in hydrothermal deposits and as a secondary mineral in Fe-containing ore veins (Rothe *et al.,* 2016). Vivianite is formed in particular where reductive conditions occur (oxygen-deficient), organic material is abundant, and phosphorus availability is increased (Rothe *et al.,* 2016). In calcareous soils, vivianite oxidizes to a weakly crystalline Fe(III) oxide (lepidocrocite) (Roldán *et al.,* 2002), which can prevent Fe deficiency in plants on these soils (Rombolà *et al.,* 2003). It has been shown that naturally formed vivianite can replace Fe in the vivianite lattice by significant amounts of Mn or Mg or trace metals, depending on the geochemical environment (Tressardi, 2000). It can, therefore, be used as a sink for metals or other impurities (Liu and Zhao, 2007; Taylor *et al.*, 2008). But, if sewage sludge is used as a fertilizer, it can also discharge heavy metals and contaminants back into the environment. Vivianite formation also seems to take place in the vicinity of easily decomposable organic material, which on the one hand promotes the formation of a reducing environment and on the

other hand serves phosphorus source. Such conditions are usually found in wastewater treatment plants or also in sediments that collect the corresponding nutrient loads with wastewater (Dodd *et al.*, 2003; Taylor *et al.*, 2008).

The release of phosphorus in soils is strongly pH dependent. While in acidic soils, phosphorus can be bound as Fe-phosphate e.g. as vivianite, in neutral and calcareous soils the Ca-phosphate hydroxyapatite can be formed, which has a low solubility under natural conditions (Gustafsson *et al.,* 2012; Walker and Syers, 1976; Yadav and Verma, 2012). Also, already mobilized phosphorus from apatite by acidification will be bound in other forms, e.g. on Fe- and Al-hydroxides (Scheffer *et al.,* 2010). With regard to the efficient use of already bound phosphorus pools in soils, the aim of this study was the characterization of long-term kinetics of phosphorus mobilization. Release experiments were conducted both in batch and with an infinite sink approach. Both systems should be compared regarding their phosphorus desorption kinetics as well as the applicability of kinetic models. The benefit of the infinite sink approach by using Flow-Through-Reactor technique is the minimal alteration of the mineral-solution system (Frossard *et al.,* 2000) and the removal of mobilized phosphorus with an infinite sink. Batch experiments are an inexpensive and simple approach (Kruse *et al.,* 2015) to determine the amount of long-term mobilized phosphorus. $CaCl_2$, $CaSO_4$, humic and citric acid were used as reaction solutions again.

The general attempt is to broaden the fundamental understanding of phosphorus fixation and mobilization in order to find suitable solutions for the optimization of soil phosphorus fertility and to lower the dependency on finite minable phosphate rock reserves. Therefore, it is necessary to improve the knowledge for sustainable use of soil phosphorus by especially understanding the inefficiency of agricultural phosphorus fertilization, as well as maintaining and

enhancing the mobilization of not available inorganic phosphorus which was already fertilized or natural bound.

2 Impact of crystalline and amorphous iron- and aluminum hydroxides on mechanisms of phosphate adsorption and desorption[1]

2.1 Abstract

Fourier-transform infrared (FT-IR) spectroscopic experiments were carried out during phosphate adsorption on highly crystalline gibbsite, poorly crystalline 2-line-ferrihydrite and amorphous iron-aluminum-hydroxide mixtures in the molar ratio 1:0, 10:1, 5:1, 1:1, 1:5, 1:10 and 0:1. The OH stretching vibrational bands were utilized to analyze changes in structural and surface OH groups during adsorption, because the position of characteristic P-O vibrational bands can shift depending on reaction conditions, pH or adsorbed phosphate content. Adsorption and desorption kinetics were studied at pH 6 and different initial phosphate concentrations to achieve varying phosphate coverage on the mineral surfaces. For gibbsite the formation of $AlHPO_4$ and Al_2HPO_4 can be assumed, while for ferrihydrite, a $FeHPO_4$ or Fe_2PO_4 complex and the precipitation of $FePO_4$ with longer equilibration time were proposed. Fe_2HPO_4 or a Fe_2PO_4 surface complex was deduced for Fe-hydroxides, an AlH_2PO_4 surface complex was identified for Al-hydroxide, and both displayed either hydrogen bonds to neighboring hydroxyl groups or hydrogen bonds to outer-sphere complexes. Fe:Al-hydroxide mixtures with high Al ratios showed a low phosphate desorption rate, while ferrihydrite and the Fe:Al-hydroxide mixtures with high Fe ratios had almost negligible desorption rates. It was concluded that within the weakly associated amorphous FeO(OH) materials, $FePO_4$ precipitated, which was bound by

[1] Published in Journal of Environmental Sciences
Elsevier
Gypser, S., Hirsch, F., Schleicher, A. M., Freese, D. (2018): Impact of crystalline and amorphous iron- and aluminum hydroxides on mechanisms of phosphate adsorption and desorption. J. Environ. Sci. **70**, 175–189.
DOI: 10.1016/j.jes.2017.12.001.

outer-sphere hydrogen bonds. With high Al ratios, desorption increased, which indicated weaker phosphate binding of both inner-sphere and outer-sphere complexes and hence, either no or minor quantities of precipitate. Ferrihydrite showed a more rigid structure and a lower extent of precipitation compared to amorphous Fe-hydroxide.

Keywords: Phosphate, Adsorption, Desorption, Surface complexation, Precipitation, FT-IR

2.2 Introduction

Sorption of phosphorus by soil minerals such as iron and aluminum-(hydr)oxides is of interest because of its critical role in terms of limitation as a nutrient for plant uptake, but also due to leaching effects and surface runoff into water bodies caused by excess fertilization, leading to eutrophication (Sims and Pierzynski, 2005). Notably, the formation of these iron and aluminum-hydroxides is characteristic during soil alteration and strongly affects phosphorus transport and bioavailability by adsorption and desorption processes. Due to the important role of phosphate in the environmental nutrient cycle, the reactions of phosphate with pedogenic iron and aluminum-hydroxides have been thoroughly studied (Arai and Sparks, 2001; Barrow, 1983; Hinsinger, 2001; Krumina *et al.,* 2016; Torrent *et al.,* 1992). A major aspect is the kinetics of adsorption and desorption on soil iron and aluminum-particles, showing a biphasic behavior including a very fast initial adsorption process during the first 2 h, followed by a slow reaction phase (Luengo *et al.,* 2006; McLaughlin *et al.,* 1977; Reddy *et al.,* 1999; Shang *et al.,* 1992; Strauss *et al.* 1997; Torrent *et al.,* 1992; Willett *et al.,* 1988). Adsorption experiments with synthetic iron and aluminum-(hydr)oxides showed the occurrence of ligand exchange and the formation of stable inner-sphere surface complexes with metal ions (Goldberg and Sposito, 2008;

Parfitt, 1979). Torrent (1997) summarized theories explaining the slower process step with the formation of initial mononuclear complexes and transformation to binuclear complexes, competition with anions on the surface or surface precipitation processes, respectively. This can also be attributed to the diffusion of phosphate into the inner particle pores of hydroxides (Chitrakar *et al.,* 2006). It was reported that the phosphate uptake increased with increasing initial phosphate concentration in the same ratio (Talebi Atouei *et al.,* 2016), while the degree of crystallinity or porosity of hydroxides affects the extent of phosphate adsorption (Parfitt, 1989). Mineral crystallinity is an important aspect in phosphate sorption processes, since soils contain amorphous, poorly crystalline and well-crystallized hydroxides during pedogenesis, offering varying properties such as specific reactive surface area (Scheffer *et al.,* 2010). Also, hydroxides occur as multi-component solids in soil systems, and affect phosphate adsorption behavior (Anderson and Benjamin, 1990).

Further investigations are needed in the area of connecting the detailed characteristics of adsorbed surface complexes with the change of binding motifs over time and their impact on desorption behavior. Gibbsite and ferrihydrite are the most common aluminum and iron hydroxides in soils, and their surface properties are well characterized; hence, they are good model minerals for investigation of phosphate surface reactions (Antelo *et al.,* 2010; Arai and Sparks, 2001; Arlidge *et al.,* 1963; Johnson *et al.,* 2002; Khare *et al.,* 2007; Krumina *et al.,* 2016; Laiti *et al.,* 1996; Li *et al.,* 2013; Lijklema, 1980; Persson *et al.,* 1996; Zheng *et al.,* 2012). The objective of this work was to detect changes in phosphate binding motifs on gibbsite, ferrihydrite and binary iron and aluminum hydroxide surfaces with varying degrees of crystallinity during short- and long-term equilibration times with varying phosphate concentration, by using Diffuse reflection (DRIFT) Fourier-transform infrared (FT-IR) spectroscopy. On the basis of these investigations, amorphous iron and aluminum hydroxide mixtures were used to compare

phosphate adsorption mechanisms. Besides the symmetric and asymmetric P-O stretching vibrations, which have been widely used for phosphate species symmetry analyses (Arai and Sparks, 2001; Krumina *et al.,* 2016; Tejedor-Tejedor and Anderson, 1990), the OH stretching bands and their changes during adsorption were included for speciation of the adsorbed phosphate surface complexes. Adsorption and desorption experiments were used to identify the different binding mechanisms and phosphate binding forms, which were detected after adsorption and contributed primarily to desorption. Furthermore, the sorption mechanism of phosphate on soil mineral particles is highly pH dependent and the phosphate binding motifs change with pH, as shown by several studies (Antelo *et al.,* 2005; Laiti *et al.,* 1998; Rahnemaie *et al.,* 2007; Weng *et al.,* 2011). With the background that eutrophication of rivers and lakes caused by over-enrichment with phosphorus is still a widespread problem, for which non-point-sources from agricultural soils are the main polluters (Carpenter *et al.,* 1998), this study focused on the pH conditions of agricultural soils, which range most frequently between pH 5.0 and 6.8 (Blume *et al.,* 2010; Scheffer *et al.,* 2010), where phosphate shows its optimal availability due to the high solubility of Fe- and Al-phosphates (Blume *et al.,* 2010; Johnson *et al.,* 2002; Scheffer *et al.,* 2010). Due to this reason, the pH for the adsorption and desorption experiments was set to a value of 6.

2.3 Materials and methods

2.3.1 Adsorbents

The commercially available synthetic adsorbent used in this study was gibbsite (analytical grade, Merck Millipore, Merck KGaA, Darmstadt, Germany). 2-line-ferrihydrite was prepared according to Schwertmann and Cornell (2008), for which 350 ml of 1 M KOH was added to

500 ml of a 0.2 M $Fe(NO_3)_3 \cdot 9\ H_2O$-solution, until a pH of 7.5 was reached. The developed precipitate was centrifuged and washed for 5 min at 12134 × g (Avanti J-25 Centrifuge, Beckman Coulter, Brea, USA), subsequently frozen, freeze-dried, and stored in a desiccator. The mixed iron-aluminum-hydroxides (Fe:Al-hydroxide) were prepared as described by Sujana *et al.* (2009), for which 0.1 M $Fe(NO_3)_3 \cdot 9\ H_2O$ and 0.1 M $Al(NO_3)_3 \cdot 9\ H_2O$ were mixed in molar ratios Fe to Al of 1:0, 10:1, 5:1. 1:1, 1:5, 1:10 and 0:1, adjusted to a pH of 6 with 5 M KOH, equilibrated for 1 h, and centrifuged for 5 min at 12134 × g. The washed precipitate was dried at 60°C and ground into a powder. All chemicals used for preparation of adsorbents were of analytical grade, and the solutions were prepared with ultrapure water. The elemental composition of the adsorbents was verified by using SEM-EDX, scanning electron microscopy (DSM 962, Zeiss, Oberkochen, Germany) with energy dispersive X-ray spectroscopy (X-Max 50 mm² with INCA, Oxford Instruments, Abingdon, Great Britain). The formation of pure $Al(OH)_3$ and FeO(OH) for the amorphous hydroxides was revealed. Determination of the adsorbent crystallization as well as amorphous structures was carried out by X-ray diffraction (XRD) using a PANalytical Empyrean powder diffractometer (Almelo, Netherlands) from GFZ Potsdam, with a theta-theta-goniometer, Cu-Kα radiation (λ = 0.15418 nm), automatic divergent and anti-scatter slits and a PIXcel3D detector. Diffraction data were recorded from 4.6° to 84.9° 2Θ with a step-size of 0.0131 and a step time of 58.4 s. The generator settings were 40 kV and 40 mA. Specific surface areas of all adsorbents used as well as the coated silica sand were determined with an Autosorb-1 (Quantachrome, Odelzhausen, Germany) using a five-point BET-measurement (Brunauer-Emmett-Teller) and nitrogen as the adsorptive medium. An outgas test was performed to verify the completed outgas procedure for each adsorbent.

2.3.2 Adsorption and desorption experiments

Phosphate adsorption was investigated with batch experiments, in which a solid-solution ratio of 1:20 was chosen for gibbsite, and a solid-solution ratio of 1:200 was chosen for ferrihydrite and the Fe:Al-hydroxide mixtures due to their high specific surface areas and P-adsorption capacity. The initial P-concentrations for the adsorption experiments were 150 µmol l^{-1} (P_{150}), 1000 µmol l^{-1} (P_{1000}) and 2000 µmol l^{-1} (P_{2000}) KH_2PO_4 for gibbsite and 1000 µmol l^{-1}, 2000 µmol l^{-1} and 5000 µmol l^{-1} (P_{5000}) KH_2PO_4 for ferrihydrite and the Fe:Al-hydroxides with a 0.01 M $CaCl_2$-background electrolyte solution, adjusted to a pH of 6 with 1 M KOH. The initial phosphate concentrations were chosen to achieve different levels of phosphate coverage of the minerals at specific time steps according to prior observed adsorption capacities for gibbsite (Borggaard *et al.,* 2005; van Emmerik *et al.,* 2007; van Riemsdijk and Lyklema, 1980) and ferrihydrite (Borggaard *et al.,* 2005; Freese *et al.,* 1999; Torrent, 1997; Willett *et al.,* 1988). After starting the adsorption experiments, the samples were horizontally shaken for 24 h at 150 revolutions min^{-1}. For phosphate measurements, the gibbsite and ferrihydrite samples were centrifuged for 15 min at 336 × g, while the Fe:Al-hydroxide samples were centrifuged for 15 min at 21572 × g to achieve a clear supernatant. The clear supernatant was filtered by using P-poor Whatman 512 1/1 filters. For FT-IR spectroscopic measurements, the remaining solid matter was dried for 24 h at 40°C. The phosphate content in the solution was measured by the method of Murphy and Riley (1962).

Prior to the desorption experiments, fine granulated, washed and calcined silica sand (particle size 0.2-0.8 mm, Merck Millipore) was coated with the adsorbents according to Scheidegger *et al.* (1993). The pure silica sand did not show any phosphate sorption. To 10 g of the adsorbent, 0.01 M of a $NaNO_3$-solution, adjusted to pH 6, was added to a final volume of 100

ml. 100 g of pure silica sand was added to the suspension and it was shaken for 24 h at room temperature. After settling of the coated sand, the supernatant was decanted and the material was washed several times with the 0.01 M $NaNO_3$-solution at pH 6, and in a final step with ultrapure water to remove hydroxide traces and soluble salts. The coated silica sand was oven-dried at 60°C for 48 h (Freese *et al.,* 1999). The content of Fe and Al of the coated silica sand was analyzed by using ICP-AES (Unicam iCAP6000 Duo, Thermo Fisher). For this test, 1 g of the coated silica sand sample was diluted into 50 ml PE-bottles and dissolved by adding 1 ml of concentrated H_2SO_4 following a 30 min ultrasonic treatment. The silica was filtered and filled up to a final volume of 50 ml. Prior to desorption, the adsorbents were preloaded with 100 ml of a 1500 µmol l^{-1} KH_2PO_4 solution. After shaking for 24 h at 150 revolutions min^{-1}, the adsorbents were centrifuged for 5 min at 2000 r min^{-1}. The supernatant was filtered and the solid matter was briefly diluted with 50 ml of ultrapure water to remove non-adsorbed phosphate. The solid matter in ultrapure water was centrifuged again and the supernatant was combined with the prior filtered supernatant to obtain a mixed sample for the measurement of adsorbed phosphate content on the hydroxide-coated silica sand. Desorption was conducted with a 0.01 M $CaCl_2$-background electrolyte solution and a solid-solution ratio of 1:20. Goethite was chosen as a reference, since the phosphate binding has been described in detail in several previous studies as either bidentate (Kubicki *et al.,* 2012; Luengo *et al.,* 2006; Tejedor-Tejedor and Anderson, 1990) or monodentate surface complexes (Kubicki *et al.,* 2012; Loring *et al.,* 2009; Persson *et al.,* 1996).

2.3.3 Fourier transform infrared spectroscopy

After adsorption experiments, the powdered samples were oven-dried at 40°C, stored overnight in a desiccator and analyzed without further treatment prior to FT-IR spectroscopic

measurements. IR spectroscopic measurements were carried out by measurement of the absorbance in the FT-IR DRIFT mode (Tensor 27 HTS-XT, Bruker, Billerica, USA) with 40 scans per sample, a wavelength range from 4000 to 400 cm^{-1}, and a resolution of 1.9 $cm^{-1.}$ For evaluation, the spectra were offset-normalized, cut-off at 500 cm^{-1} and converted to Kubelka-Munk units.

2.4 Results

2.4.1 Characterization of minerals

The amorphous nature of the Fe:Al-hydroxide mixtures, the poor crystallinity of ferrihydrite as well as the high crystallinity of gibbsite were confirmed by X-ray diffraction patterns (Fig. 3).

Gibbsite was identified as α-$Al_2O_3 \cdot 3H_2O$ with a monoclinic crystal system. The two characteristic broad bands of 2-line-ferrihydrite with *d*-values of 2.57 and 1.54 were also observed weakly in the Fe:Al-hydroxides with a predominant proportion of Fe. With increasing Al ratio, slight peaks were developed, indicating a nascent but weak crystallization process. The specific BET surface areas of the pure minerals and the minerals applied on silica are given in Tab. 1. The samples showed higher specific surface area with increasing Fe ratio. Accordingly, increasing amounts of Al in the binary systems caused a decrease in the specific surface area.

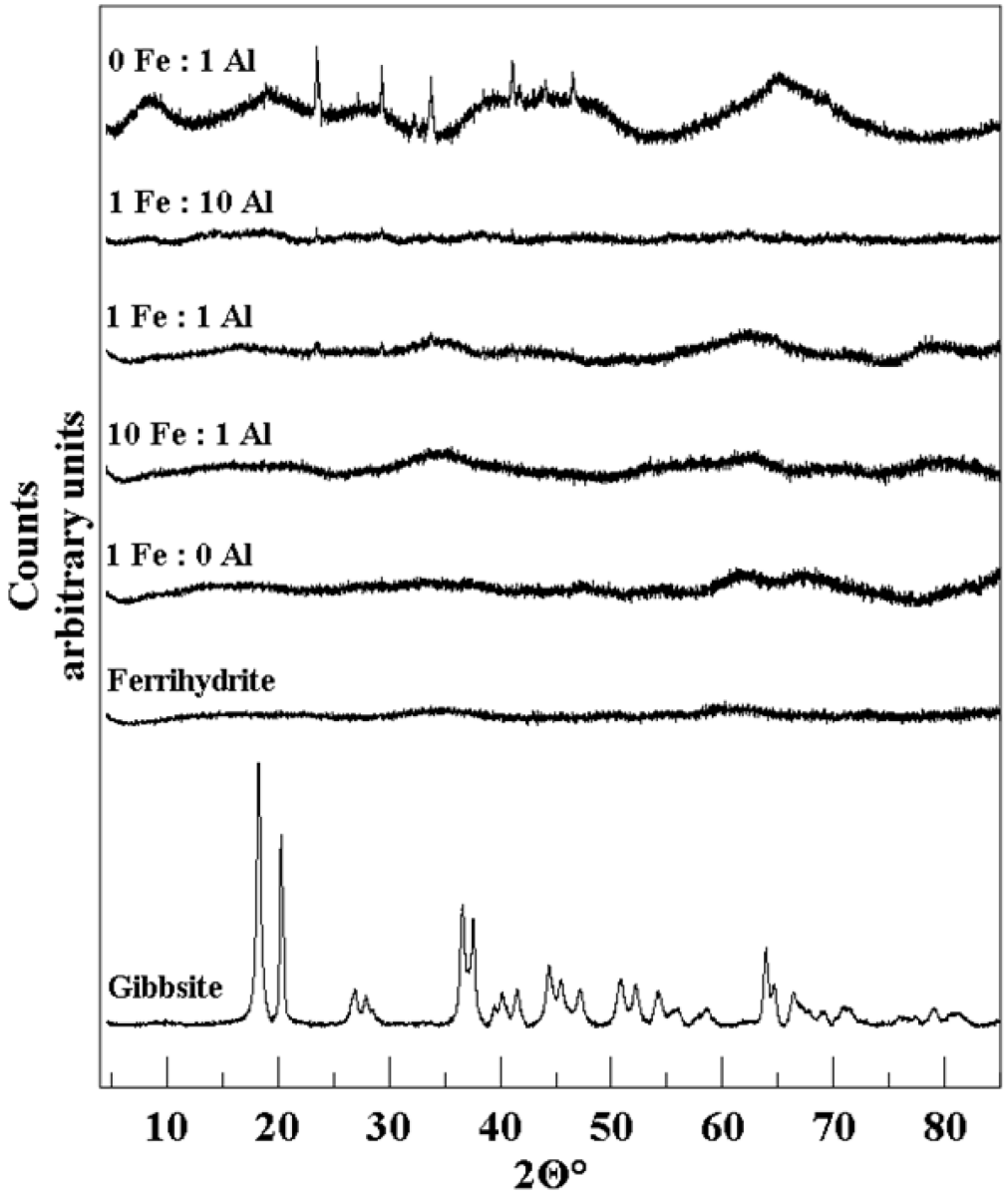

Fig. 3. X-ray diffraction patterns of gibbsite, ferrihydrite and amorphous Fe:Al-hydroxide mixtures in the ratio 1 Fe:0 Al, 10 Fe:1 Al, 1 Fe:1 Al, 1 Fe:10 Al and 0 Fe:1 Al.

Tab. 1. Specific surface of the crystalline and amorphous Fe- and Al-hydroxides and the content of Fe and Al coated on silica sand.

Mineral	**Specific surface***		**Content of Fe and Al on coated silica sand**
	pure mineral	*coated silica sand*	
	$m^2\ g^{-1}$		$mg\ g^{-1}$
Gibbsite	0.87 ± 0.0	0.08 ± 0.0	0.15
Ferrihydrite	251.75 ± 2.7	19.12 ± 2.6	39.74
1 Fe : 0 Al	297.33 ± 10.4	13.07 ± 3.0	43.84
10 Fe : 1 Al	227.07 ± 7.1	11.78 ± 1.7	35.26
5 Fe : 1 Al	203.80 ± 0.9	8.99 ± 0.2	32.44
1 Fe : 1 Al	73.69 ± 8.0	6.29 ± 0.3	24.73
1 Fe : 5 Al	0.79 ± 0.0	0.07 ± 0.0	2.16
1 Fe : 10 Al	0.75 ± 0.0	0.31 ± 0.0	3.52
0 Fe : 1 Al	1.12 ± 1.1	0.04 ± 0.0	0.09

*n = 2, Given are mean and standard deviation.

2.4.2 Kinetics of phosphate adsorption

The phosphate adsorption by gibbsite increased strongly with increasing initial phosphate concentration and totaled 100 % (3.44 µmol m^{-2}) for P_{150}, 45 % (10.40 µmol m^{-2}) for P_{1000} and 41 % (18.81 µmol m^{-2}) for P_{2000}, respectively (Fig. 4, Tab. 2), after an adsorption time of 2688 h (16 weeks).

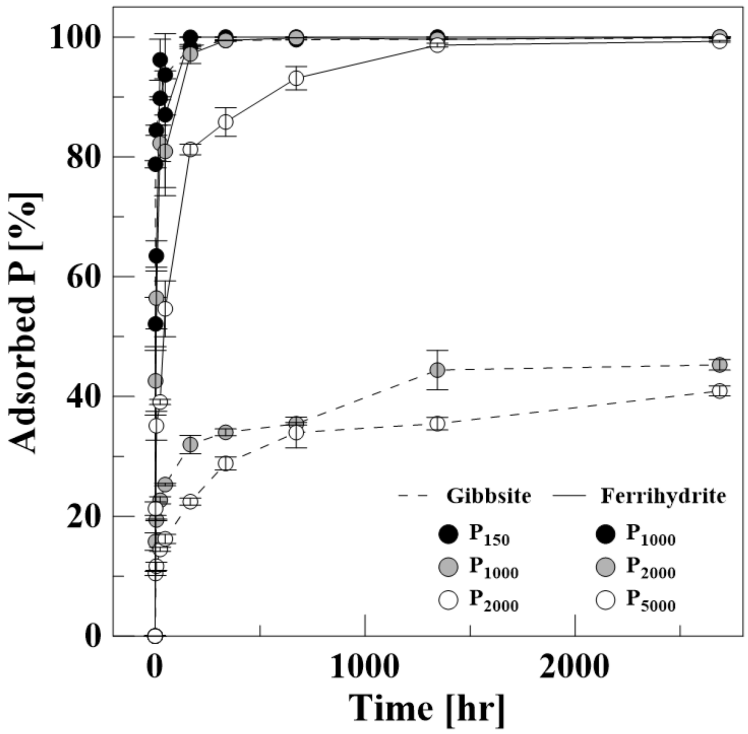

Fig. 4. P adsorption kinetics of gibbsite (P_{150}, P_{1000}, P_{2000}) and ferrihydrite (P_{1000}, P_{2000}, P_{5000}).

A comparison of the lowest initial phosphate concentration with the next level of concentration showed that an almost 6.5-fold higher phosphate solution concentration led to a 3-fold higher adsorption relative to the specific surface area. A doubling of the concentration from P_{1000} to P_{2000} gave a 1.8-fold increase, and a 5.5-fold increase compared to the phosphate adsorption for P_{150}. After a period of 2688 h nearly all of the initial phosphate concentration in the P_{150} solution was adsorbed. P_{1000} and P_{2000} had effective phosphate adsorption of 45 % and 41%, respectively. The kinetic curves also showed a continuing phosphate adsorption for P_{2000} until 2688 h of reaction time. The adsorption kinetics of ferrihydrite showed an adsorbed phosphate amount of 100 % for P_{1000} and P_{2000} (0.80 µmol m^{-2} and 1.59 µmol m^{-2}, respectively), and 99 % for P_{5000} (3.66 µmol m^{-2}) (Fig. 4). With increasing phosphate concentration, the adsorption increased in nearly the same ratio of 1:2:4.6 (adsorbed P for P_{1000}:P_{2000}:P_{5000}).

Tab. 2. P adsorption rates of gibbsite, ferrihydrite and amorphous Fe:Al-hydroxide mixtures after 2688 h and initial P concentrations of 150, 1000, 2000 and 5000 µmol l^{-1}.

	Phosphate adsorption *µmol m^{-2}*			
Initial P	*150 µmol l^{-1}*	*1000 µmol l^{-1}*	*2000 µmol l^{-1}*	*5000 µmol l^{-1}*
Gibbsite	3.44 ± 0.0	10.40 ± 0.2	18.81 ± 0.4	-
Ferrihydrite	-	0.80 ± 0.0	1.59 ± 0.0	3.66 ± 0.0
1 Fe : 0 Al	-	0.67 ± 0.0	1.35 ± 0.0	3.11 ± 0.0
10 Fe : 1 Al	-	0.88 ± 0.0	1.77 ± 0.0	4.11 ± 0.0
5 Fe : 1 Al	-	0.98 ± 0.0	1.95 ± 0.0	4.56 ± 0.1
1 Fe : 1 Al	-	2.71 ± 0.0	5.40 ± 0.0	12.57 ± 0.0
1 Fe : 5 Al	-	224.81 ± 4.8	462.48 ± 8.0	1142.20 ± 5.4
1 Fe : 10 Al	-	224.86 ± 1.1	465.30 ± 4.1	1170.62 ± 12.0
0 Fe : 1 Al	-	121.02 ± 4.7	252.80 ± 1.4	689.06 ± 17.2

n = 4, Given are mean and standard deviation.

The amount of adsorbed phosphate for the amorphous Fe:Al-hydroxides is given in Fig. 5 A-C and Tab. 2. While the adsorbed phosphate content of the Fe:Al-hydroxide mixtures with predominant Fe content and the 1 Fe: 1 Al-mixture amounted to nearly 100 % for P_{1000}, P_{2000} and P_{5000}, the Fe:Al-hydroxide mixtures with predominant Al content adsorbed lower amounts of phosphate. With increasing Al content, phosphate adsorption of 90 %, 84 % and 68 % for P_{1000}, 91 %, 86 % and 71 % for P_{2000}, and 97 %, 94 % and 82 % for P_{5000}, respectively, was measured (Fig. 5).

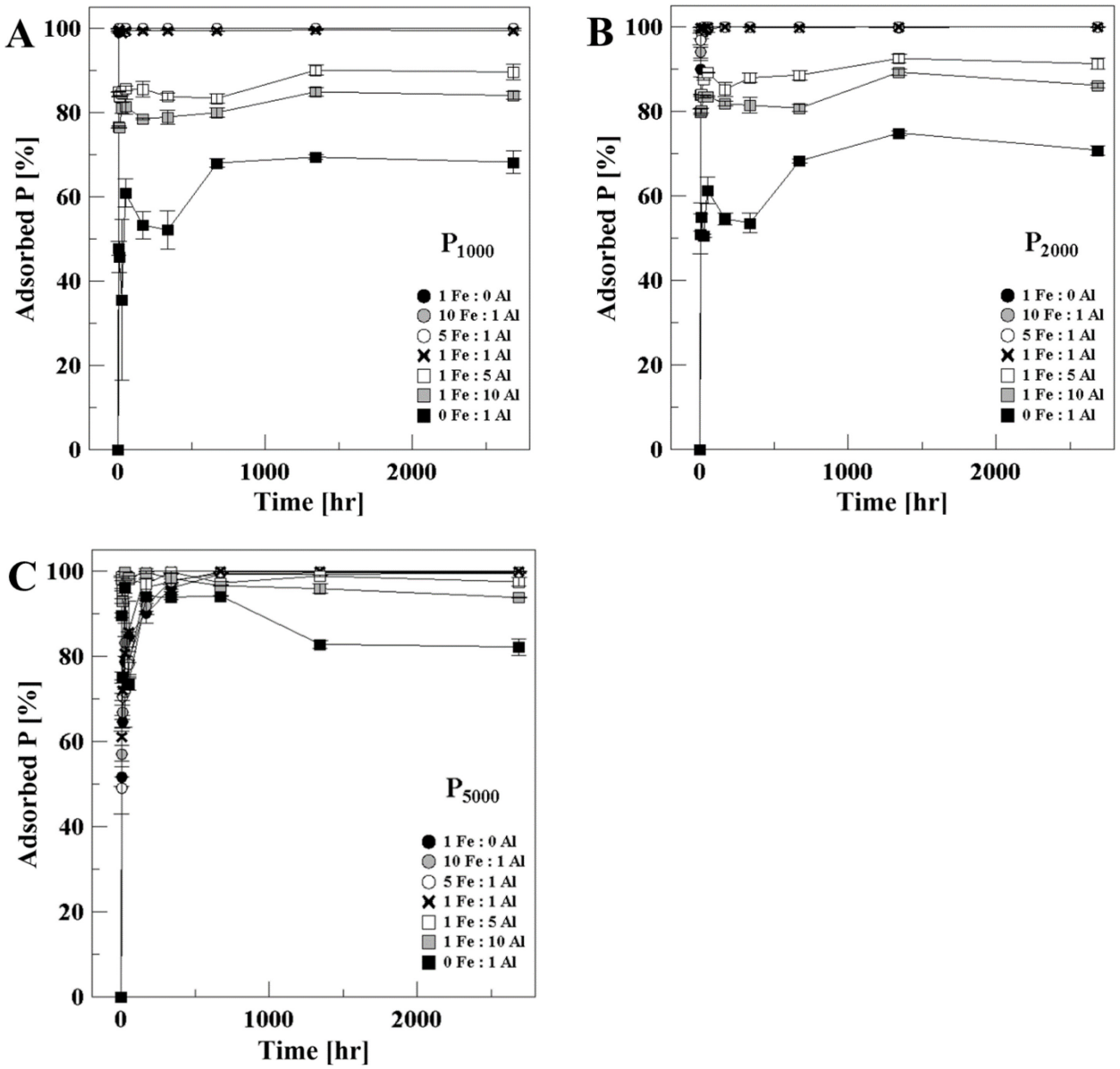

Fig. 5. P adsorption kinetic of amorphous Fe:Al-hydroxide mixtures at P_{1000}, P_{2000} and P_{5000}.

It can be seen that the amount of adsorbed phosphate relative to the specific surface area increased with increasing Al ratio, and was highest for Fe:Al-hydroxide mixtures containing 1 Fe:10 Al and decreased for 0 Fe:1 Al (Fig. 5). The adsorbed phosphate was slightly lower for pure Al-hydroxide compared to gibbsite. While the ratio of phosphate adsorption related to the initial phosphate concentration was 1:2:4.6 for the amorphous samples with predominant Fe

(including 1 Fe:1 Al), this ratio changed to 1:2.1:5.7 in the pure Al-hydroxide samples. In general, the amount of adsorbed phosphate as a percentage of the initial concentration increased pure amorphous Fe-hydroxide (1 Fe: 0 Al) compared to ferrihydrite, but substantially higher with decreasing Al-content (Fig. 6).

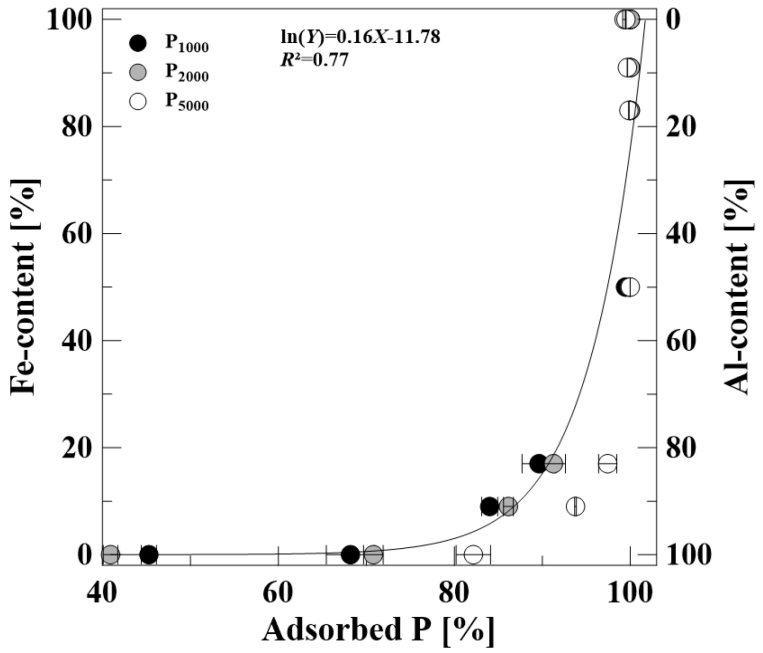

Fig. 6. Correlation of the amount of adsorbed P and the Fe- and Al-content of the mineral samples for initial P concentrations of 1000 µmol l^{-1}, 2000 µmol l^{-1} and 5000 µmol l^{-1}.

2.4.3 FT-IR spectroscopic investigation of phosphate adsorption

Several studies investigated phosphate adsorption on different hydroxyl surfaces such as goethite, ferrihydrite or gibbsite, whereupon characteristic infrared spectroscopic vibrations were analyzed. Depending on the protonation state and the symmetry of the phosphate species in solution, the observed frequencies in this study were assigned according to described frequencies

by Tejedor-Tejedor and Anderson (1990), Persson *et al.* (1996) and similar results of Arai and Sparks (2001). An overview of the described phosphate frequencies is given in Tab. 3.

Tab. 3. Described frequencies and symmetry of dissolved phosphate species.

	PO_4 symmetry	**Frequency** cm^{-1}	**Description**
PO_4^{3-}	T_d	1006	vas P-O
HPO_4^{2-}		1077	vas P-O
	C_{3v}	989	vs P-O
		847	v P-OH
$H_2PO_4^-$		1155	vas P-O
	C_{2v}	1075	vs P-O
		940	vas P-OH
		874	vs P-OH
H_3PO_4		1174	v P=O
	C_{3v}	1006	vas P-OH
		890	vs P-OH

v: vibration, vs: symmetric vibration, vas: asymmetric vibration

Using the position of characteristic P-O bands to assign the molecular symmetry of the adsorbed complex can be difficult due to peak shifts depending on reaction conditions and sample treatment, such as adsorbed phosphate content, pH or moisture (Arai and Sparks, 2001; Krumina *et al.,* 2016; Nanzyo, 1986; Persson *et al.,* 1996; Tejedor-Tejedor and Anderson, 1990; Zheng *et al.,* 2012). According to the mentioned reasons and due to the absorption bands of the minerals themselves, the vibrational bands of phosphate could not be identified, so the OH stretching vibrational bands of the FT-IR spectra were utilized to analyze changes of structural and surface OH groups during adsorption. An overview of the OH vibrations used for gibbsite, ferrihydrite and the Fe:Al-hydroxides is given in Tab. 4.

Tab. 4. Observed frequencies of OH vibrations of gibbsite, ferrihydrite and Fe:Al-hydroxides.

Frequency cm^{-1}	Description	Reference
Gibbsite		
3629	[001] plane OH non-hydrogen bond	Egorova and Lamberov, 2015; Kloprogge *et al.*, 2002; Novák *et al.*, 1990; Phambu *et al.*, 2000
3542	interlayer OH hydrogen bond	Egorova and Lamberov, 2015; Novák *et al.*, 1990
3510	lateral OH	Phambu *et al.*, 2000
3402 3384	} in plane OH	Egorova and Lamberov, 2015
1139 982	} in plane deformation OH	Ruan *et al.*, 2001b
919	deformation OH from Al(OH)Al non-hydrogen bond	Ruan *et al.*, 2001b; Frost, 1998
892 824	} out of plane deformation OH	Kloprogge *et al.*, 2002
Ferrihydrite		
3575	surface and structural OH	Russel, 1979; Tüysüz *et al.*, 2008
1661	H_2O	Myronyuk *et al.*, 2016; Rout *et al.*, 2012; Tüysüz *et al.*, 2008
1539	Fe-O	Tüysüz *et al.*, 2008
1426 761	} Fe-OH	Rout *et al.*, 2012; Tüysüz *et al.*, 2008
Fe-Al-Hydroxides		
3616 - 3433	surface and structural OH non-hydrogen bond > 3500 < hydrogen bond	Hass *et al.*, 2000; Russel, 1979; Tüysüz *et al.*, 2008
1635	H_2O	Myronyuk *et al.*, 2016
1401 - 1458	Fe/Al-O	Tüysüz *et al.*, 2008
1352 - 1375	Fe/Al-OH	Rout *et al.*, 2012; Tüysüz *et al.*, 2008
1050 990 809	} Al-OH	
760	Fe-OH	Rout *et al.*, 2012; Tüysüz *et al.*, 2008

2.4.3.1 Gibbsite

The IR spectrum of pure gibbsite showed seven vibrational bands in the range from 3629 cm^{-1} to 3402 cm^{-1}. The pronounced band at 3629 cm^{-1} with a shoulder at 3612 cm^{-1}, and the bands at 3542 cm^{-1} and 3510 cm^{-1} are assigned to stretching vibrations of non-hydrogen-bonded terminal OH-groups in the [001] plane of the crystal (Egorova and Lamberov, 2015; Kloprogge *et al.,* 2002; Novák *et al.,* 1990; Phambu *et al.,* 2000), interlayer hydrogen-bonded OH-groups between gibbsite slabs (Egorova and Lamberov, 2015; Novák *et al.,* 1990) and lateral hydroxyl groups (Phambu *et al.,* 2000), respectively. Vibrations at 3402 cm^{-1} and 3384 cm^{-1} can be assigned to OH-groups in the plane of gibbsite layers (Egorova and Lamberov, 2015). Bands at 1139 cm^{-1}, 982 cm^{-1} and 919 cm^{-1} can be described as in-plane deformation vibrations of OH-groups and correspond to bands in the hydroxyl stretching region (Ruan *et al.,* 2001a), while bands at 892 cm^{-1} and 824 cm^{-1} belong to out-of-plane deformation OH-vibrations (Kloprogge *et al.,* 2002). Kolesova and Ryskin (1959) reported that the bending hydroxyl vibration at 1139 cm^{-1} was influenced by hydrogen bonds, while the 982 cm^{-1} and 919 cm^{-1} bands were due to bending vibrations of weakly interacting hydroxyl groups. Thus, the band around 919 cm^{-1} can be assigned to a non-hydrogen-bond hydroxyl deformation vibration of an Al(OH)Al-group (Frost, 1998; Ruan *et al.,* 2001a).

During phosphate adsorption, only minor intensity changes were detected in the IR spectrum of gibbsite. To better discern the observed vibrational changes during phosphate adsorption, the OH-stretching region was cut between the different peaks and offset-normalized (Fig. 7). While the intensity of the of non-hydrogen-bonded terminal OH-groups in the [001] plane of the crystal at 3629 cm^{-1} decreased over time for P_{150} and P_{1000}, this peak increased during the first week of adsorption and decreased in the remaining adsorption period for P_{2000}. A slight

shift of the shoulder at 3612 cm^{-1} to lower wavelength can be observed. The peak of the interlayer hydrogen-bonded OH-groups at 3542 cm^{-1} also decreased over time for all initial phosphate concentrations. The vibration of the lateral hydroxyl groups at 3510 cm^{-1} showed a similar increasing intensity for all initial phosphate concentrations and a slight shift to lower wavelength during the adsorption process. Vibrations of the OH-groups in the plane of the gibbsite layers between 3425 cm^{-1} and 3380 cm^{-1} increased very weakly for P_{150}, and more intensely for P_{2000}, but after an adsorption time of 2688 h the intensity of the peak leveled out at the base level. Somewhat similar changes were apparent for the vibrational bands at 1139 cm^{-1}, 982 cm^{-1}, 919 cm^{-1} and 892 cm^{-1} (Fig. 7).

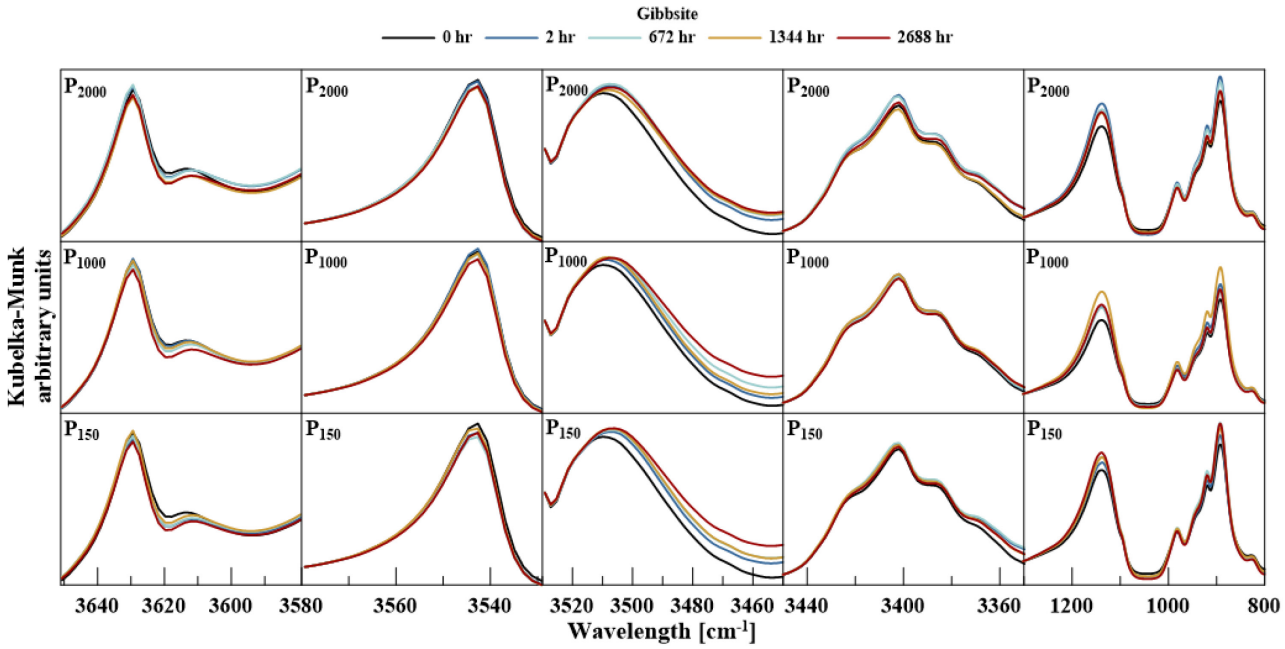

Fig. 7. Edited FT-IR spectra of gibbsite during P adsorption.

For P_{150} and P_{1000}, the peak intensities increased with increasing adsorbed phosphate concentration until an adsorption time of 1344 h, and decreased in the last measured adsorption

step of 2688 h. For P_{2000}, the peak intensities increased until an adsorption time of 2 h and started decreasing with further adsorption steps. In general, the intensities increased with phosphate adsorption, but no discrete P-O vibrations or shifted bands were observed during the process of phosphate adsorption.

2.4.3.2 Ferrihydrite

In the IR spectrum of pure ferrihydrite, three bands were identified (Fig. 8A and 8C). The broad adsorption band around 3575 cm^{-1} can be associated with surface-bonded and structural OH-groups (Russell, 1979; Tüysüz *et al.,* 2008). A broad band occurred, including two distinctive vibrations at 1661 cm^{-1} and 1426 cm^{-1}, which are attributed to H_2O and Fe-OH vibrations, respectively (Rout *et al.,* 2012; Tüysüz *et al.,* 2008), and a less distinctive vibration at 1539 cm^{-1}, associated with a Fe-O vibration (Tüysüz *et al.,* 2008). A sharp band at 761 cm^{-1} can be assigned to the bending vibration of OH-groups of Fe-OH (Rout *et al.,* 2012). At the start of phosphate adsorption, a vibrational band with a weak shoulder appeared at lower wavelength, at 1125 cm^{-1} (P_{1000}). With increasing initial phosphate concentration, this band shifted to 1130 cm^{-1} for P_{2000} and to 1140 cm^{-1} for P_{5000}. The broad vibrational band in the range of 1661 cm^{-1} to 1426 cm^{-1} degenerated, and only a weak vibration at 1664 cm^{-1} remained. The Fe-OH band at 764 cm^{-1} showed a decreasing intensity for P_{1000} and P_{2000} at the beginning of the adsorption experiments, but increased to the initial value after 2688 h of reaction time. For P_{5000}, the Fe-OH band had a consistently lower intensity during the whole adsorption time. Also, the intensity of the OH-vibration at 3575 cm^{-1} decreased during the adsorption process; however, this decrease was permanent only for P_{5000} after 2688 h.

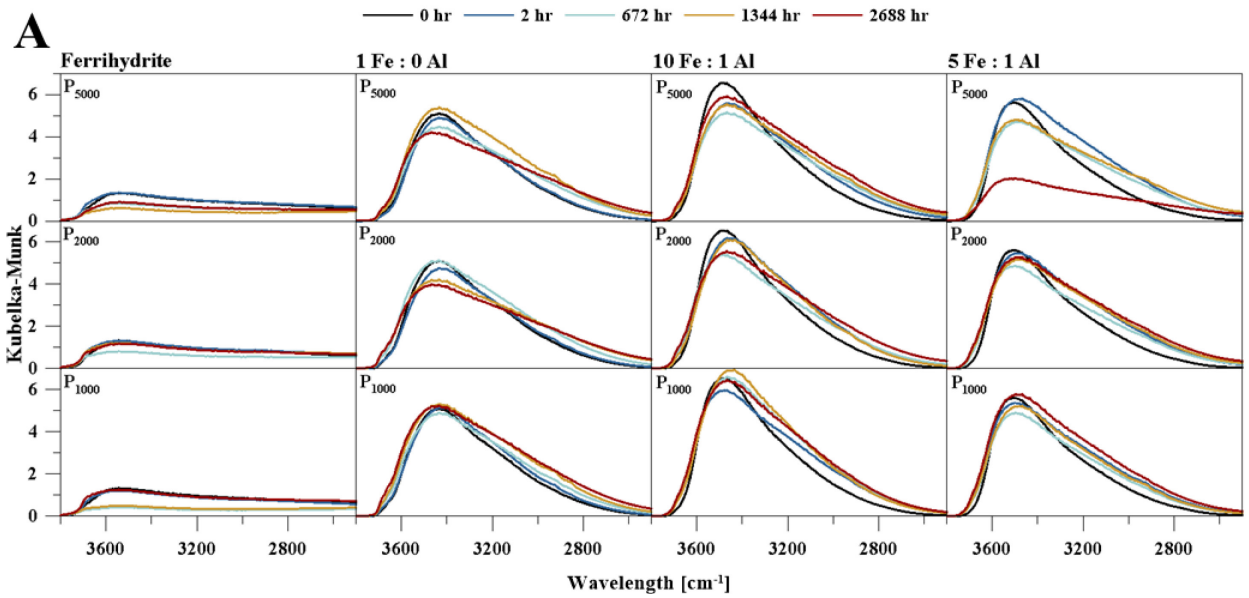
A
0 hr
2 hr
672 hr
1344 hr
2688 hr
Ferrihydrite
1 Fe : 0 Al
10 Fe : 1 Al
5 Fe : 1 Al
P5000
P2000
P1000
Kubelka-Munk
Wavelength [cm-1]

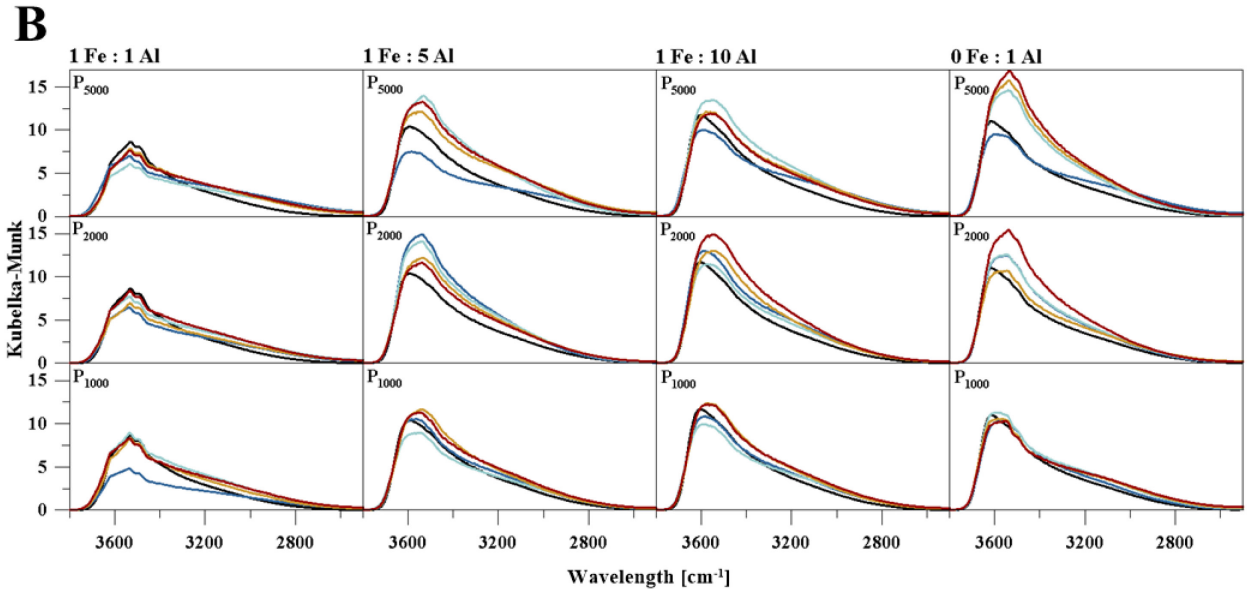
B
1 Fe : 1 Al
1 Fe : 5 Al
1 Fe : 10 Al
0 Fe : 1 Al
P5000
P2000
P1000
Kubelka-Munk
Wavelength [cm-1]

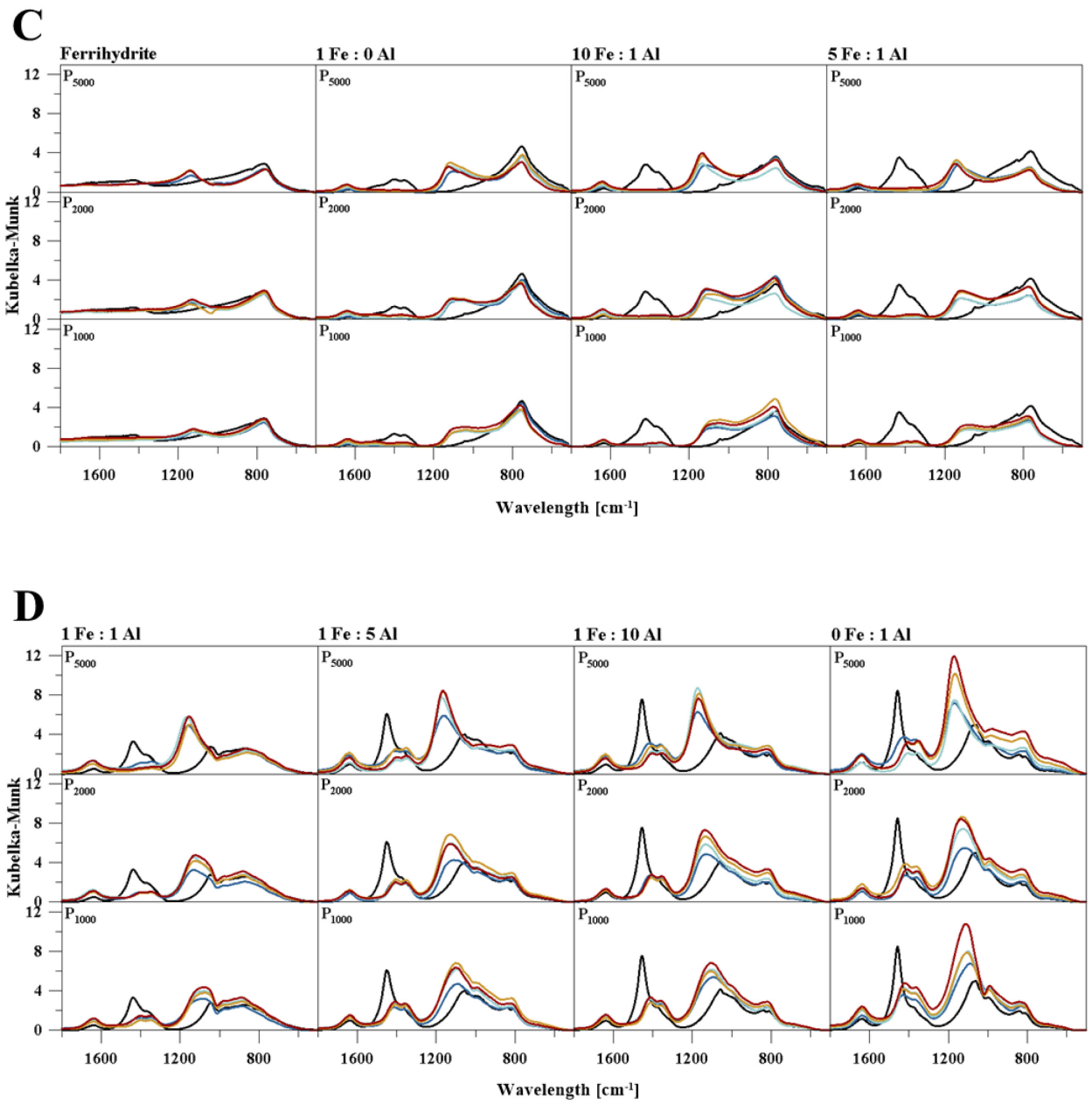

Fig. 8. FT-IR spectra of ferrihydrite and amorphous Fe:Al-hydroxide mixtures 1 Fe:0 Al, 10 Fe:1 Al, 5 Fe:1 Al and 1 Fe:1 Al, 1 Fe:5 Al, 1 Fe:10 Al and 0 F e:1 Al in the OH stretching region from 3800 to 2500 cm^{-1} (A, B) and in the OH stretching region from 1800 to 500 cm^{-1} (C, D) during phosphate adsorption. Please notice the different scaling of the Kubelka-Munk units in (A) and (B).

2.4.3.3 Amorphous Fe: Al-hydroxide

The IR spectra of the amorphous Fe:Al-hydroxides showed a vibrational band in the OH-stretching region in the range from 3745 cm^{-1} to 2645 cm^{-1}, which generally can be assigned to structural and surface-bonded OH-groups (Fig. 8). While the width of the band stayed constant during transition, the intensity increased and the peak shifted to higher wavelength (from 3433 cm^{-1} to 3616 cm^{-1}) with increasing Al-content (Fig. 9).

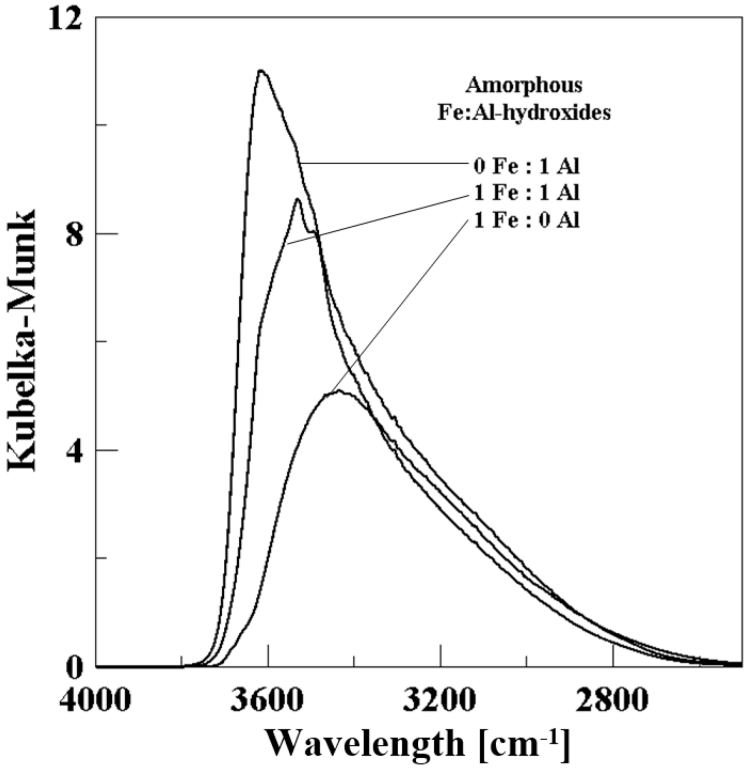

Fig. 9. FT-IR spectra of amorphous Fe:Al-hydroxide mixtures in the OH stretching region.

This could indicate the preferred formation of hydrogen-bonded OH-groups in Fe-hydroxides and the formation of non-hydrogen-bonded OH-groups in Al-hydroxides (Hass *et al.,* 2000), or an increasing amount of structural instead of surface-bound OH in Fe-hydroxides

(Russell, 1979). The splitting and shifting of this vibration is obvious in the 1 Fe:1 Al-hydroxide sample.

The amorphous Fe-hydroxide showed similar vibrations to those of the poorly crystalline ferrihydrite (Fig. 10). A characteristic band between 751 cm^{-1} and 761 cm^{-1} with two small features at higher wavelength on the slope can be found for both samples. By comparison with the ferrihydrite infrared spectrum, it can be deduced that this vibrational band in the amorphous sample was associated specifically with Fe-OH bonding. With increasing Al ratio, a shift of this vibration to higher wavelength at 1068 cm^{-1} was observed, which can be assigned to Al-OH bonding due to the lower atomic mass of Al compared to Fe, and hence, the higher vibrational frequency. A weak band of ferrihydrite at 1661 cm^{-1}, which can also be found in the spectrum of amorphous Fe-hydroxide at 1634 cm^{-1}, and more pronounced in Al-hydroxide at 1639 cm^{-1}, can be assigned to the bending mode of molecular H_2O-groups (Myronyuk *et al.,* 2016; Schwertmann and Fischer, 1973) (Fig. 10). A wide difference can be observed according to a set of vibrational bands in the wavelength range of 1350 cm^{-1} to 1500 cm^{-1}, which is very weak in the ferrihydrite spectrum, more pronounced in the amorphous Fe-hydroxide, and strong in the Al-hydroxide spectrum. The IR spectrum of gibbsite showed no band in this wavelength range. This band with multiple vibrations was assigned as Fe-O and Fe-OH for ferrihydrite (see above) and can be correlated to Fe-O and Fe-OH vibrations in the Fe-hydroxide sample. Due to the slight shift to higher frequency in the Al-hydroxide, the vibration can also be correlated to Al-O and Al-OH vibrations.

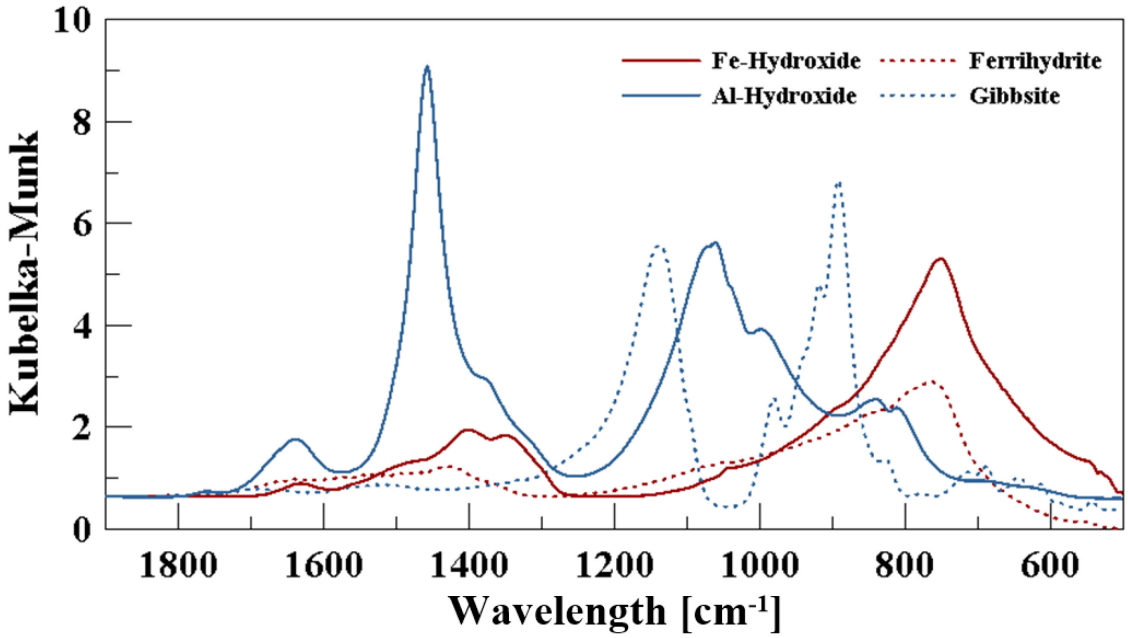

Fig. 10. Comparison of FT-IR spectra of pure amorphous Fe:Al-hydroxides, ferrihydrite and gibbsite in the wavelength range from 1900 cm^{-1} to 500 cm^{-1}.

During phosphate adsorption a new band around 1100 cm^{-1} appeared, which can be assigned to P-O bonding (Krumina *et al.,* 2016; Persson *et al.,* 1996; Sun and Xue, 2013; Tejedor-Tejedor and Anderson, 1990), while the precise position depends on the Fe:Al ratio and the P-concentration (Fig. 8). This band belonged to observed reference fundamental frequencies of the vibration of the PO_4 in $H_2PO_4^-$, which are described in Tab. 3. The IR spectra of the Fe:Al-hydroxides showed broad vibrational bands in the range of 510 cm^{-1} to 1210 cm^{-1} prior to the phosphate adsorption; hence, other phosphate vibrations were overlaid or poorly observable. As the ratio of Fe to Al changed, the broad band changed in this wavelength range and the suggested overlaid phosphate peaks were visible at about 995 cm^{-1} and 815 cm^{-1}. Certainly, this possible P-O band could also be due to the integrated Al-OH vibration. Also, the frequencies of the set of

peaks changed with increases in the adsorbed phosphate concentration and Fe:Al ratio, and the clear and sharp asymmetric P-O vibration around 1100 cm^{-1} will be used for further analysis.

A further change in the IR spectra during phosphate adsorption can be observed in the OH-binding regions. For the pure Fe-hydroxide sample, the peak of the OH-stretching vibration shifted with increasing adsorbed phosphate concentration from 3433 cm^{-1} to 3467 cm^{-1}, and the intensity decreased with adsorption time and increasing initial phosphate concentration. The Fe-O and Fe-OH vibrations at 1401 cm^{-1} and 1352 cm^{-1} decreased immediately with the adsorption process and disappeared completely at P_{5000}. The Fe-OH band at 751 cm^{-1} shifted slightly to 761 cm^{-1} for P_{1000}, but the shift was reversed with higher adsorbed phosphate concentration. In addition, the intensity of this band decreased with increasing phosphate adsorption. The H_2O band at 1634 cm^{-1} was observable at all times and increased from P_{1000} to P_{5000}. Overall, the infrared spectra showed a fast adsorption process in the beginning and almost no further changes over time. Only the OH stretching vibration showed long-term changes. In the 10 Fe:1 Al-hydroxide sample, the OH stretching band shifted from 3485 cm^{-1} to 3469 cm^{-1} and the intensity decreased with increasing initial phosphate concentration. The observed changes were similar to those of the 1 Fe:0 Al-hydroxide samples. The intensities showed more differentiated long-term changes. The OH-stretching vibration for the 5 Fe:1 Al-hydroxide sample shifted from 3502 cm^{-1} to 3487 cm^{-1}, and the intensity also decreased with increasing initial phosphate concentration. This was more distinctive in the P_{5000} samples. The intensities of the Fe- OH band at 760 cm^{-1} decreased as well; again, this decrease was stronger in the beginning and a slight increase for P_{1000} and P_{2000} was observed. The 1 Fe:1 Al-hydroxide showed a differentiation of the OH-stretching vibration with three peaks at 3623 cm^{-1}, 3532 cm^{-1} and 3490 cm^{-1}, which were still visible in the in the phosphate adsorption spectra. The peak at 3532 cm^{-1} shifted slightly to 3535 cm^{-1}, and the peak at 3490 cm^{-1} shifted to 3496 cm^{-1}, respectively. The intensities of the

bands decreased with increasing phosphate adsorption, but in comparison to the pure hydroxide sample the vibrational band intensity increased with adsorption time. Also, the intensities of Fe-OH-Al vibrations in the range from 1049 cm^{-1} to 857 cm^{-1} increased slightly with the adsorbed phosphate concentration for P_{1000} and P_{2000}. Additionally, the intensity of both the Fe-O and Al-O as well as the Fe-OH and Al-OH vibrations at 1439 cm^{-1} and 1364 cm^{-1}, respectively, decreased in general, but stayed visible for P_{1000} and P_{2000}. They were observable for P_{5000} samples until an adsorption time of 2 h. The OH band of the 1 Fe:5 Al-hydroxide sample shifted from 3592 cm^{-1} to 3560 cm^{-1} and the intensity increased with increasing initial phosphate concentration, but decreased with adsorption time, especially in P_{2000}. For the 1 Fe:10 Al-hydroxide, the OH stretching vibration shifted from 3603 cm^{-1} to 3550 cm^{-1}. The intensity increased with increasing adsorbed phosphate concentration, but decreased for all treatments in the beginning of the adsorption process, and for P_{5000} after an adsorption time of 672 h. The Fe-OH vibration intensity slightly increased over time, while that of the Al-OH vibration seemed to decrease in P_{5000}. For the pure Al-hydroxide, the OH-stretching band showed a broadening of the peak at P_{1000} and P_{2000}, and a shift from 3616 cm^{-1} to lower wavelength, resulting in three apparent peaks (3572 cm^{-1}, 3534 cm^{-1}, 3499 cm^{-1}) at P_{5000}. The two peaks at 3534 cm^{-1} and 3499 cm^{-1} were only slightly visible in the pure spectra. Also, the intensity of this vibration increased with adsorption time and adsorbed phosphate concentration. The Al-OH vibrations at 1068 cm^{-1}, 995 cm^{-1}, 839 cm^{-1} and 809 cm^{-1} increased in intensity more strongly over time compared to the Fe-dominated hydroxide samples the same was true for the P-O vibration. Also, the H_2O band at 1639 cm^{-1} was observable at all times and increased from P_{1000} to P_{5000}. The Al-O band at 1458 cm^{-1} decreased and shifted to lower wavelength, whereas the Al-OH vibration at 1375 cm^{-1} shifted only slightly to lower frequency but increased during adsorption. However, an asymmetric P-O vibration at around 1150 cm^{-1} could be observed. In general, the P-O vibration

shifted during the transition from pure Fe-hydroxide to pure Al-hydroxide from lower to higher frequency. This was more pronounced for higher adsorbed phosphate concentrations. The wavelength shifted from 1110 cm^{-1} to 1131 cm^{-1} for P_{2000} and from 1128 cm^{-1} to 1174 cm^{-1} for P_{5000}, respectively.

2.4.4 Phosphate desorption

Gibbsite and the pure Al-hydroxide showed the highest phosphate release capacities, with 42.6 % and 38.2 % after 1344 h (Fig. 11). Both showed slightly lower desorption rates compared to a desorption rate of 47.9 % for goethite, as a well characterized crystalline Fe-hydroxide (treated by the same method). Hydroxide mixtures with a predominant ratio of Al had a substantially lower rate of phosphate release compared to gibbsite or the pure Al-hydroxide, with 1.5 % for 1 Fe:5 Al and 5.5 % for 1 Fe:10 Al, respectively. Ferrihydrite and the pure Fe-hydroxide showed almost no or very minor phosphate desorption, with 0.3 % and 0.1 % after 1344 h, respectively, and the 1 Fe:1 Al-hydroxide had a similar low phosphate release of 0.1 %. For the 10 Fe:1 Al and 5 Fe:1 Al samples, a desorption rate of 0 % was determined; however, the residual phosphate concentrations were close to or under the detection limit. The initial desorption rate within the first 2 h was high, but decreased after 168 h. Due to the relatively low amount adsorbed onto the minerals coated on silica prior to desorption, possible vibrational bands of phosphate were overlaid by the distinctive bands of the silica sand.

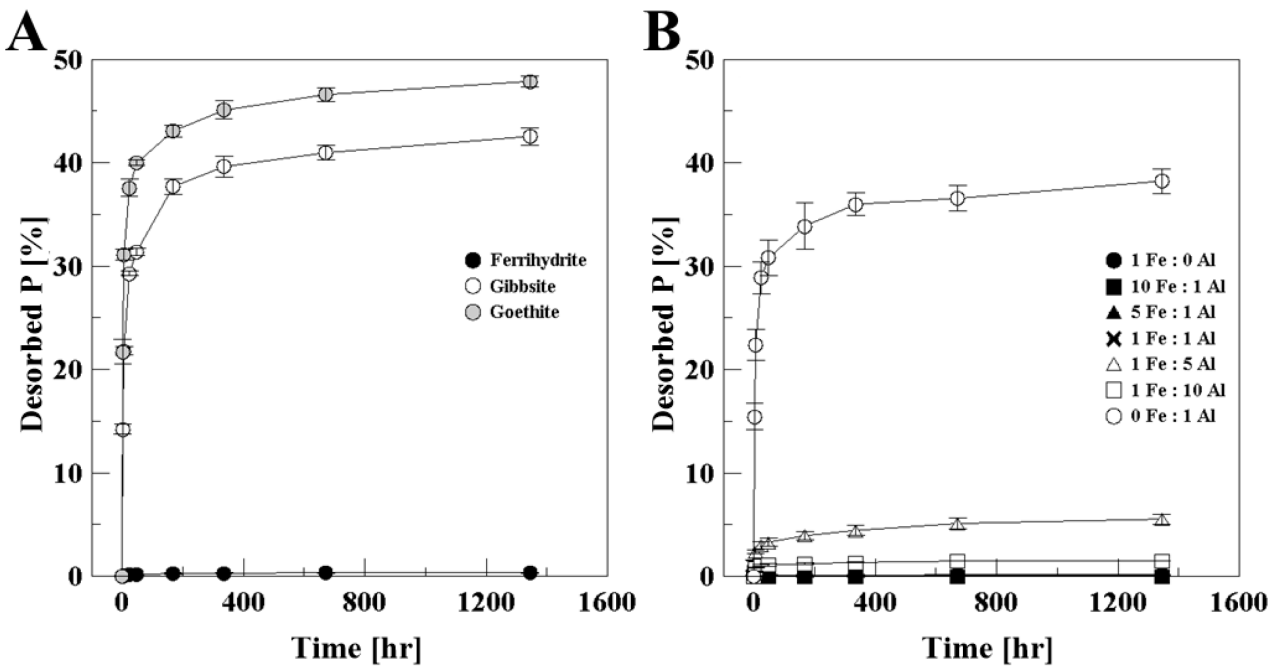

Fig. 11. P desorption kinetics of gibbsite, ferrihydrite and goethite (A), and amorphous Fe:Al-hydroxide mixtures in 0.01 M $CaCl_2$ at pH 6 (B).

2.5 Discussion

2.5.1 FT-IR spectroscopic experiments during phosphate adsorption

2.5.1.1 Gibbsite

For gibbsite, several studies have described the formation of inner-sphere complexes between phosphate and the alumina surface in combination with outer-sphere complexation. Zheng *et al.* (2012) reported that at lower pH with $H_2PO_4^-$ as the dominant phosphate species, the inner-sphere surface complex between phosphate and the alumina surface is of the diprotonated monodentate type, with hydrogen-bonding to outer-sphere complexes, or the monoprotonated bidentate binuclear type with the same symmetry. It was possible that both binding forms existed

simultaneously. Van Emmerik *et al.* (2007) described a mixture of inner-sphere and weakly bound outer-sphere complexes depending on pH and phosphate concentration, with predominantly inner-sphere complexes found at a pH of 6.5. It was suggested that monodentate inner-sphere complexes are bound to singly coordinated reactive Al-OH sites on the edge of the gibbsite crystals (Parfitt *et al.,* 1977; van Emmerik *et al.,* 2007).

The increase and slight shift of the lateral Al-OH groups was a result of additional OH groups formed during adsorption of AlH_2PO_4 complexes, while in-plane OH groups were not affected by the adsorption process. With increasing equilibration time, the Al-OH peaks decreased, which can be due to reduced protonation and the formation of $AlHPO_4$ and Al_2HPO_4. The constant increase of adsorption at long reaction times, at which no equilibrium plateau was reached, led to the conclusion that precipitated $AlPO_4$ seemed to be formed as well (Johnson *et al.,* 2002; van Emmerik *et al.,* 2007; van Riemsdijk and Lyklema, 1980; Zheng *et al.,* 2012). Laiti *et al.* (1998) described the initial formation of a monodentate inner-sphere complex as a precursor for a formed $AlPO_4$ phase, which was low at pH 6, but increased substantially at pH 7. Johnson *et al.* (2002) described a decrease in the relative amount of $AlPO_4$ precipitate formation with increasing pH due to the increasing solubility of $AlPO_4$ at pH values around 6. In this case, the adsorption experiments were conducted at pH 6, where the relative amount of $AlPO_4$ precipitate is limited by its increasing solubility as mentioned above, and Al- or Fe-phosphates were described as having their optimal phosphate availability (Blume *et al.,* 2010; Johnson *et al.,* 2002). Nevertheless, amorphous aluminum phosphate can be formed, for which the extent of precipitation is limited by the phosphate concentration. It was implied that surface precipitates, which do not necessarily need to be formed by surface reactions, may occur on the Al_2-OH face sites of the gibbsite crystal in close contact with water molecules or surface hydroxyl groups (van Emmerik *et al.,* 2007).

With regard to the described P-O vibration in Tab. 3, a distinctive band should appear around 1155 cm^{-1}. Other than a change in intensity, no distinctive P-related vibrational change was observed. The visibility of this band can be hindered by the Al-OH vibration. With the lowering of symmetry of the adsorbed phosphate species, the symmetric P-O band shifted to higher wavelength. Laiti *et al.* (1996) described this phenomenon of poorly resolved P-O bands, which was caused by the low symmetry of the complexes on the aluminum oxide surface and differences in the structural environment, which led to four vibrational bands and a weaker interaction of phosphate and alumina. They formulated, amongst others, $AlHPO_3$ and AlH_2PO_4 surface complexes with similar low symmetry (C_1). Connor and McQuillan (1999) described a general C_s symmetry for monodentate monoprotonated, monodentate diprotonated and bidentate monoprotonated adsorbed phosphate species with four vibrational bands, similar to the result of Laiti *et al.* (1996). A lowering in symmetry can also occur due to the influence on surface complexes by hydrogen bonds (Arai and Sparks, 2001). Hence, a differentiation between surface complex and precipitation could not be well evaluated solely by consideration of the P-O peak. Both adsorption processes, on the plane and on the edge of the gibbsite crystal, respectively, proceeded more slowly with lower initial phosphate concentration. Due to the significantly lower specific surface area compared to ferrihydrite but higher amount of adsorbed phosphate over time, the continuously increasing phosphate adsorption without reaching an equilibrium plateau, also observed by Lookman (1995), and the minor changes of the infrared spectra, can be interpreted according to additional formation of outer-sphere complexes.

2.5.1.2 Ferrihydrite

Previous studies divided the adsorption process into three stages, in which the first two stages included the formation of bidentate binuclear surface complexes and the third stage involved the formation of three bonds between phosphate and iron for both migration and precipitation, respectively (Nanzyo, 1986; Parfitt, 1979, 1989), since a long equilibration time resulted in the formation of a stable mineral-phosphate phase (Persson *et al.,* 1996). Also, Nanzyo (1986) specified the adsorption of amorphous iron phosphate and partly bidentate binuclear surface complexes. Further studies also described a bidentate binuclear complex as the dominant surface species of adsorbed phosphate (Khare *et al.,* 2007; Nanzyo, 1986; Parfitt, 1979), specified as prevalently nonprotonated (Antelo *et al.,* 2010; Arai and Sparks, 2001). Krumina *et al.* (2016) and Borggaard *et al.* (2005) also suggested the formation of a mononuclear monodentate surface complex between phosphate and ferrihydrite.

When orthophosphate ions were added to the reactive metal-hydroxide surface groups by ligand exchange, surface (and structural) OH or H_2O molecules were released and a phosphate surface complex was formed (Goldberg and Sposito, 2008; Parfitt *et al.,* 1975; Torrent *et al.,* 1992b), which would be observed by a decrease in the intensity of the OH stretching band. Certainly, the OH vibrations of the adsorbed phosphate species were also included in this vibrational band (Persson *et al.,* 1996; Tejedor-Tejedor and Anderson, 1990). On the basis of similar changes in the FT-IR spectra and corresponding to findings in the goethite structure reported by Ruan *et al.* (2001b), it was assumed that the Fe-O and Fe-OH bands at 1539 cm^{-1} and 1426 cm^{-1} correspond to the Fe-OH bending vibration at 761 cm^{-1}. Also, the degeneration of the Fe-OH bending band showed the release of OH groups by attached phosphate and the development of Fe-O-P bonds. The observed P-O band at 1125 cm^{-1}, with a weak shoulder around 1055 cm^{-1}, can be assigned to the bands of the $H_2PO_4^-$ phosphate species, forming a

$FeHPO_4$ surface complex, also described by Tejedor-Tejedor and Anderson (1990). This can be supported by only minor variation of the OH stretching vibration, indicating almost no change of bound OH groups at low phosphate content and short equilibration time. However, with continuing equilibration time, the OH band intensity decreased, indicating the conversion of $FeHPO_4$ to Fe_2PO_4. Also, the Fe-OH band increased in intensity and did not reach a steady state until higher adsorbed phosphate content, indicating liberation of reactive OH sites. A possible explanation can be the precipitation of $FePO_4$, as shown by Nanzyo (1988), with longer equilibration time.

With increasing phosphate concentration, the decrease of the OH band continued with longer equilibration time and showed less strong reversibility. In addition to the P-O peak at 1130 cm^{-1} with a weak shoulder at 1065 cm^{-1}, a new weak peak at 1012 cm^{-1} appeared. These are in good agreement with the earlier reported $H_2PO_4^-$ bands. Including the permanently decreased Fe-OH band at P_{5000}, possible surface complexes could be Fe_2PO_4 or $FePO_4$, according to Tejedor-Tejedor and Anderson (1990), the latter of which had a higher C_{3v} symmetry, which is not consistent with the P-O peak position. Fe_2PO_4 was more reasonable; certainly, the phosphate peak position indicated a lower symmetry. Arai and Sparks (2001) explained possible molecular configurations and mentioned the symmetry lowering effect of hydrogen bonds.

2.5.1.3 Amorphous Fe: Al-hydroxide mixtures

In general, the FT-IR spectra of amorphous Fe- and Al-hydroxides differed regarding the OH stretching vibration region. A shift of the OH vibrational band to lower wavelength can be related to the formation of hydrogen bonds (Al-Abadleh and Grassian, 2003) within the mineral sample. Hence, one possible explanation could be a higher amount of hydrogen bonds in the Fe-

hydroxide samples and hence, hydrogen bond-affected binding sites, while the Al-hydroxide samples developed predominantly free OH groups. Another explanation could be the predominant formation of bulk OH groups in the Fe-hydroxide compared to more surface OH groups in Al-hydroxide samples (Russell, 1979). The latter case by itself would not explain the highly different specific surface areas. The observed formation of $Al(OH)_3$ and FeO(OH) led to the conclusion that the iron(III) oxide-hydroxide was mainly associated by hydrogen bonds, while the aluminum hydroxide was mainly associated by covalent OH bonds (Hass *et al.,* 2000). Also, the OH stretching vibration for Al-hydroxides increased compared to the Fe-dominated samples. Including also the increasingly intense molecular H_2O band at 1639 cm^{-1}, it was concluded that the Al-hydroxides contained more molecular water compared to the Fe-hydroxides, which was not removed during desiccation. Myronyuk *et al.* (2016) described a decrease of the specific surface area as a result of a reduced water adsorption, and hence, in lower intensity OH stretching bands. Despite a more intense OH stretching vibration, Al-hydroxide had a lower specific surface area. It can be concluded that the higher amount of molecular water, which was not attached on possible binding sites and was removed during the outgassing procedure, increased the OH band but not the specific surface area. The shift of the OH vibration during the adsorption process to higher wavelength in the Fe-hydroxides and to lower wavelength in the Al-hydroxides showed both the formation of hydrogen bond- as well as non-hydrogen bond-affected OH groups.

Similar to the ferrihydrite samples, the P-O peak shifted continuously to higher frequency with increasing adsorbed phosphate. The highest wavelength was observed in the pure Al-hydroxide samples with a value of 1174 cm^{-1} and the lowest in the pure Fe-hydroxide samples, with 1128 cm^{-1}. Besides the phosphate loading, this can be explained by the lower atomic mass of the associated Al ions compared to the Fe ions, similar to the Fe/Al-OH vibrations.

The FT-IR spectra of amorphous Fe-hydroxide showed an increase of molecular water for all concentration levels, but a decrease of OH groups until P_{2000} adsorption. Also, the bending Fe-OH vibration at 751 cm^{-1} decreased more strongly with increasing adsorbed phosphate content due to the release of OH groups from the surface. It was concluded that OH groups released from the mineral surface formed H_2O molecules, which were located within the amorphous particle structure and protected from the exsiccation process after adsorption. The Fe-O and Fe-OH bands around 1400 cm^{-1} and 1350 cm^{-1} were affected during adsorption and disappeared from P_{1000} to P_{5000}, since the binding changed to Fe-O-P, which was reflected in a broad stretching vibration with a peak at 1102 cm^{-1}. A number of vibrations could not be observed; however, a lower symmetry than T_d for PO_4^{3-} can be concluded on the basis of the peak position. Compared to the ferrihydrite sample, the Fe-OH vibrations were shifted to lower wavelength, which indicated the influence of the hydrogen bonds on the peak position. For P_{1000}, a $FeHPO_4$, Fe_2HPO_4 or a $Fe_2H_2PO_4$ surface complex can be assumed according to the minor changes observed for the OH band. The OH band shift from 3433 cm^{-1} to 3467 cm^{-1} suggested the adsorption of covalently bonded (Shirodkar *et al.,* 1990) as well as hydrogen-bonded phosphate complexes. The amount of hydrogen-bonded phosphate seemed to be higher than in the ferrihydrite samples. The residual Fe-O and Fe-OH bands at 1401 cm^{-1} and 1352 cm^{-1} showed that not all possible surface sites were occupied during adsorption. With increasing phosphate adsorption, the OH peak decreased continuously, indicating the loss of free and hydrogen-bonded OH groups, and hence, the formation of a $FePO_4$ (C_{3v}), Fe_2PO_4 (C_{2v}) or Fe_2HPO_4 (C_1) surface complex (Tejedor-Tejedor and Anderson, 1990). Even if no phosphate vibrations were detected, the Fe-O-P peak was observed at slightly higher wavelength, which revealed the formation of a complex with symmetry lower than C_{2v}. Thereby, Fe_2HPO_4 or Fe_2PO_4 were possible binding motifs, which can also be affected by additional molecular environmental conditions, lowering the symmetry. This can occur in

hydrogen bonds to neighboring hydroxyl groups or hydrogen bonds to outer-sphere complexes. Since no maximum adsorption capacity was reached in the kinetic experiments, the still-available OH groups can be related to free Fe-OH binding sites or the adsorbed protonated phosphate species.

In contrast, for the pure amorphous Al-hydroxide, the flattening of the OH peak and the stronger appearance of integrated vibrations in the Al-hydroxide samples showed the increase of hydrogen-bonded molecules and the simultaneous decrease of free OH groups. While the Fe-hydroxide showed one distinctive band beside the P-O peak at a wavelength below 1000 cm^{-1}, the Al-hydroxides had two vibrations. However, a conclusion regarding the symmetry of the adsorbed complex cannot be drawn due to the mineral-specific absorption bands, but if the OH stretching vibration is taken into account, the formation of $AlHPO_4$, AlH_2PO_4 or Al_2HPO_4 could be assumed. With increasing phosphate content, the OH peak increased strongly, indicating the preferred formation of AlH_2PO_4 (Zheng *et al.,* 2012) and either the binding on neighboring Al ions by hydrogen bonds or the development of outer-sphere complexes. This was also suggested by the less-strong degeneration and slight shift of the Al-O and Al –OH vibrations in the range from 1460 cm^{-1} to 1350 cm^{-1}, leading to the conclusion that not all binding sites were affected by phosphate adsorption with increasing Al ratio, resulting in a low probability of a multidentate binding mechanism, and a change of the molecular environment by formation of hydrogen bonds.

While 10 Fe:1 Al-hydroxide mixtures indicated the predominant formation of precipitated and hydrogen-bonded phosphates, the 5 Fe:1 Al-hydroxide mixtures showed a distinctive inner-sphere complexation, developing a nonprotonated mineral-phosphate complex. The 1 Fe:1 Al-hydroxide mixture showed an observable separation of the integrated OH stretching peaks, which showed that especially the free OH groups were influenced during adsorption, while a shift to a higher or lower amount of hydrogen bonds was not observed. The 1 Fe:5 Al- and 1 Fe:10 Al-

hydroxide samples showed a similar complexation mechanism for P_{1000} and P_{5000}, but a different spectral response for P_{2000}. Kinetic experiments involved a similar amount of phosphate adsorption for both mixtures, certainly higher compared to pure Al-hydroxide. Anderson and Benjamin (1990) assumed a dominant type of particle interaction and its influence on surface reactions for binary hydroxide systems. However, the fluctuating intensity of the OH vibration of the mixed hydroxides could reveal the simultaneous presence of phosphate binding mechanisms, linked either to amorphous Fe-hydroxide or Al-hydroxide, overlaid in the FT-IR spectra and hence, not able to be clearly analyzed by the spectroscopic experiments performed.

2.5.2 Kinetics of adsorption and desorption

One aspect influencing the phosphate adsorption behavior in soil systems is the impact of dissolved ions. Amongst others, Ca^{2+} is an important cation in the solution phase of natural systems. Therefore, it is necessary to work with an electrolyte background solution during sorption experiments, and it was found that an increase of ionic strength of the background electrolyte solution resulted in an increase of phosphate adsorption due to the addition of negative charge, which decreases the electrostatic repulsive force and induces Ca^{2+} adsorption, leading to a more positive charge on the surface (Antelo *et al.,* 2005; Talebi Atouei *et al.,* 2016). Arai and Sparks (2001) determined this effect for Na^{+}, and the formation of outer-sphere complexes by electrostatic interaction. If the adsorbed phosphate ions were bound by forming outer-sphere complexes, the symmetry reduction was caused only by protonation and not by phosphate binding onto the mineral surface. The vibrational bands should appear at similar wavelengths for the dominant phosphate species at a given pH (Arai and Sparks, 2001).

According to the adsorption capacities for gibbsite and ferrihydrite given in the literature, the actual amount of adsorbed phosphate, in particular for ferrihydrite, was larger than earlier reported values (Borggaard *et al.,* 2005; van Emmerik *et al.,* 2007; van Riemsdijk and Lyklema, 1980). Especially for the amorphous Al-hydroxide, the formation of outer-sphere complexes was assumed due to the high phosphate adsorption compared to the low specific reactive surface area. As already mentioned, the observed infrared spectra with the averaged vibrational bands of phosphate (Kubicki *et al.,* 2012) and the absorption bands of the minerals themselves prevent an accurate description of the symmetry and protonation mode of surface complexes. However, the shift of the P-O vibration to higher wavelength and the sharp band profile as well as the pH of 6 indicated the formation of H_2PO_4 outer-sphere complexes. An increasing phosphate concentration strengthened this effect, and led to a higher ratio of adsorbed phosphate compared to initial phosphate concentration, as shown in the adsorption measurements. If $H_2PO_4^-$ was bound by weak hydrogen-bonded outer-sphere complexes, desorption experiments should lead to a higher phosphate release compared to stronger covalent inner-sphere binding. Since the FT-IR spectra of Fe-hydroxide indicated a higher amount of hydrogen bonds both before and during adsorption, the phosphate desorption rate should be higher compared to Al-hydroxide. The opposite was observed, leading to the conclusion that during adsorption, as a result of the weakly associated FeO(OH) molecules, $FePO_4$ precipitate was formed, which was bound by outer-sphere hydrogen bonds and not dissolved during desorption due to the low solubility (Blume *et al.,* 2010; Scheffer *et al.,* 2010). The slightly higher desorption rate (0.14 %) of pure Fe-hydroxide compared to Fe-Al-hydroxide mixtures with predominant Fe (0 %) showed a slightly higher amount of desorbable and hence, less stably bound phosphate on pure Fe-hydroxide samples. This indicated the binding of phosphate on already precipitated $FePO_4$ due to fewer available Fe-OH reaction sites. With increasing Al content and decreasing Fe content in the Fe-Al-hydroxide mixtures, the lower

amount of Fe contributed completely to the precipitation of adsorbed phosphate, and the contribution of phosphate bound to Al during desorption can either be neglected or was superimposed by the precipitated $FePO_4$. With high Al ratios, desorption increased, which indicated weaker phosphate bonding of both inner-sphere and outer-sphere types, respectively. Ferrihydrite had a slightly higher desorption rate compared to amorphous Fe-hydroxide, which can be explained by the more rigid structure of the former and a lower extent of precipitation.

The surface speciation of phosphate on goethite at near-neutral pH was reported as bidentate (Rahnemaie *et al.,* 2007), and assuming that no other binding motif was present, the following conclusions for gibbsite were made: phosphate adsorption on gibbsite could not be weaker than bidentate due to having desorption rates in the same range as goethite. The slightly lower phosphate release can be explained by $AlPO_4$ precipitation between gibbsite layers. Nevertheless, weakly bound outer-sphere complexes that can readily desorb from the mineral surface represented a higher amount of total desorbed phosphate compared to strong bound inner-sphere complexation.

2.5.3 Crystallinity

The OH groups in the layers of gibbsite showed only minor and nonpermanent changes in intensity, so it was concluded that no phosphate was bound within the crystal structure. The amorphous Al-hydroxides were characterized by a less-rigid crystal structure, which led to better accessibility of reactive sites within the particle structure and hence, a higher amount of adsorbed phosphate relative to the reactive surface. Also, the poorly crystalline character of ferrihydrite enabled the migration of phosphate into the mineral particles, where phosphate started to form surface complexes as shown by Willett *et al.* (1988) and described by Parfitt (1989). This was

observed with the increase of molecular water within the particle structure, and not affected by desiccation as well. Hence, the amorphous structure can affect the extent of precipitation by better accessibility of both surface and structural reactive binding sites, respectively.

2.6 Conclusions

For gibbsite, phosphate adsorption occurred mainly on the surface of the particles, while in-plane reaction sites were not affected, and with increasing reaction time, the formation of $AlHPO_4$ and Al_2HPO_4 can be assumed. Due to an increase of adsorption during long-term reaction times, the precipitation of $AlPO_4$ on the Al_2OH face sites or hydrogen-bonded outer-sphere complexes were concluded. The differentiation between surface complexes and precipitation could not be well evaluated solely by consideration of the P-O peak, and the absorption bands of the minerals themselves prevented an accurate description of the symmetry and protonation mode of the surface complex, so that the lower symmetry of the adsorbed phosphate complex can be interpreted according the formation of outer-sphere complexes. For ferrihydrite, the initial appearance of a $FeHPO_4$ surface complex, conversion to a $FeHPO_4$ or Fe_2PO_4 complex and the precipitation of $FePO_4$ with longer equilibration time were described. Fe_2HPO_4 or a Fe_2PO_4 surface complex were deduced for Fe-hydroxides, and an AlH_2PO_4 surface complex for Al-hydroxide, and both revealed either hydrogen bonds to neighboring hydroxyl groups or hydrogen bonds to outer-sphere complexes. Gibbsite and pure Al-hydroxide had the highest phosphate release capacities, but were slightly lower compared to goethite as reference. The Fe:Al-hydroxide mixtures with high Al ratios showed a substantially lower phosphate desorption rate compared to gibbsite or pure Al-hydroxide, while ferrihydrite and the Fe:Al-hydroxide mixtures with high Fe ratios had almost no or a minor desorption rate. These results

led to the conclusion that even a higher quantity of weak hydrogen bonds did not enhance desorption and as a result of the weakly associated amorphous FeO(OH) molecules, and $FePO_4$ precipitate was formed, which was bound by outer-sphere hydrogen bonds and not dissolved during desorption due to its low solubility. Fe:Al-hydroxide mixtures indicated the precipitation of $FePO_4$ as well which, because of the lower Fe amount, completely contributed to precipitation. With high Al ratios, desorption increased, indicating weaker phosphate binding of both inner-sphere and outer-sphere complexes and hence, either no or a minor quantity of precipitation. The less-rigid structure of amorphous hydroxides led to the higher accessibility of reactive sites within the particle structure and a higher amount of migrated and adsorbed phosphate relative to the reactive surface area. Ferrihydrite had a slightly higher desorption rate compared to amorphous Fe-hydroxide, which can be explained by the more-rigid structure of the former and a lower extent of precipitation. Phosphate binding on gibbsite could not be weaker than bidentate due to having desorption rates in the same range as goethite. Further investigations should deal with the questions of how different inorganic and organic desorption solutions influence phosphate binding during desorption, and if they can affect the mobilization of precipitated phosphate.

3 Crystallization of single and binary iron- and aluminum hydroxides affect phosphorus desorption [2]

3.1 Abstract

In acidic soils, phosphorus availability is affected by its strong affinity for mineral surfaces, especially Fe- and Al-hydroxides. Plant roots have developed adaptive strategies to enhance the availability of phosphorus, including producing and exuding low-molecular-weight organic acids with a high affinity for phosphorus that competes with high-molecular-weight organic ligands formed during humification and mineralization. The aim of this study was to characterize the kinetics and mechanism of phosphorus desorption from Fe- and Al-hydroxides of variable crystallinity, as well as binary Fe:Al-hydroxide mixtures. Long-term desorption experiments (56 days) were conducted with $CaCl_2$, $CaSO_4$, citric acid, and humic acid as competitive sorptives. $CaCl_2$ and $CaSO_4$ were selected as general inorganic sorptives and citric and humic acids were selected as organic ligands produced by organisms in the rhizosphere or following humification. The cumulative phosphorus desorption increased following the order $CaCl_2$ < $CaSO_4$ < humic acid < citric acid. Amorphous ferrihydrite and Fe-rich Fe:Al-hydroxides exhibited much less desorption when exposed to inorganic solutions than the crystalline and Al-rich Fe:Al-hydroxide mixtures. Models of the desorption data suggest phosphorus desorption with citric acid is diffusion-controlled for ferrihydrite and Fe-rich amorphous Fe:Al-hydroxides. When humic acid was the sorptive, metal-organic complexes accumulated in the solution. The

[2] Published in Journal of Plant Nutrition and Soil Science
Wiley-VCH
Gypser, S., Schütze, E., Freese, D. (2019): Crystallization of single and binary iron- and aluminum hydroxides affect phosphorus desorption. J. Plant Nutr. Soil Sci. **182**, 741–750.
DOI: 10.1002/jpln.201700543.

results suggest organic compounds, especially citric acid, are more important for liberating phosphorus from Fe- and Al-minerals than inorganic ions present in the soil solution.

Keywords: $CaCl_2$, $CaSO_4$, Humic acid, Citric acid, Dissolution, Complexation

3.2 Introduction

Non-point-sources from agricultural soils are still mainly responsible for causing eutrophication of rivers and lakes by over-enrichment with phosphorus (Carpenter *et al.,* 1998). Only small amounts of applied phosphorus fertilizers remain available to plants (Sample *et al,.*1980). In acidic soils, phosphorus availability is affected by adsorption, desorption and precipitation reactions on soil particle surfaces. Due to the fundamental role of phosphorus in the environment, phosphorus reactions in soils and on model substances have been intensively studied (Arai and Sparks, 2001; Barrow, 1983; Hinsinger, 2001; Torrent *et al.,* 1992).

Plants have developed a range of adaptive strategies to enhance the availability of phosphorus from soils, which includes the exudation of low-molecular-weight organic acids (Bais *et al.,*2006; Chen *et al.,* 2004; Jones, 1998). Among these organic acids, citric acid is often detected at a higher concentration in the rhizosphere and is described as more effective than other organic acids in mobilizing inorganic phosphorus (Johnson and Loeppert, 2006; Kpomblekou-A and Tabatabai, 2003). Beside low-molecular-weight organic acids, such as citric, malic or oxalic acid, high-molecular-weight organic compounds formed during humification and mineralization, such as humic or fulvic acid, play an important role in soil environment and phosphorus mobilization. Various studies have investigated the influence of humic substances on phosphorus

in soils and found they reduced phosphorus fixation and increased phosphorus availability to plants (e.g. Hua *et al.,* 2008; Jones, 1998).

The specific properties of minerals and hydroxides influence their characteristic behavior in soil systems, such as the specific surface area or degree of crystallinity. Nevertheless, the influence of the mineral crystallinity on soil sorption behavior is not well explained. Hydroxides can have different crystallinity such as completely crystallized minerals or fine crystalline minerals with an amorphous basic structure (short-range-ordered), affecting phosphorus sorption processes (Goldberg and Sposito, 2008; Gypser *et al.,* 2018; Parfitt, 1979) and hence, phosphorus release and mobilization. In the following, the investigated hydroxides are only classified into "crystalline" and "amorphous", which is oriented to the phase analysis by X-ray diffraction. Therefore, the aim of this study was to characterize the kinetics and mechanism of phosphorus desorption on crystalline and amorphous single Fe- and Al-hydroxides and on binary Fe:Al-hydroxide systems. Long-term desorption experiments were performed in order out to measure the desorption kinetics of phosphorus on various mineral surfaces and detect fast (easily bound) and slow (strongly bound) releasable phosphorus over time. As desorption solutions, $CaCl_2$ and $CaSO_4$ were chosen to represent the ionic strength of the soil solution and humic and citric acid are model organic ligands representing humic substances and plant exudates, respectively. Goethite and gibbsite were used as model substances of crystalline Fe- and Al-hydroxides, whereas synthesized Fe- and Al-hydroxide mixtures represented the amorphous fraction appearing in soils. Ferrihydrite was used as a transitional Fe-hydroxide with a predominant amorphous character, bridging between the initial amorphous hydroxide structure and crystalline goethite during pedogenesis.

3.3 Materials and methods

3.3.1 Fe- and Al-hydroxides

The synthetic and commercially available adsorbents investigated in this study were goethite (99 %, Alfa Aesar, Haverhill, Massachusetts, USA) and gibbsite (Merck Millipore, Merck KGaA, Darmstadt, Germany), which were of analytical grade. A 2-line-ferrihydrite was prepared according to (Schwertmann and Cornell, 2008), at which a 1 M KOH was added to 500 ml of a 0.2 M $Fe(NO_3)_3 \cdot 9\ H_2O$-solution, until a pH of 7.5 was reached. The developed precipitate was centrifuged and washed for 5 min at 12134 × g (Avanti J-25 Centrifuge, Beckman Coulter, Brea, USA), subsequently frozen, freeze-dried, and stored in a desiccator. The mixed iron-aluminum-hydroxides (Fe:Al-hydroxides) were prepared as described by (Sujana *et al.,* 2009), by mixing 0.1 M $Fe(NO_3)_3 \cdot 9\ H_2O$ and 0,1 M $Al(NO_3)_3 \cdot 9\ H_2O$ were mixed in molar ratios of 1:0, 10:1, 5:1. 1:1, 1:5, 1:10 and 0:1, and brought to a pH of 6 with 5 M KOH. After equilibration for 1 h, the precipitate was centrifuged for 5 min at 12134 × g, washed several times with ultrapure water to remove soluble salts, dried at 60°C and ground into a powder. All chemicals used for the preparation of adsorbents were of analytical grade and the solutions were prepared with ultrapure water.

Elemental composition of the adsorbents was verified using SEM-EDX, scanning electron microscopy (DSM 962, Zeiss, Oberkochen, Germany) with energy dispersive X-ray spectroscopy (X-Max 50 mm² with INCA, Oxford Instruments, Abingdon, Great Britain). The final resulting mineral phase of pure $Al(OH)_3$ and FeO(OH) for the amorphous hydroxides was identified. Determination of the adsorbent crystallization as well as amorphous structures was performed by X-ray diffraction (XRD), using an Empyrean powder diffractometer (PANalytical , Almelo, Netherlands), with a theta-theta-goniometer, Cu-Kα radiation (λ = 0.15418 nm), automatic

divergent and anti-scatter slits and a PIXcel3D detector. Diffraction data were recorded from 4.6° to 84.9° 2Θ with a step-size of 0.0131, a step time of 58.4 s, and generator settings of 40 kV and 40 mA (for details see Gypser *et al.,* 2018).

3.3.2 Desorption experiments

Earlier adsorption experiments have shown varying characteristics regarding the centrifugation and filtration behavior of the considered hydroxides. Hence, prior to the desorption experiments, silica sand was coated with the hydroxides according to (Scheidegger *et al.,* 1993), to ensure a similar sample treatment (e.g. centrifugation times and revolutions). The silica sand used (particle size 0.2 – 0.8 mm, Merck Millipore) was finely granulated, washed and calcined. 10 g of the hydroxide was combined with a 0.01 M $NaNO_3$-solution, adjusted to pH 6, resulting in a final volume of 100 ml. 100 g of pure silica sand was added to the suspension before it was shaken for 24 h at room temperature. After the coated sand had settled, the supernatant was decanted and the material was washed three to five times with the 0.01 M $NaNO_3$-solution at pH 6 to achieve a clear supernatant. In a final step it was washed again with ultrapure water to remove hydroxide traces and soluble salts. The coated silica sand was oven dried at 60°C for 48 h following the description from (Freese *et al.,* 1999). To achieve a complete mixing and, thus, to maximize the coating of the silica sand with the hydroxides, two circuits of the coating procedure were performed, one for the experiments with inorganic $CaCl_2$ and $CaSO_4$ and one for organic humic acid and citric acid desorption solutions. The extent of the coating of the silica sand was analyzed by complete dissolution of coatings and determination of Fe and Al by using ICP-AES (Unicam iCAP6000 Duo, Thermo Fisher Scientific, Waltham, Massachusetts, USA). Therefore, 1 g of the coated silica sand sample was diluted into 50 ml PE-bottles and dissolved by adding

1 ml of concentrated H_2SO_4, followed by a 30 min ultrasonic treatment. The suspension was filtered and filled up with deionized water to a final volume of 50 ml.

To preload the silica-hydroxide mixtures with phosphorus, 200 ml of a 2 mM KH_2PO_4 solution and a 0.01 M $CaCl_2$ background solution were added to the mixtures. After shaking horizontally for 24 h at 150 motions min^{-1}, the hydroxides were centrifuged for 5 min at 929 × g (Allegra X-12R Benchtop Centrifuge, Beckman Coulter). The supernatant was filtrated with P-poor Whatman 512 1/1 filters and the solid matter was immediately diluted with 50 ml of ultrapure water to remove not adsorbed phosphorus. It was centrifuged again and the supernatant was added to a mixed sample. The extent of adsorbed phosphorus was determined according to the same method as used for the extent of the coating.

This study is focused on the pH conditions of agronomic soils, which range most frequently between pH 5.0 and 6.8 where phosphate minerals are very soluble (Blume *et al.,* 2010; Johnson *et al.,* 2002; Scheffer *et al.,* 2010). Therefore, a pH of 6 was set for desorption to prevent precipitation during the experiments. Desorption experiments were conducted with organic (humic acid, citric acid) and inorganic ($CaCl_2$, $CaSO_4$) solutions, adjusted to a pH of 6 by addition of either KOH or HNO_3. To reach this, 2.5 g of the coated silica sand was placed in 100 ml PE-bottles and 50 ml of 0.01 M $CaCl_2$ or 0.01 M $CaSO_4$ were added to each bottle. 5 g of the coated silica sand was used for desorption with 50 ml of 2 g l^{-1} humic acid and citric acid (Alfa Aesar) due to the higher desorption capacity of low molecular organic acids (Gerke, 1994). A concentration of 2 g l^{-1} for both humic and citric acid was selected to provide a concentration similar to that of the $CaCl_2$ and $CaSO_4$. Due to its complex composition, no molecular weight data are available for humic acid. Therefore, the sample weight of approximately 1.9 g l^{-1} for citric acid was calculated, which corresponds to a concentration of 0.01 M, and hence, a concentration of 2 g l^{-1} was used for the organic acids. This concentration is higher than the

values commonly measured in rhizosphere and soil (0 – 50 µmol) (Guppy *et al.,* 2005; Strobel, 2001).

For the desorption experiments, treatment solutions were added to the samples (4 replicates), shaken at 150 motions min^{-1}, and centrifuged for 15 min at 2091 × g. After this, the supernatant was filtered for measurement of phosphorus. Next, 50 ml of fresh desorption solution was added to the samples. During the first 24 h the samples were shaken continuously. This was only interrupted for the sampling after 2 and 6 h. Afterwards the samples were shaken once a week for 15 min. The hydroxides were adjusted to pH 6 during the coating procedure and then again after the addition of the organic and inorganic solutions. The pH was controlled at regular intervals and remained stable. The amount of desorbed phosphorus was determined by subtracting the measured desorbed phosphorus content in the solution from the initial adsorbed phosphorus content. Microbial activity and contaminations were inhibited by acid washing of all materials involved with 10 % HNO_3 prior to experiments. For the desorption treatments with organic acids, the C_{Total} content of the organic solutions was measured with a TOC-Analyzer (TOC-Vcph and TOC5000, Shimadzu, Kyoto, Japan) before desorption and after eight weeks of reaction time.

3.3.3 Equations and mechanisms of desorption kinetics

The cumulative phosphorus desorption depending on time was calculated for each hydroxide and desorption solution and different kinetic models were fitted to the data. Kinetic analyses were performed with the objective to fit the experimental data to a proper kinetic model and to study the influence of different desorption solutions on desorption kinetics from selected

contrasting phosphorus adsorbents. The following models and their corresponding linear equations were used:

Elovich $$Q_t = \frac{1}{\beta}\ln(\alpha\beta) + \frac{1}{\beta}\ln t \quad (1)$$

Exponential $$\ln Q_t = \ln a + b \ln t \quad (2)$$

Parabolic $$Q_t = Q_0 + k_P\, t^{1/2} \quad (3)$$

where Q_t is the amount of desorbed phosphorus at time t in mg P mg^{-1} Hydroxide, Q_0 is the initial phosphorus concentration in the solution, α and a are the initial phosphorus desorption constants in mg P mg^{-1} Hydroxide min^{-1}, β and b are the desorption rate constants in mg P mg^{-1} Hydroxide min^{-1}, and k_P is the diffusion rate constant. The selected models were applied to obtain kinetic parameters that could provide information about differences of time-dependent phosphorus desorption. All models were tested by using least-square regression analysis to determine their applicability on the phosphorus desorption kinetics of the investigated Fe- and Al-hydroxides. Statistical analyses were performed with SigmaPlot (Systat Software Inc., San Jose, California, USA).

3.4 Results

3.4.1 Characterization of hydroxides

The elemental composition of the adsorbents (except for 1 Fe:5 Al and 5 Fe:1 Al), were determined using SEM-EDX. The numbers of washing steps affect the amount of hydroxide coated on the silica sand and, thus, the initially adsorbed phosphorus concentration. Therefore,

the hydroxides to be treated with inorganic reaction solutions have concentrations of Fe, Al and, initial P which differ from the hydroxides to be treated with organic reaction solutions (Tab. 5).

Tab. 5. Elemental composition (SEM-EDX) of the pure minerals and amount of Fe, Al and P of the used Fe-Al-hydroxides coated on silica sand.

Hydroxide	**SEM-EDX**			**Coating****			
	Elemental composition			**Fe- and Al- content on coated silica sand**		**Initial P content on hydroxide**	
	Fe	Al	O	Inorganic	Organic	Inorganic	Organic
	wt%			*mg g^{-1} SiO_2*		*mg mg^{-1} Hydroxide*	
Goethite	69.3	0.00	30.1	0.31	0.41	0.14	1.15
Gibbsite	0.00	36.2	62.0	0.15	0.60	0.46	0.91
Ferrihydrite	68.6	0.00	25.1	39.74	51.05	0.01	0.02
1 Fe : 0 Al	55.35	0.00	35.89	43.84	19.29	0.01	0.03
10 Fe : 1 Al	44.88	2.40	43.16	35.26	19.64	0.02	0.04
5 Fe : 1 Al	-	-	-	32.44	39.71	0.02	0.02
1 Fe : 1 Al	30.71	15.81	43.71	24.73	19.35	0.01	0.04
1 Fe : 5 Al	-	-	-	2.16	3.50	0.09	0.28
1 Fe : 10 Al	11.62	28.88	41.48	3.52	6.85	0.11	0.11
0 Fe : 1 Al	0.00	34.81	59.89	0.09	2.28	0.66	0.46

3.4.2 Efficiency of desorption

After eight weeks of desorption time, the samples treated with citric acid had the highest phosphorus desorption kinetics. The efficiency of the desorption solutions generated the following sequence: $CaCl_2$ < $CaSO_4$ < humic acid < citric acid. The crystalline Fe-hydroxide goethite had a higher phosphorus desorption than gibbsite or the amorphous Fe:Al-hydroxide

mixtures for all considered desorption solutions (Tab. 6). While the lowest phosphorus desorption extent of 48 % of the initial phosphorus loading was measured from $CaCl_2$, the citric acid treatment increased the phosphorus desorption extent up to 91 %. Slightly lower desorption kinetics were detected for gibbsite and amorphous Al-hydroxide with 43 % and 38 % phosphorus desorption extent, respectively from $CaCl_2$, and 83 % and 89 % extent of phosphorus desorption, respectively, from citric acid. The amorphous Fe:Al-hydroxide mixtures showed the lowest phosphorus desorption, since the extent of desorption decreased with a decreasing predominant Fe content.

Tab. 6. Total P desorption after eight weeks of desorption time by using desorption solutions $CaCl_2$, $CaSO_4$, humic acid and citric acid at pH 6.

Hydroxide	**$CaCl_2$**	**$CaSO_4$**	**Humic Acid**	**Citric Acid**
	*Desorbed P %**			
Goethite	47.9 ± 0.5	57.4 ± 1.4	87.2 ± 18.1	90.5 ± 0.0
Gibbsite	42.6 ± 0.8	45.5 ± 0.9	69.3 ± 2.9	82.8 ± 0.4
Ferrihydrite	0.3 ± 0.1	0.4 ± 0.0	1.5 ± 0.0	8.6 ± 0.2
1 Fe : 0 Al	0.1 ± 0.0	0.3 ± 0.0	5.1 ± 0.7	48.8 ± 5.2
10 Fe : 1 Al	0.0 ± 0.0	0.6 ± 0.0	3.8 ± 0.6	27.6 ± 1.6
5 Fe : 1 Al	0.0 ± 0.0	0.7 ± 0.0	0.3 ± 0.0	8.2 ± 0.4
1 Fe : 1 Al	0.1 ± 0.1	1.4 ± 0.1	1.3 ± 0.0	6.7 ± 0.0
1 Fe : 5 Al	5.5 ± 0.5	8.9 ± 0.4	28.4 ± 1.5	75.9 ± 1.8
1 Fe : 10 Al	1.5 ± 0.0	3.3 ± 0.0	4.7 ± 0.2	54.2 ± 7.3
0 Fe : 1 Al	38.2 ± 1.2	44.6 ± 0.6	35.8 ± 2.8	89.1 ± 0.0

***** % of the initial adsorbed P, n = 4, Given are mean and standard deviation

From the $CaCl_2$ treatment, the mixtures from 1 Fe:0 Al to 1 Fe:1 Al with a predominant Fe content exhibited little to no desorption, with aqueous phosphorus concentrations often below detection limit. However, the extent of phosphorus desorption increased with an increasing Al content. The 1 Fe:10 Al mixture showed lower desorption than 1 Fe:5 Al and 0 Fe:1 Al.

Compared to $CaCl_2$, desorption from $CaSO_4$ increased slightly for the investigated hydroxides. The humic acid treatment clearly increased desorption and the extent amounted to 87 % for goethite, 69 % for gibbsite and to 5 %, 4 % and 28 % for 1 Fe :0 Al, 10 Fe:1 Al, and 1 Fe:5 Al, respectively. The ferrihydrite and 1 Fe: 10 Al samples exhibited a slight desorption extent, amounting to 2 and 5 %, respectively. However, the humic acid treatment with the 5 Fe:1 Al, 1 Fe:1 Al and 0 Fe:1 Al hydroxides exhibited a lower desorption extent than the $CaSO_4$ treatment.

3.4.3 Kinetics of phosphorus desorption

During the first 24 h, fast initial phosphorus desorption took place, succeeded by a slower stage (Fig. 12). If the total desorbed P is evaluated in terms of a faster and a slower stage, most samples released a greater amount of phosphorus in the first 48 h, ranging between 63 % and 100 % from the $CaCl_2$ treatment and between 57 % and 81 % from $CaSO_4$ (Fig. 13). Only ferrihydrite, 1 Fe:0 Al, and 10 Fe:1 Al showed a lower extent of phosphorus desorption, between 45 % and 53 % from the $CaCl_2$ treatment. Also, the extent of desorbed phosphorus from humic acid was the highest within the first 48 h for all hydroxides, from 57 % to 100 %. For desorption with citric acid, these kinetics were only observed with goethite, gibbsite, 1 Fe: 10 Al and 0 Fe: 1 Al. In this treatment, more phosphorus was desorbed in the second, slower phase.

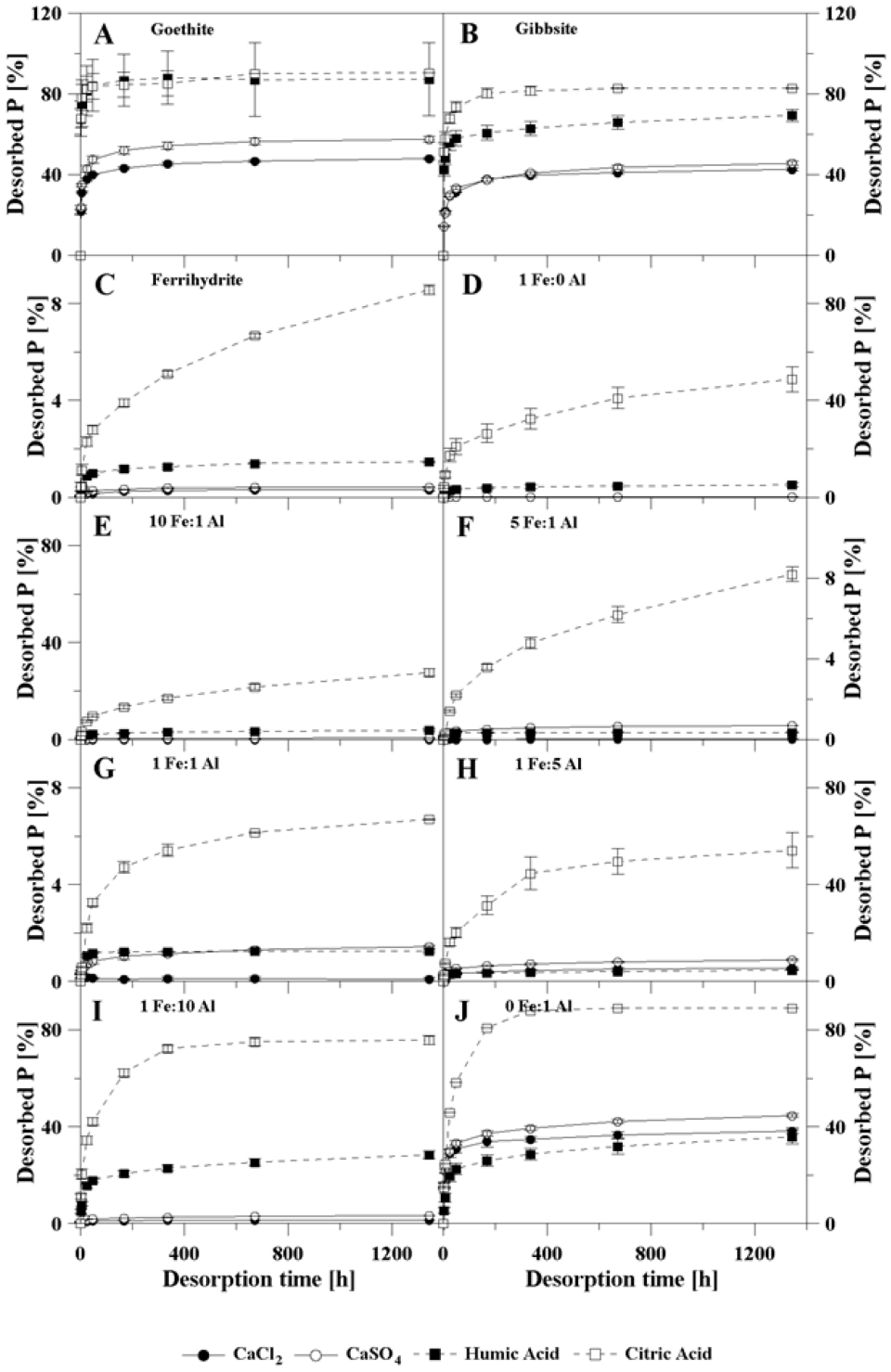

Fig. 12. Desorption kinetics of (A) goethite, (B) gibbsite, (C) ferrihydrite, (D) 1 Fe:0 Al, (E) 10 Fe:1 Al, (F) 5 Fe:1 Al, (G) 1 Fe:1 Al, (H) 1 Fe:5 Al, (I) 1 Fe:10 Al and (J) 0 Fe:1 Al by using desorption solutions $CaCl_2$, $CaSO_4$, humic acid and citric acid at pH 6.

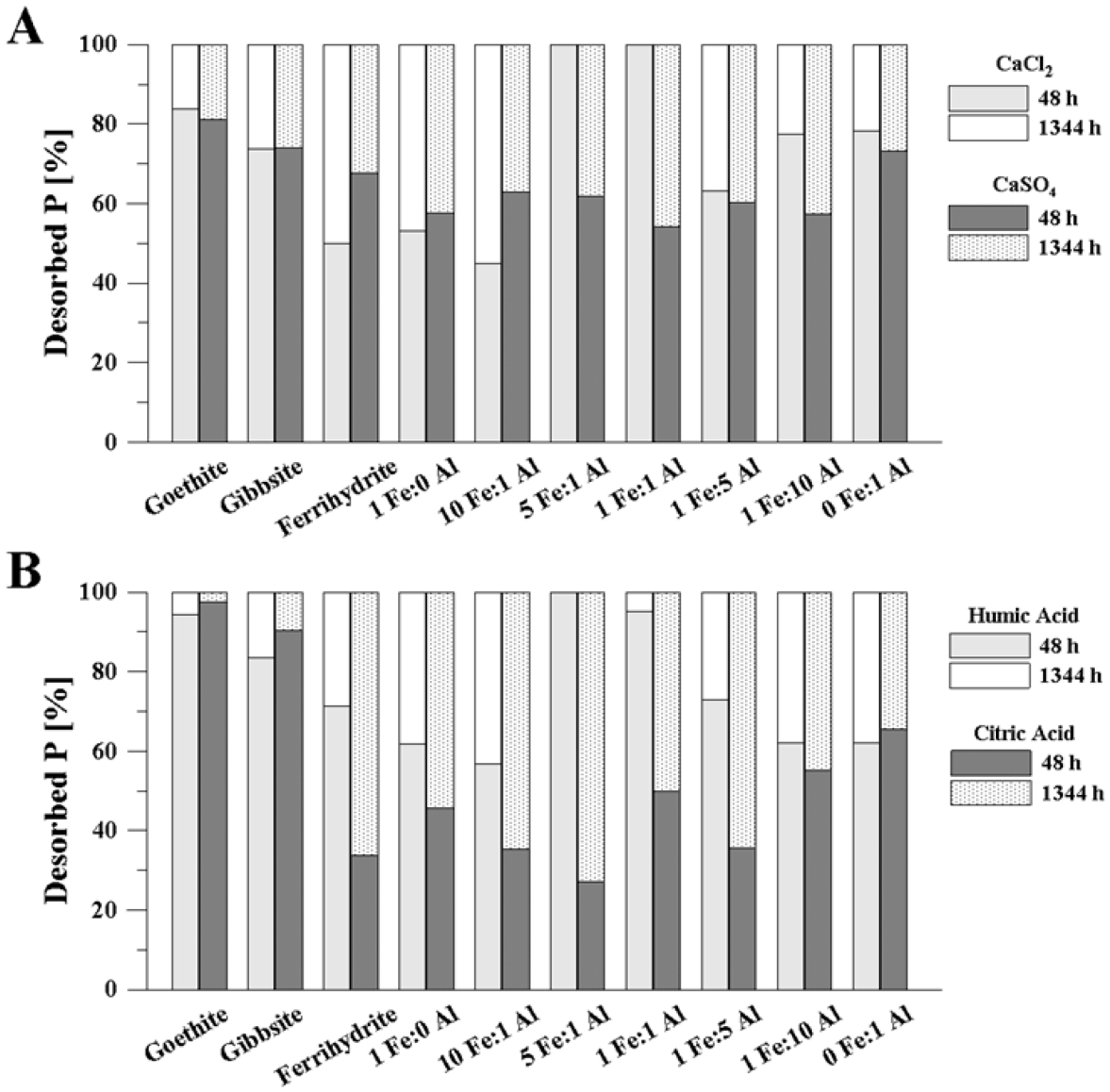

Fig. 13. Extent of desorbed P related to the extent of total desorbed P (= 100 %) after 48 h and 1344 h desorption time for (A) $CaCl_2$ and $CaSO_4$ and (B) humic acid and citric acid.

The coefficients of determination (R^2) for the applied kinetic models indicated that the kinetics of phosphorus desorption for all treatments fitted best with the Elovich equation (mean R^2 = 0.98 to 0.92), followed by the Exponential function (mean R^2 = 0.94 to 0.86), and the Parabolic function (mean R^2 = 0.84 to 0.68) (Tab. 7). The missing R^2 values for 10 Fe:1 Al,

5 Fe:1 Al, and 1 Fe:1 Al were due to the proximity of the desorbed phosphorus concentration to the detection limit and the restricted applicability of the kinetic models in this concentration range. The Elovich and Exponential function equations were most suitable to describe the phosphorus kinetics and for this reason, the kinetic parameters obtained from both models were calculated (Tab. 7). The kinetic parameters obtained from Elovich showed the highest initial phosphorus desorption for goethite and 0 Fe:1 Al from the $CaCl_2$ and $CaSO_4$ treatments, while gibbsite had the highest values from the humic and citric acid treatments. The desorption rate constant over time revealed the highest desorption for goethite from the $CaCl_2$, $CaSO_4$ and citric acid treatment, and lower, but similar values for gibbsite and 0 Fe:1 Al. Desorption from humic acid showed 1/β in a similar range for goethite, gibbsite and 0 Fe:1 Al. In general, α and 1/β were very low for ferrihydrite and nearly all Fe:Al-hydroxides, except for 0 Fe:1 Al, due to the low amount of desorbed phosphorus.

The kinetic parameters obtained from the Exponential function showed the highest initial desorption for 0 Fe:1 Al from both $CaCl_2$, and $CaSO_4$ treatments, followed by gibbsite and goethite. A reversed sequence was observed for the humic and citric acid treatment. The desorption rate constant over time decreased for the amorphous Fe:Al-hydroxides with increasing Al content from the $CaCl_2$ and $CaSO_4$ treatments. In the humic acid treatment, the values of b decreased with a declining, but predominant Fe content, and increased with a predominant upsurge in Al content. Conversely, from the citric acid treatment, the desorption rate constant increased with a decreasing, but predominant Fe content, and decreased with an increasing, but predominant Al content. In general, the values of b were lower for the crystalline than for the amorphous hydroxides. Constant relationships between the kinetic parameters and the Fe or Al content of the hydroxides or desorption solutions were not observed.

Tab. 7. Coefficients of determination (R^2) and standard errors (S.E.) for the kinetic equations used to describe the kinetic release of P after 1344 h desorption time and the kinetic parameters of the selected Elovich and Exponential function equations for P desorption from $CaCl_2$, $CaSO_4$, humic acid and citric acid.

Hydroxide	Treatment	Elovich				Exponential				Parabolic	
		R^2	S.E.	α	$1/\beta$	R^2	S.E.	a	b	R^2	S.E.
Goethite	$CaCl_2$	0.96^{***}	0.00	2.66	0.01	0.92^{**}	0.08	0.03	0.11	0.68^{*}	0.01
	$CaSO_4$	0.95^{***}	0.00	0.95	0.01	0.88^{**}	0.11	0.04	0.13	0.66^{*}	0.01
	Humic	0.87^{**}	0.03	$5.9 \cdot 10^{8}$	0.03	0.85^{**}	0.04	0.80	0.04	0.52^{*}	0.06
	Citric	0.87^{**}	0.03	$8.0 \cdot 10^{8}$	0.03	0.85^{**}	0.04	0.81	0.04	0.64^{*}	0.05
Gibbsite	$CaCl_2$	0.97^{***}	0.01	0.48	0.02	0.91^{**}	0.13	0.07	0.16	0.71^{**}	0.03
	$CaSO_4$	0.98^{***}	0.01	0.32	0.02	0.92^{**}	0.12	0.07	0.17	0.75^{**}	0.03
	Humic	0.98^{***}	0.01	$8.9 \cdot 10^{3}$	0.03	0.96^{***}	0.03	0.39	0.07	0.79^{**}	0.04
	Citric	0.94^{***}	0.03	$8.5 \cdot 10^{2}$	0.05	0.92^{**}	0.05	0.47	0.08	0.64^{*}	0.07
Ferrihydrite	$CaCl_2$	0.98^{***}	0.00	$6.1 \cdot 10^{-6}$	$6.4 \cdot 10^{-6}$	0.93^{**}	0.22	$5.6 \cdot 10^{-6}$	0.32	0.82^{**}	0.00
	$CaSO_4$	0.99^{***}	0.00	$1.6 \cdot 10^{-5}$	$7.5 \cdot 10^{-6}$	0.93^{***}	0.17	$1.1 \cdot 10^{-5}$	0.25	0.78^{**}	0.00
	Humic	0.98^{***}	0.00	$1.3 \cdot 10^{-4}$	$3.6 \cdot 10^{-5}$	0.91^{**}	0.18	$6.8 \cdot 10^{-5}$	0.23	0.76^{**}	0.00
	Citric	0.93^{**}	0.00	$9.0 \cdot 10^{-5}$	$2.3 \cdot 10^{-4}$	0.96^{***}	0.20	$9.5 \cdot 10^{-5}$	0.42	0.98^{***}	0.00
1 Fe : 0 Al	$CaCl_2$	0.96^{***}	0.00	$1.6 \cdot 10^{-6}$	$2.5 \cdot 10^{-6}$	0.82^{**}	0.50	$1.1 \cdot 10^{-6}$	0.43	0.86^{**}	0.00
	$CaSO_4$	0.97^{***}	0.00	$7.8 \cdot 10^{-6}$	$4.6 \cdot 10^{-6}$	0.94^{***}	0.16	$6.3 \cdot 10^{-6}$	0.26	0.80^{**}	0.00
	Humic	0.98^{***}	0.00	$4.0 \cdot 10^{-4}$	$2.0 \cdot 10^{-4}$	0.89^{**}	0.23	$2.7 \cdot 10^{-4}$	0.27	0.76^{**}	0.00
	Citric	0.97^{***}	0.00	$1.3 \cdot 10^{-3}$	$2.0 \cdot 10^{-3}$	0.95^{***}	0.19	$1.4 \cdot 10^{-3}$	0.34	0.95^{***}	0.00
10 Fe : 1 Al	$CaCl_2$	-	-	-	-	-	-	-	-	-	-
	$CaSO_4$	0.99^{***}	0.00	$2.5 \cdot 10^{-5}$	$1.1 \cdot 10^{-5}$	0.90^{**}	0.21	$1.7 \cdot 10^{-5}$	0.26	0.77^{**}	0.00
	Humic	0.99^{***}	0.00	$3.0 \cdot 10^{-4}$	$1.9 \cdot 10^{-4}$	0.93^{**}	0.19	$2.4 \cdot 10^{-4}$	0.27	0.84^{**}	0.00
	Citric	0.94^{***}	0.00	$5.9 \cdot 10^{-4}$	$1.5 \cdot 10^{-3}$	0.96^{***}	0.21	$5.8 \cdot 10^{-4}$	0.43	0.97^{***}	0.00
5 Fe : 1 Al	$CaCl_2$	-	-	-	-	-	-	-	-	-	-
	$CaSO_4$	0.99^{***}	0.00	$2.5 \cdot 10^{-5}$	$1.5 \cdot 10^{-5}$	0.94^{***}	0.17	$2.0 \cdot 10^{-5}$	0.27	0.84^{**}	0.00
	Humic	0.72^{**}	0.00	$3.5 \cdot 10^{-4}$	$7.0 \cdot 10^{-6}$	0.71^{**}	0.26	$2.7 \cdot 10^{-5}$	0.16	0.38^{0}	0.00
	Citric	0.92^{**}	0.00	$5.4 \cdot 10^{-5}$	$2.4 \cdot 10^{-4}$	0.96^{***}	0.32	$2.8 \cdot 10^{-5}$	0.61	0.98^{***}	0.00
1 Fe : 1 Al	$CaCl_2$	-	-	-	-	-	-	-	-	-	-
	$CaSO_4$	0.99^{***}	0.00	$7.7 \cdot 10^{-5}$	$2.2 \cdot 10^{-5}$	0.98^{***}	0.08	$4.5 \cdot 10^{-5}$	0.21	0.87^{**}	0.00
	Humic	0.80^{**}	0.00	$8.7 \cdot 10^{-4}$	$6.1 \cdot 10^{-5}$	0.75^{**}	0.28	$1.7 \cdot 10^{-4}$	0.20	0.45^{0}	0.00
	Citric	0.99^{***}	0.00	$2.0 \cdot 10^{-4}$	$4.5 \cdot 10^{-4}$	0.91^{**}	0.38	$1.3 \cdot 10^{-4}$	0.48	0.84^{**}	0.00

Continued on next page

Hydroxide	Treatment	Elovich				Exponential				Parabolic	
		R^2	S.E.	α	$1/\beta$	R^2	S.E.	a	b	R^2	S.E.
1 Fe : 5 Al	$CaCl_2$	0.99^{***}	0.00	$3.4 \cdot 10^{-3}$	$5.1 \cdot 10^{-4}$	0.97^{***}	0.08	$1.3 \cdot 10^{-3}$	0.18	0.89^{**}	0.00
	$CaSO_4$	0.99^{***}	0.00	$4.8 \cdot 10^{-3}$	$8.3 \cdot 10^{-4}$	0.98^{***}	0.07	$2.1 \cdot 10^{-3}$	0.19	0.89^{**}	0.00
	Humic	0.99^{***}	0.00	0.02	0.01	0.91^{**}	0.19	0.02	0.25	0.80^{**}	0.01
	Citric	0.98^{***}	0.01	0.04	0.03	0.94^{***}	0.19	0.03	0.30	0.78^{**}	0.04
1 Fe : 10 Al	$CaCl_2$	0.96^{***}	0.00	$2.2 \cdot 10^{-3}$	$1.5 \cdot 10^{-3}$	0.88^{**}	0.14	$5.8 \cdot 10^{-4}$	0.15	0.74^{**}	0.00
	$CaSO_4$	0.98^{***}	0.00	$2.3 \cdot 10^{-3}$	$3.7 \cdot 10^{-4}$	0.99^{***}	0.05	$9.6 \cdot 10^{-4}$	0.18	0.93^{**}	0.00
	Humic	0.93^{***}	0.00	$2.4 \cdot 10^{-3}$	$5.8 \cdot 10^{-4}$	0.84^{**}	0.25	$1.1 \cdot 10^{-3}$	0.23	0.70^{**}	0.00
	Citric	0.97^{***}	0.00	$3.6 \cdot 10^{-3}$	0.01	0.95^{***}	0.25	$3.2 \cdot 10^{-3}$	0.44	0.90^{**}	0.01
0 Fe : 1 Al	$CaCl_2$	0.95^{***}	0.01	2.75	0.02	0.88^{**}	0.11	0.11	0.13	0.67^{*}	0.03
	$CaSO_4$	0.99^{***}	0.01	0.81	0.03	0.94^{***}	0.10	0.11	0.15	0.76^{**}	0.04
	Humic	0.99^{***}	0.01	0.05	0.02	0.89^{**}	0.22	0.03	0.26	0.80^{**}	0.02
	Citric	0.96^{***}	0.03	0.10	0.06	0.91^{**}	0.22	0.07	0.28	0.71^{**}	0.08

^{0} not significant at $p < 0.05$, *significant at $p < 0.05$, **significant at $p < 0.01$, ***significant at $p < 0.001$

3.4.4 Desorption mechanism of humic and citric acid

During the desorption procedure, a brownish gelatinous precipitate appeared in the sample solutions treated with humic acid. For this reason, C_{Total} was measured after eight weeks of desorption time, which decreased for all hydroxide samples in the humic acid treatment. From the citric acid treatment, C_{Total} fluctuated around the initial C content of the citric acid and no distinctive change in C_{Total} was observed (Fig. 14). Correlations between the initial phosphorus content, expressed in mg mg^{-1} hydroxide, desorbed phosphorus in mg l^{-1}, and desorbed phosphorus, in % and the loss of C_{Total} in mg l^{-1} from the desorption solution revealed no relationship. The amount of Fe or Al in the desorption samples also indicated no relation to the loss of C_{Total}.

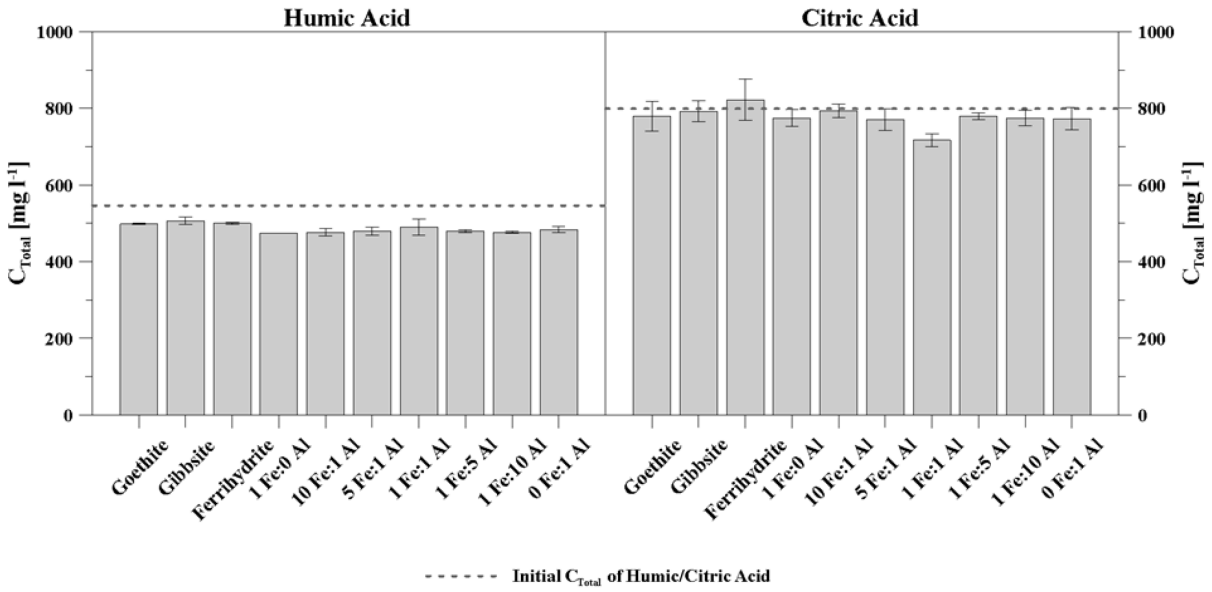

Fig. 14. C_{Total} in mg l^{-1} in the desorption solutions humic acid and citric acid after eight weeks of desorption time (n = 2).

3.5 Discussion

3.5.1 Efficiency of desorption

The organic acids desorbed more phosphorus than the inorganic background solutions, at which point the citric acid had the highest phosphorus desorption capability in the sequence $CaCl_2$ < $CaSO_4$ < humic acid < citric acid. This was supported by findings of prior studies, which measured a higher phosphorus desorption from Fe- and Al-phosphates by the use of citric acid than other organic acids (Harrold and Tabatabai, 2006; Lazo *et al.,* 2017; Wei *et al.,* 2010; Xu *et al.,* 2004). However, the efficiency of all desorption solutions investigated in this study showed differences between crystalline and amorphous hydroxides. The amorphous ferrihydrite and Fe:Al-hydroxides dominated by Fe released very little phosphorus in the $CaCl_2$ solutions. The slightly higher release of phosphorus from $CaSO_4$ could be explained by the higher affinity of

SO_4^{2-} to adsorb on the hydroxide surface than Cl^-. Nevertheless, due to the higher valence and ionic radius of PO_4^{3-} and the higher affinity for binding on the hydroxide surface (Blume *et al.,* 2010; Scheffer *et al.,* 2010), $CaCl_2$ and $CaSO_4$ were regarded as weak desorption solutions. The crystalline goethite, gibbsite, and the amorphous Fe:Al-hydroxides with a predominant Al content, on the other hand, had distinctively higher cumulative phosphorus release from $CaCl_2$ and $CaSO_4$, ranging between 38 % and 57 % of desorbed phosphorus after eight weeks of desorption. This suggests a less stable phosphorus binding on the crystalline hydroxides than the amorphous hydroxides and an influence of the Al content in Fe:Al-compounds. The cumulative desorption was also clearly higher for the organic ligand solutions, especially with the ligand citric acid, which exhibited two-fold higher desorption for goethite, gibbsite, and pure amorphous Al-hydroxide and even 36 fold higher desorption for 1 Fe : 10 Al than $CaCl_2$.

3.5.2 Kinetics of phosphorus desorption

The phosphorus desorption from the Fe- and Al-hydroxides showed a biphasic behavior with a rapid initial stage until 48 h desorption time, followed by a slower second desorption phase (Krumina *et al.,* 2016; Smet *et al.,* 1998; Wang *et al.,* 2015). While the crystalline hydroxides goethite and gibbsite had the main phosphorus desorption during the initial fast desorption step for all reaction solutions, ferrihydrite revealed a stronger and ongoing phosphorus desorption during the slower second desorption phase, especially from citric acid, where 66 % of adsorbed phosphorus was desorbed in long-term. Similar results were observed for the amorphous Fe- and Al-hydroxide mixtures with a predominant Fe content, whereas this biphasic behavior was more pronounced for the citric acid desorption. The amount of desorbed phosphorus in the first desorption stage increased with increasing Al content. Both the different efficiency of the

hydroxides and the biphasic desorption behavior indicated different binding mechanisms of phosphorus to the hydroxide surfaces of different crystallinity (Gypser *et al.,* 2018; Wang *et al.,* 2015).

The time-dependent phosphorus desorption data were modeled with the Elovich, Exponential, and Parabolic functions and, based on R^2, the data fitted better to the Elovich equation, followed by the Exponential equation. This suggests that phosphorus was desorbed from Fe- and Al-hydroxides by chemisorption reactions, which corroborated previous studies with phosphorus desorption from soils (Shariatmadari *et al.,* 2006; Steffens, 1994; Wang *et al.,* 2015). For $CaCl_2$, $CaSO_4$, and humic acid, the calculated kinetics parameters showed a fast initial desorption step, followed by a slow reaction phase. This biphasic kinetic behavior revealed a rapid desorption of nonspecific adsorbed phosphorus from low-affinity sites and a slower step of desorption of specifically adsorbed phosphorus from high-affinity sites, which has been previously suggested by Wang *et al.* (2013). However, for ferrihydrite and the Fe:Al-hydroxides with a predominant Fe content, slightly higher or similar R^2 were observed for the citric acid treatment, using the Parabolic function. When the Elovich equation was applied, phosphorus desorption over time was higher than the initial desorption rate, and hence, a pronounced second desorption step was observed, indicating a stronger and continuous desorption effect on specific and heavily adsorbed phosphorus. This suggested a delayed release and a diffusion-controlled process during phosphorus desorption. The application of the Parabolic function also allowed modelling a second desorption mechanism after diffusion, which consisted of the dissolution of the adsorbents in the case of citric acid (e.g. Duputel *et al.,* 2013; Goyne *et al.,* 2006; Henintsoa *et al.,* 2017; Ström *et al.,* 1994; Wang *et al.,* 2005). Hence, in soils, a combination of desorption processes took place, depending on the formation of pedogenic crystalline or amorphous Fe:Al-hydroxides, according to pedogenesis and soil chemical properties.

3.5.3 Desorption mechanism of inorganic and organic solutions

The analyses of desorption kinetics revealed varying amounts of desorbed phosphorus during the aforementioned biphasic desorption process, but also the fact that the efficiency of phosphorus desorption differed distinctively between crystalline and amorphous hydroxides. An explanation of this variable desorption behavior could be supported by the already different specific and nonspecific phosphorus binding mechanisms (Wang *et al.,* 2013) on the hydroxide surfaces during adsorption. Due to the important role of phosphorus in the environmental nutrient cycle, extensive adsorption experiments with pedogenic Fe- and Al-hydroxides were carried out and revealed ligand exchange and the formation of stable inner-sphere surface complexes with metal ions (e.g. Arai and Sparks,, 2007; Goldberg and Sposito, 2008; Johnson *et al.,* 2002; Krumina *et al.,* 2016; van Emmerik *et al.,* 2007; Zheng *et al.,* 2012). Also, the diffusion of phosphorus into the inner particle pores of hydroxides was reported (Chitrakar *et al.,* 2006), and it was shown that the phosphorus uptake increased with increasing initial phosphorus concentration (Talebi Atouei *et al.,* 2016). However, in a meta-analysis, Gérard (2016) compared phosphorus adsorption equilibria across multiple studies and found that measured phosphate binding capacity differed even for similar hydroxides. This may be explained by varying experimental conditions, such as the specific reactive surface area, reaction time, pH, solid-solution ratio or background electrolytes (Antelo *et al.,* 2005; Talebi Atouei *et al.,* 2016). Mineral crystallinity and single, binary, or multi-component hydroxide systems also play an important role in phosphorus ad- and desorption processes (Anderson and Benjamin, 1990), because their chemical composition also affects phosphorus binding motifs (e.g. Khare *et al.,* 2005; van Emmerik *et al.,* 2007; Zheng *et al.,* 2012). For the considered synthetic model hydroxides, Gypser *et al.* (2018) used phosphorus adsorption experiments and Fourier-transform infrared spectroscopic investigations to identify the different binding mechanisms of phosphorus on

crystalline and amorphous hydroxides at pH 6. Gypser *et al.* (2018) showed that phosphorus binding on crystalline minerals occurred essentially on the hydroxide surface and not within the crystal structure. Amorphous Al-hydroxides, which are characterized by a less rigid crystal structure, revealed a higher accessibility of reactive sites within the particle structure. In our experiments, the amorphous character of ferrihydrite and of Fe-hydroxides likely enabled the diffusion of phosphorus into the mineral particle, where phosphorus started to form stable surface complexes and precipitate as shown by Willett *et al.* (1988) and Parfitt (1989). Hence, the amorphous structure affects the extent of precipitation because both surface and structural reactive sites are more accessible (Gypser *et al.,* 2018).

Ion exchange can play an important role in the retention and release of plant available nutrients (Blume *et al.,* 2010; Scheffer *et al.,* 2010), but also in the substitution of phosphorus in the soil solution by anions (Dean and Rubins, 1947). While the anion exchange of adsorbed phosphorus by Cl^- and SO_4^{2-} ions was more effective for the weaker adsorbed phosphorus on the crystalline hydroxides goethite and gibbsite as well as the pure amorphous Al-hydroxide, the Fe:Al-hydroxide mixtures with a predominant Fe content likely had strongly adsorbed phosphorus, which is rarely removed by these ions. Mobilization of inorganic phosphorus by organic acids was described by various processes: I. dissolution of low soluble minerals (e.g. Ca-, Fe-, and Al-phosphates), II. direct ligand exchange and replacement of phosphorus by anions of organic acids on ligand exchange surfaces, and III. formation of metal-organic complexes with Fe or Al and, as a consequence, the blocking of phosphorus adsorption sites (Bais *et al.,* 2006; Chen *et al.,* 2004; Johnson and Loeppert, 2006; Jones, 1998; Kpomblekou-A and Tabatabai, 2003; Lan *et al.,* 1995). The decrease of C_{Total} from the humic acid treatment can be explained by the process of ligand exchange on the mineral surface, but the formation of precipitate supported the accumulation of metal-organic complexes in the desorption solution instead (Lazo *et al.,* 2017;

Masset *et al.,* 2000). This effect was not observed from citric acid and the nearly constant C_{Total} content suggested neither a ligand exchange nor the formation of metal-organic complexes. It was rather emphasized that the hydroxides were dissolved and either the adsorbed or precipitated phosphorus was mobilized. This finding is supported by prior studies, which detected a Fe and Al release during phosphorus desorption and the promoted dissolution of phosphate minerals and adsorbents by the use of citric acid (Gerke, 1994; Gerke *et al.,* 1994; Goyne *et al.,* 2006; Henintsoa *et al.,* 2017; Ström *et al.,* 1994; Wang *et al.,* 2005). An addition of citrate can increase the dissolved Fe and Al, as well as the K and Si concentrations, which are attributed to the dissolution of clay minerals. The release of these ions was measured in an experiment of (Duputel *et al.,* 2013) for an additional 100 µM of citric acid, and it was reported that, on the contrary, low citrate concentrations (< 20 µM) were responsible for a decrease of available phosphorus for the investigated soil. This was explained by a large adsorption of citrate, which enhanced Ca^{2+} adsorption and facilitated the binding of phosphorus through Ca-bridging reactions (citrate-Ca-P). In our study, we did not measure dissolved Fe and Al in the reaction solutions.

3.6 Conclusion

Long-term desorption experiments were performed in order to characterize the kinetics of phosphorus desorption from crystalline and amorphous Fe- and Al-hydroxides. The cumulative phosphorus desorption by organic acids was higher than the inorganic background solutions in the order $CaCl_2$ < $CaSO_4$ < humic acid < citric acid. The efficiency of the desorption solutions showed differences between the crystalline and amorphous hydroxides. The inorganic solutions facilitated greater phosphorus release from the crystalline goethite, gibbsite, and the amorphous

Fe:Al-hydroxide mixtures dominated by Al than from the amorphous ferrihydrite and Fe:Al-hydroxides dominated by Fe. In order to verify the impact of organic acids on hydroxide dissolution, further desorption experiments employing various concentrations of organic acids at different pH levels and the measurement of changing Fe and Al concentrations in the reaction solutions are necessary. It can be stated that phosphorus adsorbed on crystalline hydroxides can be more easily mobilized than phosphorus adsorbed on amorphous Fe- and Al-hydroxides. Citric acid, which is exuded by plant roots, has an important impact on improving the phosphorus availability of soils, especially those containing amorphous Fe- and Al-hydroxides.

This study points to the presence of easily and strongly bound phosphorus as well as the mineral crystallinity, which affects the extent of phosphorus desorption. This should be considered with regard to concerns about the exhaustion of global phosphorus reserves and as a result, adapted soil management strategies. These strategies should take into account the amount of phosphorus, which is already fixed in soils and contribute to a directed mobilization of these phosphorus pools. Both humic substances, as well as root exudates, have a positive effect on phosphorus bioavailability. With regard to their effectiveness, the influence of organic components in the rhizosphere should be given greater consideration, e.g. through the use of phosphorus mobilizing catch crops on agricultural soils.

4 Phosphorus release from vivianite and hydroxyapatite by organic and inorganic compounds [3]

4.1 Abstract

Based on recent mining rates and the exhaustion of global phosphorus reserves, the mobilization of phosphorus already stored in soils and the recovery from secondary resources such as Ca- and Fe-phosphates is required. The Ca-phosphate hydroxyapatite is well known as a resource for fertilizer whereas vivianite is formed in waterlogged soils and sediments. During sludge treatment, the formation of vivianite has been identified, being the major Fe-phosphate. Long-term phosphorus release of both hydroxyapatite and vivianite has been studied by applying different inorganic ($CaCl_2$, $CaSO_4$) and organic (citric and humic acid) reagents in batch experiments. $CaCl_2$ and $CaSO_4$ were chosen to represent the soil solution, while citric and humic acid as organic constituents affects phosphorus availability in the rhizosphere and during the process of humification. Additionally, the Flow-Through-Reactor technique with infinite sink has been applied to study the long-term release kinetics of phosphorus. The cumulative phosphorus release by organic acids was higher than by inorganic compounds. The cumulative release rates of FTR with $CaCl_2$ had a higher release of phosphorus compared to batch. The infinite sink application has caused a continuously high concentration gradient between the solid and liquid phase leading to higher desorption rates compared to the batch technique. The predominant amount of the totally released phosphorus over time was available during short-term. While inorganic anion exchange preferentially took part at easily available binding sites, organic acids

[3] Published in Pedosphere
Elsevier
Gypser, S., Freese, D. (2020): Phosphorus release from vivianite and hydroxyapatite by organic and inorganic compounds. Pedosphere **30**, 190–200.
DOI: 10.1016/S1002-0160(20)60004-2.

affect the more heavily available binding sites, which can be embedded within the mineral structure. The results showed that organic compounds, especially citric acid, play a superior role compared to inorganic soil solution constituents during recovery of already stored phosphorus from the tertiary phosphates vivianite and hydroxyapatite.

Keywords: Anion exchange, Batch, Citric acid, Dissolution, Flow-Through Reactor, Humic acid, Hydroxyapatite, Ligand exchange, Phosphorus recovery

4.2 Introduction

The deficiency of phosphorus affects agricultural soils and limiting biomass productivity in terrestrial ecosystems worldwide (Elser *et al.,* 2007). Over 80 % of applied phosphorus fertilizer can become immobilized and hence, restricted for plant uptake as a result of reactions with the soil solid phase such as adsorption or precipitation (Zhu *et al.,* 2018). Due to the fundamental role of phosphorus in the environment, phosphorus reactions in soils and on model substances have been thoroughly studied (Arai and Sparks, 2001, 2007; Barrow, 1983; Hinsinger, 2001; Torrent *et al.,* 1992).

Based on recent mining rates there are concerns about global phosphorus reserves and its exhaustion (Cordell *et al.,* 2009; Cordell and White, 2010). Since phosphorus cannot be synthesized by organisms from other elements, the demand of mineral phosphorus fertilizers is covered by mineable rock phosphates. One strategy to minimize the dependence on mineable phosphate reserves is the mobilization of phosphorus already stored in soil and the recovery from Fe- and Ca-phosphates while avoiding undesired leaching. Soil inorganic phosphorus occurs in a number of different forms and several pools were identified: rapidly solubilized and mobilized

phosphorus from adsorption reactions by surface complexation and slowly exchangeable phosphorus, which is strongly adsorbed on Fe- or Al-hydroxides or precipitated in Fe-, Al- or Ca-phosphates (Lookman *et al.,* 1997). While in waterlogged soils and sediments Fe-phosphate vivianite has developed (Rothe *et al.,* 2016), in neutral and calcareous soils the Ca-phosphate hydroxyapatite has occurred, which has a low solubility under natural conditions (Gustafsson *et al.,* 2012; Walker and Syers, 1976; Yadav and Verma, 2012). Both vivianite and hydroxyapatite are pedogenic minerals and primary resources of phosphorus in terrestrial ecosystems, but also in aquatic systems (Rothe *et al.,* 2016). But sewage sludge is a remarkable secondary source for phosphorus as well (Wilfert *et al.,* 2016) and prior studies verified the Fe-phosphate mineral vivianite in surplus and digested sludge (Frossard *et al.,* 1997; Ghassemi and Recht, 1971; Seitz *et al.,* 1973; Wilfert *et al.,* 2018).

The release of phosphorus in soils is strongly pH dependent and during pedogenesis, phosphorus can be mobilized from apatite by acidification, but will be bound in other forms, e.g. on Fe- and Al-hydroxides (Scheffer *et al.,* 2010). Several approaches have been investigated to increase phosphorus availability in soils. These include the use of soil P activators (Zhu *et al.,* 2018) such as I. bio-inoculants and bio-fertilizers, containing phosphorus solubilizing microorganisms and phosphatase enzymes (Behera *et al.,* 2014; Chesti *et al.,* 2013*;* Ji *et al.,* 2014; Kalsi *et al.,* 2016; Khan *et al.,* 2014; Li *et al.,* 2015; Liu *et al.,* 2016; Mukherjee and Sen, 2015; Othman and Panhwar, 2014; Owen *et al.,* 2015; Sharma *et al.,* 2013), II. organic matter, containing low-molecular-weight organic acids, humic acids, lignin, crop residue, biochar or manure (Andersson *et al.,* 2015; Basak, 2018; Dai *et al.,* 2016; Damon *et al.,* 2014; Espinosa *et al.,* 2017; Guppy *et al.,* 2005; Yuan *et al.,* 2016) and III. zeolites and other materials, used as cation exchangers (Fadaeerayeni *et al.,* 2015; García-Domínguez *et al.,* 2015; Parab *et al.,* 2015; Yang *et al.,* 2015).

However, plants can enhance the phosphorus availability in case of demand by the exudation of organic acids (Bais *et al.,* 2006; Hinsinger, 2001; Hou *et al.,* 2018; Jones, 1998). The mobilization of inorganic phosphorus by organic acids was explained by various processes, which include: I. dissolution of low soluble phosphate minerals, II. direct ligand exchange and replacement of phosphorus by anions of organic acids, and III. formation of metal-organic complexes with Fe or Al and thus the blocking of phosphorus adsorption sites (Bais *et al.,* 2006; Chen *et al.,* 2004; Johnson and Loeppert, 2006; Kpomblekou-A and Tabatabai, 2003). Besides other organic acids such as oxalic or malic acid, citric acid was often detected in higher concentration in the rhizosphere and was described as an effective solubilizer for inorganic phosphorus (Henintsoa *et al.,* 2017; Johnson and Loeppert, 2006; Kpomblekou-A and Tabatabai, 2003). But in addition to those low-molecular-weight organic acids, also high-molecular-weight acids played an important role in phosphorus mobilization. Humic or fulvic acids, which were formed during humification and mineralization, reduced phosphorus fixation and increased its availability to plants (Hua *et al.,* 2008; Jones, 1998).

While several studies focused on phosphorus release from Ca-phosphates by organic acids (Gharabaghi *et al.,* 2009; Taghipour and Jalali, 2013; Xu *et al.,* 2004) or phosphorus solubilizing microorganisms (Khan *et al.,* 2014; Li *et al.,* 2015), no studies on phosphorus release from vivianite have been carried out so far. It should also be considered that during investigations of the kinetics and mechanisms of phosphorus release in soils, a multi-component system must be taken into account which, in addition to phosphates, also contains Ca, Fe or Al hydroxides or organic matter. Thus, depending on the soil composition there may be varying results regarding the P release as well as the applicability of kinetic models. With regard to an efficient use of already bound phosphorus, the aim of this study was to characterize long-term kinetics of phosphorus mobilization from the pure minerals vivianite and hydroxyapatite as well as the

detection of rapidly and slowly available phosphorus over time. This will serve to identify the specific mechanisms of phosphorus mobilization on the phosphates and to estimate their potential as usable phosphorus source. In the experiments, vivianite and hydroxyapatite were compared as they both represent a primary phosphorus resource. Synthetic vivianite and hydroxyapatite were used as model substances to investigate the different binding strength and hence, accessibility of phosphorus within the mineral structure. $CaCl_2$, $CaSO_4$, humic and citric acid were used as reaction solutions, at which $CaCl_2$ and $CaSO_4$ were chosen to represent the main constituents of the soil solution. Humic and citric acid were chosen to compare the influence of humification and plant exudate in the rhizosphere on phosphorus solubilization from minerals. The amount of available inorganic phosphorus can be determined by long-term release kinetics, which include both immediately as well as very slow available phosphorus (Frossard *et al.,* 2000; Hacker *et al.,* 2017). Release experiments were conducted both in batch and with an infinite sink approach. The benefit of the infinite sink approach by using Flow-Through-Reactor technique (FTR) is the minimal alteration of the mineral-solution system (Frossard *et al.,* 2000) and the removal of mobilized phosphorus with the infinite sink without accumulation in the reaction solution, resulting in a new binding or precipitation in the solution or on the mineral surface (Kaupenjohann and Wilcke, 1995). In contrast, batch experiments are an inexpensive and simple approach (Kruse *et al.,* 2015) to determine the amount of long-term mobilized phosphorus. Previous to the kinetic experiments, the pH of the minerals and the reaction solutions was adjusted to 6. Therefore, the effect of humic and citric acid on phosphorus release was comparable to the inorganic compounds, representing the soil solution. Also phosphorus revealed its high availability in a pH range from 5.0 to 6.8 due to the high solubility of both Fe- and Ca-phosphates (Johnson *et al.,* 2002; Scheffer *et al.,* 2010). It was hypothesized that citric acid, which has been characterized as a strong solvent, is significantly more effective than humic acid,

and that the inorganic components have minor influence on phosphorus release. Also it will be investigated whether the organic constituents differ in their mechanism of phosphorus mobilization and whether dissolution at a near neutral pH of 6 can still be considered as a release mechanism. Finally, the comparability of the applied kinetics models with different experimental methods will be discussed.

4.3 Materials and methods

4.3.1 Phosphate minerals

The Fe-phosphate vivianite ($Fe_3^{2+}[PO_4]_2 \cdot 8H_2O$) was prepared adapted from the method of (Eynard *et al.,* 1992). To 250 ml of a 0.035 M H_3PO_4-solution solid $FeSO_4$ were added, resulting in a 0.05 M $FeSO_4$-solution. The pH of the solution was adjusted to 6 with 5 M KOH. The precipitation was centrifuged for 5 min at 2090 × g (Allegra X-12R Benchtop Centrifuge, Beckman Coulter) and washed several times with ultrapure water. The prepared vivianite was dried at 40°C. Using a mortar and pestle, the solid was ground into a powder. All chemicals used for the preparation of vivianite were of analytical grade and the solutions were prepared with ultrapure water. The Ca-phosphate hydroxyapatite ($Ca_5[OH(PO_4)_3]$) was synthetic, commercially available (Acros Organics, Thermo Fisher Scientific, Massachusetts, USA) and of analytical grade. The composition of each phosphate mineral was determined by using X-ray diffraction (XRD) using an Empyrean powder diffractometer (PANalytical) with Cu Kα radiation (λ = 0.15418 nm), theta-theta-goniometer, 2 kW X-ray generator (Spellman), automatic divergent and anti-scatter slits and PIXcel^{3D} detector. Diffraction data were recorded from 4.6° to 84.9° 2ϴ with a step-size of 0.0131 and a step time of 58.4 s.

4.3.2 Phosphorus release experiments

The release of phosphorus was conducted by using batch and Flow-Through-Reactor technique, at which prior to the experiments fine granulated, washed and calcined silica sand (particle size 0.2 – 0.8 mm, Merck Millipore) was coated with the phosphate minerals according to (Scheidegger *et al.,* 1993). Therefore, similar sample treatment (e.g. centrifugation times and revolutions) and sufficient pore space to keep a constant flow rate during the FTR-experiments were ensured. Samples for the phosphorus measurement were taken after 2, 6, 24, 48, 168, 336, 672 and 1344 h. This corresponds to a total duration of 8 weeks. A pH of 6 of the minerals was adjusted by a previous silica sand coating procedure. After addition of the organic and inorganic solutions, the pH was controlled at regular intervals and remained stable.

4.3.2.1 Preparation of coated silica sand

To 10 g of the phosphate minerals, a 0.01 M $NaNO_3$-solution, adjusted to pH 6, was added to a final volume of 100 ml. Than 100 g of pure silica sand was added to the suspension and it was shaken for 24 h at room temperature. After settling of the coated sand the supernatant was decanted and the material was washed three to five times with the 0.01 M $NaNO_3$-solution at pH 6 and in a final step with ultrapure water to remove not adsorbed phosphorus traces and soluble salts. The coated silica sand was oven dried at 60°C for 48 h (Freese *et al.,* 1999). The extent of the coating of the silica sand with the phosphate minerals as well as the initial phosphorus content were analyzed by using ICP-AES (Unicam iCAP6000 Duo, Thermo Fisher Scientific, Massachusetts, USA).

4.3.2.2 Batch experiment

Batch solubilization experiments were performed with organic (humic acid $C_9H_9NO_6$, citric acid $C_6H_8O_7$) and inorganic ($CaCl_2$, $CaSO_4$) reaction solutions at pH 6. Therefore, 2.5 g of the coated silica sand was placed in 100 ml PE-bottles and 50 ml of 0.01 M $CaCl_2$ or $CaSO_4$ were added to each sample. 5 g of the coated silica sand were used for the organic batch solubilization with 50 ml of 2 g l^{-1} humic acid and citric acid (Alfa Aesar, Haverhill, Massachusetts, USA), respectively, due to the higher release capacity of low molecular organic acids (Gerke, 1994). The samples (4 replicates) were shaken for 24 h at 150 motions min^{-1}, centrifuged for 15 min at 2091 × g (Allegra X-12R Benchtop Centrifuge, Beckman Coulter, Brea, USA) and the supernatant was filtrated by using P-poor Whatman 512 1/1 filters. Following, 50 ml of fresh reaction solution was added to the samples.

4.3.2.3 FTR-experiment

Flow-Through-Reactor (FTR) release experiments were conducted according to (Grolimund *et al.,* 1995), modified by (Freese *et al.,* 1999) to compare the cumulative phosphorus release rate with the batch setup and $CaCl_2$ as reaction solution. A scheme of the used model is presented in Fig. 15. The experiment was conducted by placing 10 g of dried silica sand, coated with vivianite or hydroxyapatite, in the first reactor. For each mobilization step, 5 g of an infinite sink, which adsorbed the extracted phosphorus from the samples, were placed in a second reactor and was replaced by a fresh one for the measurement of desorbed phosphorus. This infinite sink was prepared as described by (Scheidegger *et al.,* 1993), modified by (Freese *et al.,* 1999). While continuous stirring, 1 M KOH were added to 750 ml of a 0.2 M $Fe(NO_3)_3 \cdot 9\ H_2O$-solution, until a pH of 6 was reached. Following, 2 kg of pure silica sand (acid washed and calcined, Merck

Millipore, Merck KGaA, Darmstadt, Germany) were added to the homogeneous suspension and the mixture was shaken at room temperature for 24 h. The following steps were similar to the procedure of coating of silica sand as described above. The reactors were arranged in a closed-loop setup and filled with 30 ml 0.01 M $CaCl_2$-solution. The reaction solution circulated with a flow-rate of 2.5 ml min^{-1}, continuously pumped by a multichannel peristaltic pump. For the measurement of the phosphorus content after each reaction step, the infinite sink was rinsed with ultrapure water into 50 ml PE-bottles and dissolved by adding 1 ml of 98 % H_2SO_4, followed by an ultrasonic treatment for 30 min. The samples (2 replicates) were filtered and filled up to a final volume of 50 ml.

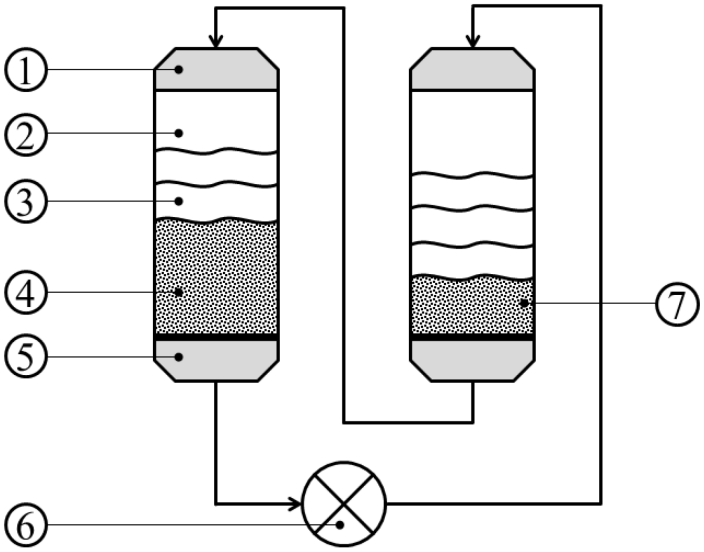

Fig. 15. Setup of the Flow-Through-Reactor desorption experiments with (1) top of the reactor chamber, (2) intermediate, (3) desorption solution, (4) phosphate-coated silica sand, (5) bottom of the reactor chamber with filter holder, membrane filter and silicon gasket, (6) peristaltic pump and (7) infinite sink.

4.3.2.4 Microbial activity and carbon content

Microbial activity and contaminations were inhibited by acid washing all used materials with 10 % HNO_3. The C_{Total} content of the organic reaction solutions was measured by using a TOC-Analyzer (TOC-Vcph and TOC5000, Shimadzu, Kyoto, Japan) after eight weeks of reaction time.

4.3.3 Kinetics of phosphorus release

The cumulative phosphorus release depending on time was calculated for each mineral and reaction solution. Different kinetic models (Aharoni and Sparks, 1991) were fitted to the data, while the following equations were used:

Elovich $$Q_t = \frac{1}{\beta}\ln(\alpha\beta) + \frac{1}{\beta}\ln t \quad (1)$$

Exponential $$\ln Q_t = \ln a + b \ln t \quad (2)$$

Parabolic $$Q_t = Q_0 + k_P\, t^{1/2} \quad (3)$$

where Q_t is the amount of released phosphorus at time t in mg P mg^{-1} Mineral, Q_0 is the initial phosphorus concentration in the solution, α and a are the initial phosphorus release constants in mg P mg^{-1} Mineral min^{-1}, β and b are the phosphorus release rate constants in mg P mg^{-1} Mineral, and k_P is the diffusion rate constant in m s^{-1}. Q_0 equals a value of 0 at the beginning of the experiments. All models were tested by using least-square regression analysis to determine their applicability on the phosphorus release kinetics of the investigated phosphate minerals. Statistical analyses were performed with SigmaPlot (Systat Software Inc., San Jose, California, USA).

4.4 Results

4.4.1 Characterization of phosphate minerals

The composition of the synthetic phosphate minerals vivianite and hydroxyapatite was verified by using XRD (Fig. 16). Hydroxyapatite was identified as $Ca_5(PO_4)_3(OH)$ with a hexagonal crystal system. Characteristic bands with *d*-values of 3.45, 2.80, 2.73, 1.94, 1.84 and 1.72 (bands with > 30 % intensity) were observed (Fig. 16A). Vivianite was identified as $Fe_3(PO_4)_2 \cdot 8H_2O$ with a monoclinic crystal system. Numerous bands were shown in the XRD pattern and distinctive *d*-values of 6.76, 4.93, 3.87, 3.22, 2.98, 2.73 and 2.44 (bands with > 50 % intensity) were observed (Fig. 16B).

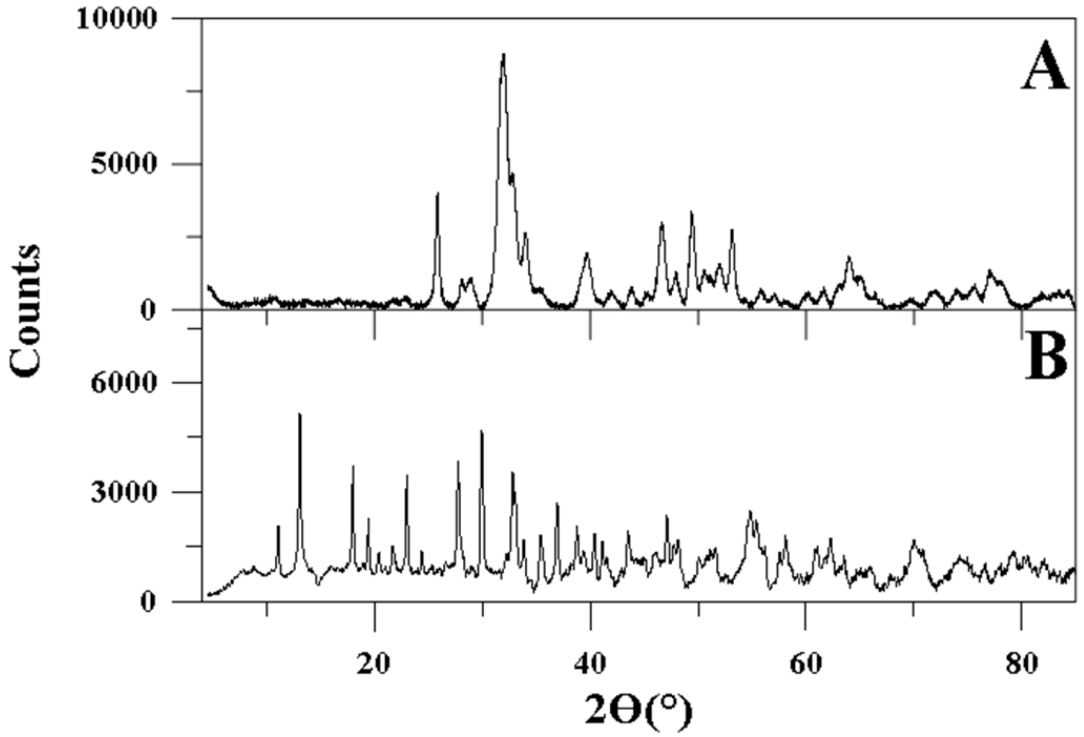

Fig. 16. XRD patterns of (A) hydroxyapatite and (B) vivianite.

The determined extent of coating and the initial phosphorus amount of vivianite and hydroxyapatite were given in Ta. 8. The calculated mobilization rate was expressed in mg P mg^{-1} Mineral.

Tab. 8. Amount of Fe, Ca and P of the used phosphate minerals and the infinite sink coated on silica sand.

Mineral	**Fe- and Ca- content on coated silica sand**	**Initial P content***
	mg g^{-1} SiO2	*mg mg^{-1} Mineral*
Vivianite	6.50	0.27 ± 0.01
Apatite	15.85	0.33 ± 0.03
Infinite Sink	3.61	0.00 ± 0.00

*n = 2, Given are mean and standard deviation.

4.4.2 Efficiency of phosphorus release

The lowest phosphorus release of vivianite and hydroxyapatite was measured for the $CaCl_2$ treatment with 1.4 and 0.9 %, respectively, and had a similar amount for $CaSO_4$ with 1.7 and 0.9 % released phosphorus, respectively (Tab. 9). Higher release of phosphorus was detected by using humic acid. They amounted 8.1 % for vivianite and 22.1 % for hydroxyapatite. After eight weeks of reaction time, samples treated with citric acid had the highest phosphorus release with 83.9 % for vivianite and 94.0 % for hydroxyapatite. The FTR experimental setup for the $CaCl_2$ treatment showed clearly higher cumulative release rates for both minerals. They amounted 25.1 % for vivianite and 8.9 % for hydroxyapatite, respectively which was 18-fold and 10-fold higher compared to the batch experimental setup.

Tab. 9. Total P release after 1344 h as well the percentages of P release in the two reaction time periods of 0-48 and 48-1344 h related to the amount of total desorbed P by using desorption solutions $CaCl_2$, $CaSO_4$, humic acid and citric acid at pH 6.

Mineral		Batch				FTR
		$CaCl_2$	$CaSO_4$	Humic Acid	Citric Acid	$CaCl_2$
		Desorbed P %				
Vivianite	0-48 h	59.8 ± 2.5	62.2 ± 0.1	55.4 ± 0.2	52.4 ± 0.8	43.8 ± 24.5
	48-1344 h	40.2 ± 2.5	37.8 ± 0.1	44.6 ± 0.2	47.6 ± 0.8	56.2 ± 24.5
	Total	1.4 ± 0.1	1.7 ± 0.1	8.1 ± 0.1	83.9 ± 14.7	25.1 ± 3.4
Apatite	0-48 h	69.4 ± 6.0	57.9 ± 1.4	80.6 ± 1.3	85.5 ± 1.6	25.8 ± 21.2
	48-1344 h	30.6 ± 6.0	42.1 ± 1.4	19.4 ± 1.3	14.5 ± 1.6	74.2 ± 21.2
	Total	0.9 ± 0.1	0.9 ± 0.0	22.1 ± 1.4	94.0 ± 0.0	8.9 ± 4.4

n = 4, Given are mean and standard deviation.

4.4.3 Kinetics of phosphorus release

It can be seen that during the first 24 to 48 h, a fast initial process of phosphorus release took place, followed by a slower reaction step (Fig. 17). For the batch experiments, all sample treatments had their prevailed phosphorus release (> 50 % from total phosphorus release) within the first 48 h. It was in the range between 60 and 70 % for vivianite and hydroxyapatite in the $CaCl_2$ treatment and between 62 and 58 % in the $CaSO_4$ treatment, respectively (Tab. 9). Especially for the organic acid treatments, the release was higher for hydroxyapatite compared to vivianite and amounted 55 and 81 % for humic acid and 52 and 86 % for citric acid, respectively. Though the $CaCl_2$ FTR treatment had a substantial higher phosphorus release compared to the batch method, but the discharge within the first 48 h was lower with 44 % for vivianite and 26 % for hydroxyapatite.

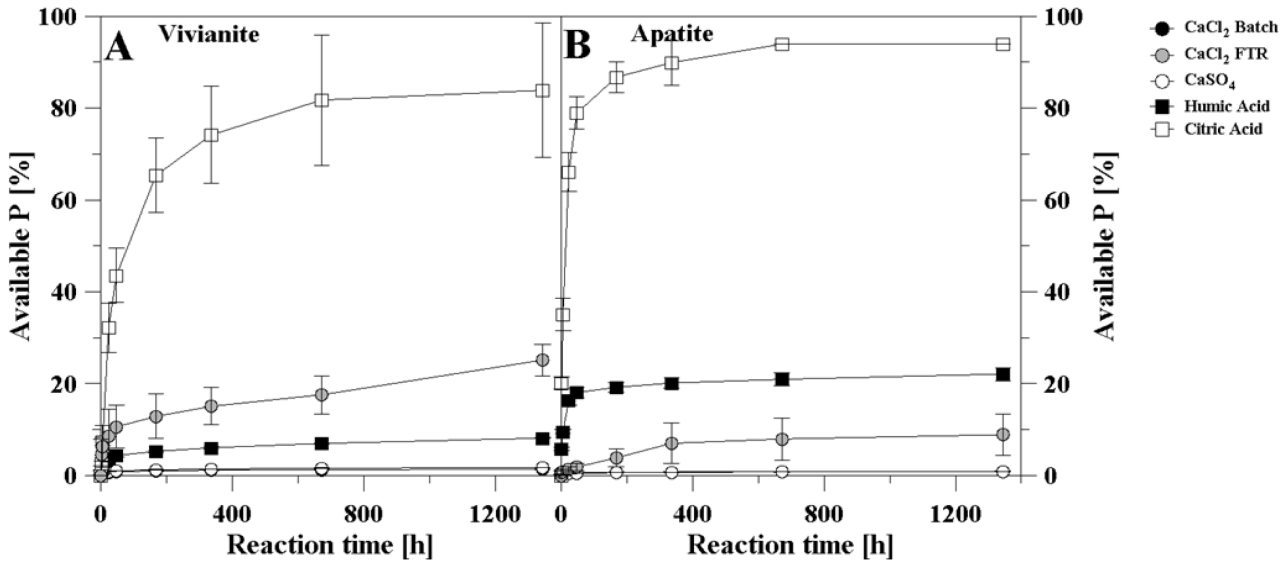

Fig. 17. P release kinetics of (A) vivianite and (B) hydroxyapatite by using $CaCl_2$, $CaSO_4$, humic acid and citric acid at pH 6. Please note that results of the batch experiments using CaCl2 and CaSO4 solutions were so close that the latter was overlaid.

The coefficients of determination (R^2) of the applied kinetic models were compared and revealed that the kinetics of phosphorus release for the batch experiments fitted best with the Elovich equation (R^2 = 0.99 to 0.91), followed by the Exponential function (R^2 = 0.94 to 0.83) (Tab. 10). However, for the kinetics of the FTR experiments the data fitted best with the Parabolic (R^2 = 0.99) and the Exponential function (R^2 = 0.99 to 0.98). The kinetic parameters obtained from the Elovich and Exponential function showed a higher initial phosphorus release during batch experiments of hydroxyapatite compared to vivianite for $CaCl_2$, humic and citric acid (Tab. 10). This value was nearly in the same range for both minerals during the $CaSO_4$ treatment. The release rate constant over time, calculated with the Elovich equation, was higher for hydroxyapatite within the $CaCl_2$ and $CaSO_4$ treatment, higher for vivianite within the humic acid treatment and in a similar range for both minerals during the citric acid treatment. The

calculated release rate constant using the Exponential equation showed higher values for vivianite overall. However, for the FTR experiment, the kinetic parameter revealed a higher initial phosphorus release and a higher release rate constant over time of vivianite compared to hydroxyapatite. The diffusion rate constant of the Parabolic function, which fitted best for FTR, was 2-fold higher for vivianite ($7.0 \cdot 10^{-3}$ m s^{-1}) compared to hydroxyapatite ($3.3 \cdot 10^{-3}$ m s^{-1}). In general, the kinetic parameters were higher for phosphorus release by using organic compounds compared to inorganic compounds.

Tab. 10. Coefficients of determination (R^2) and standard errors (S.E.) for the kinetic equations used to describe the kinetic release of P after 1344 h desorption time, and kinetic parameters of the selected Elovich and Exponential function equations for P release.

Mineral	Treatment	Elovich				Exponential				Parabolic	
		R^2	S.E.	α	$1/\beta$	R^2	S.E.	a	b	R^2	S.E.
Vivianite	$CaCl_2$	0.99***	0.00	$8.2 \cdot 10^{-4}$	$4.7 \cdot 10^{-4}$	0.91**	0.22	$6.0 \cdot 10^{-4}$	0.27	0.81**	0.00
	$CaSO_4$	0.99***	0.00	$7.9 \cdot 10^{-4}$	$6.1 \cdot 10^{-4}$	0.90**	0.25	$6.3 \cdot 10^{-4}$	0.30	0.83**	0.00
	Humic	0.99***	0.00	$3.7 \cdot 10^{-3}$	$2.9 \cdot 10^{-3}$	0.94***	0.18	$3.3 \cdot 10^{-3}$	0.29	0.88**	0.00
	Citric	0.98***	0.01	0.02	0.04	0.87**	0.50	0.01	0.52	0.79**	0.05
	$CaCl_2$ FTR	0.91*	0.03	0.01	0.04	0.98***	0.15	0.01	0.45	0.99***	0.01
Apatite	$CaCl_2$	0.96***	0.00	0.01	$3.1 \cdot 10^{-4}$	0.87**	0.16	$1.1 \cdot 10^{-3}$	0.16	0.77**	0.00
	$CaSO_4$	0.99***	0.00	$7.4 \cdot 10^{-4}$	$3.9 \cdot 10^{-4}$	0.93**	0.18	$5.6 \cdot 10^{-4}$	0.26	0.86**	0.00
	Humic	0.91**	0.01	$3.3 \cdot 10^{-3}$	0.29	0.83**	0.21	0.02	0.19	0.61*	0.01
	Citric	0.91**	0.03	0.19	0.04	0.83**	0.26	0.08	0.23	0.60*	0.06
	$CaCl_2$ FTR	0.80**	0.02	$2.7 \cdot 10^{-3}$	0.02	0.99***	0.10	$1.6 \cdot 10^{-3}$	0.60	0.99***	0.00

*significant at $p < 0.05$, **significant at $p < 0.01$, ***significant at $p < 0.001$

4.4.4 C_{Total} during humic and citric acid treatment

After eight weeks of reaction time, the samples of the humic acid treatments showed the formation of a brownish precipitate. For this reason, C_{Total} was measured in the sample solutions, which was 546 mg l^{-1} for humic acid and 800 mg l^{-1} for citric acid. For the humic acid treatment, C_{Total} decreased about 13.2 % for vivianite and 9.5 % for hydroxyapatite, respectively (Fig. 18). For the citric acid treatment, C_{Total} fluctuated with 96.5 % and 100.7 % for vivianite and hydroxyapatite around the initial C_{Total} content of the citric acid. Correlations between the amount of desorbed phosphorus in %, and the initial phosphorus concentration in mg mg^{-1} mineral to the C_{Total} content in mg l^{-1} from the reaction solution revealed no relationship.

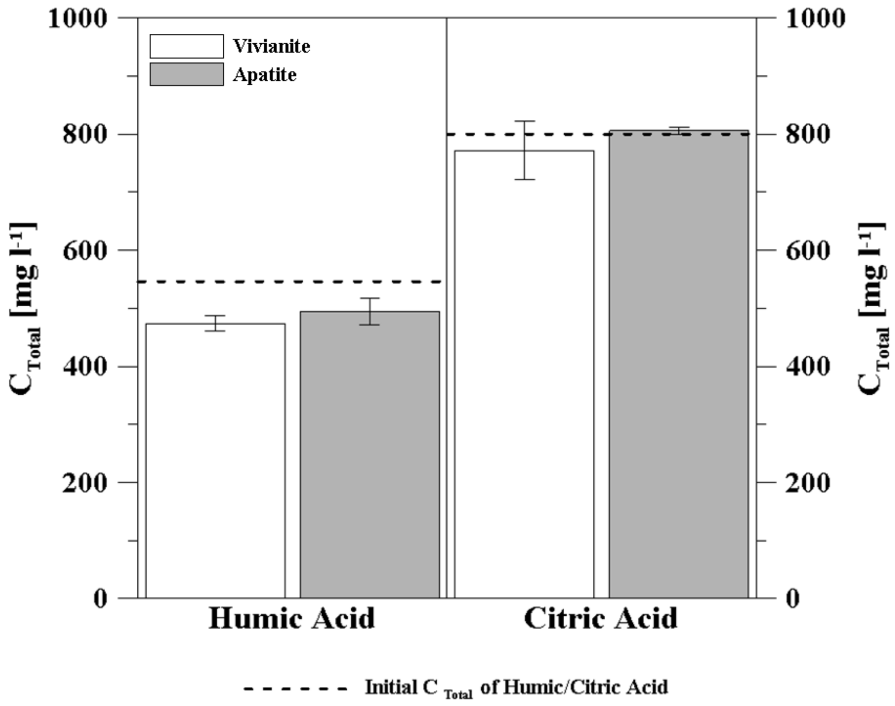

Fig. 18. C_{Total} in mg l^{-1} in humic acid and citric acid after eight weeks of reaction time (n = 2).

4.5 Discussion

4.5.1 Efficiency of phosphorus release

The cumulative phosphorus release by organic acids was greater than by inorganic background solutions at which the capability to solubilize phosphorus followed the order $CaCl_2 \leq CaSO_4$ < humic acid < citric acid. The higher cumulative release rate of vivianite compared to hydroxyapatite by using $CaCl_2$ and $CaSO_4$ indicated a slightly better anion exchange capacity of vivianite, but a minor impact of the used inorganic solutions on mobilization of phosphorus in general. While humic acid increased the availability of inorganic bound phosphorus, a distinctive effect of citric acid for both vivianite and hydroxyapatite was measured. Though, the higher standard deviation of the vivianite samples did not permit an accurate conclusion with regard to a varying capability of citric acid to mobilize phosphorus compared to hydroxyapatite. Prior studies have shown a positive effect of hydroxyapatite as a phosphorus fertilizer on plant growth (Basak, 2019; Giroto *et al.,* 2015; Xiong *et al.,* 2018). Since hydroxyapatite is also a water-insoluble form of phosphorus, the influence of inorganic components is rather small (Taşkın *et al.,* 2018).

Ion exchange plays an important role for the plant availability of nutrients (Scheffer *et al.,* 2010) and the mobilization of phosphorus by anions (Dean and Rubins, 1947). However, compared to the influence of organic compounds, the inorganic anion exchange has an inferior standing. Previous findings supported the beneficial effect of organic acids and especially citric acid during phosphorus release from soils (Gerke, 1994; Henintsoa *et al.,* 2017; Taghipour and Jalali, 2013) and phosphate minerals (Harrold and Tabatabai, 2006; Johnston and Miller, 1959; Lazo *et al.,* 2017; Wei *et al.,* 2010; Xu *et al.,* 2004). Beside the hydrogen ions especially the carboxyl groups of organic acids have a strong effect on the amount of dissolved phosphorus. A higher quantity of carboxyl groups can increase phosphorus release, but the structure of the acid

itself can have a limiting effect (Johnston, 1952; Johnston and Miller, 1959; Xu *et al.,* 2004). In this case, the amount of carboxyl groups was related to C_{Total}, which was 546 mg l^{-1} for humic acid and 800 mg l^{-1} for citric acid. According to this, citric acid seemed to be more effective in phosphorus release, which was observed in this study as well. Othieno (1973) reported an even detrimental effect of humic acid on the phosphorus availability to wheat by adding humic acid, which makes it necessary to take into account that humic acid may also act as phosphorus adsorbing surface (Zhu *et al.,* 2018). A further aspect could be the more complex structure of humic acid, which on the one hand can act as a physical barrier on the mineral surface and reduces phosphorus affinity to soil colloids (Rosa *et al.,* 2018; Wang *et al.,* 2016), but on the other hand can possibly limiting desorption within the mineral structure and hence, the effectiveness of humic acid during phosphorus mobilization.

The processes, which were described during mobilization of inorganic phosphorus by organic acids, are mainly the direct ligand exchange and replacement of phosphorus by organic anions, the formation of metal-organic complexes and blocking of possible adsorption sites, and the dissolution of low soluble minerals (Bais *et al.,* 2006; Chen *et al.,* 2004; Johnson and Loeppert, 2006; Kpomblekou-A and Tabatabai, 2003). The decrease of C_{Total} in the humic acid treatment can indicate the mechanism of ligand exchange on the mineral surface, but the accumulation of precipitate in the sample solution can also refer to the formation of metal-organic complexes (Lazo *et al.,* 2017; Masset *et al.,* 2000). A decrease of C_{Total} was not measured for citric acid and as a result, ligand exchange with organic anions and the formation of metal-organic complexes were excluded as possible reaction mechanisms. It can be assumed that phosphorus mobilization was induced by the dissolution of the minerals itself (Fig. 5), which can be supported by findings of prior studies, which observed the release of Fe or Al by using citric

acid for phosphorus solubilization (Duputel *et al.,* 2013; Gerke, 1994; Gerke *et al.,* 1994; Goyne *et al.,* 2006; Henintsoa *et al.,* 2017; Ström *et al.,* 1994).

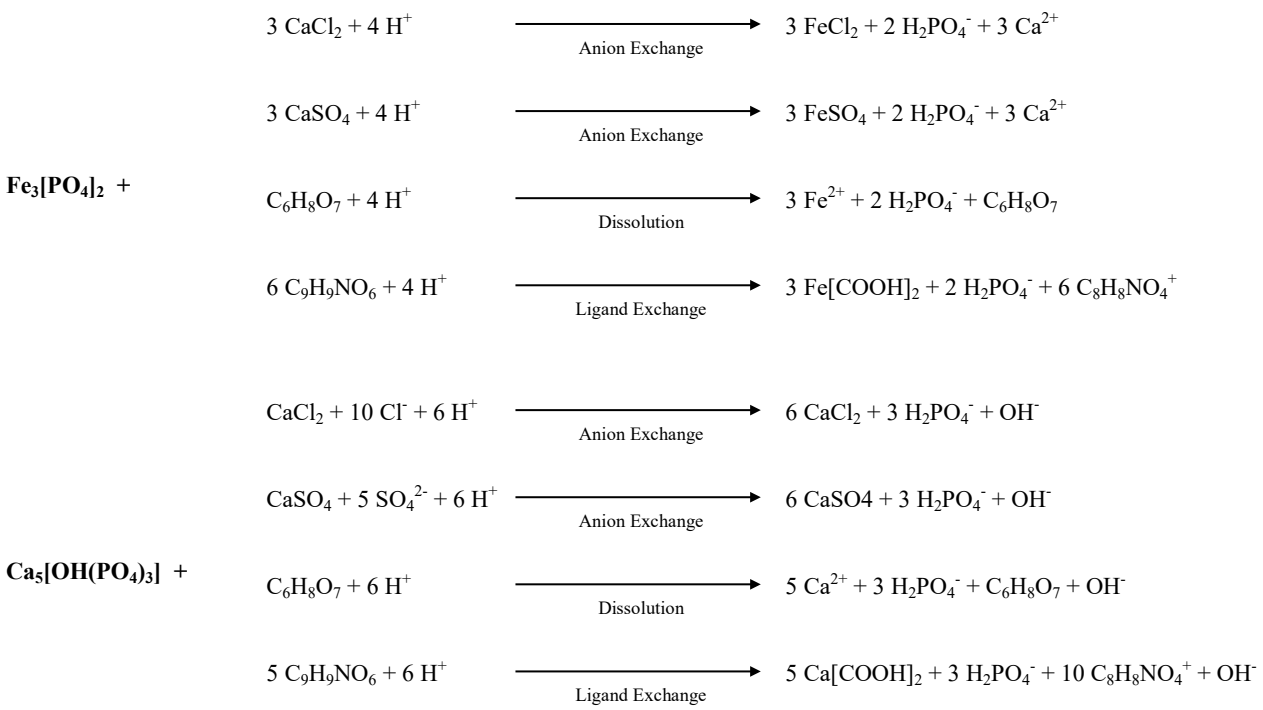

Fig. 19. Possible chemical reactions of vivianite and hydroxyapatite during desorption with $CaCl_2$, $CaSO_4$, citric acid and humic acid at pH 6.

These data revealed that organic acids often increased the dissolution of phosphate minerals and hence, the availability of inorganic phosphorus. To confirm the dissolution of both vivianite and hydroxyapatite, the Fe- and Ca-concentrations would have to be determined after desorption. In this study, no dissolved Fe and Al were determined in the reaction solutions and if measured, the initial under-saturation of all investigated reaction solutions towards the minerals must also be taken into account. Duputel *et al.* (2013) have measured the release of Fe, Al, K and Si from complex clay minerals during the addition of 100 µM of citric acid. Most of the studies were

performed under acidic or alkaline experimental conditions, at which the pH is a highly important factor for phosphorus leaching (Lazo *et al.,* 2017). In particular the effect of citric acid was explained by the lower pH of the acid itself in comparison to the soil solution for solubilize minerals and phosphorus release (Henintsoa *et al.,* 2017; Ström *et al.,* 1994). Previous to the kinetic experiments, the pH of the minerals and the reaction solutions was adjusted to 6 and a decrease of the solution pH during the test duration was excluded by measurement. Therefore, the experimental conditions for phosphorus release by using humic and citric acid were comparable to the inorganic compounds, representing the soil solution. Also phosphorus revealed its high availability in an overlapping pH range from 5.0 to 6.8 due to the high solubility of both Fe- and Ca-phosphates (Johnson *et al.,* 2002; Scheffer *et al.,* 2010). Johnson and Loeppert (2006) reported that low weight organic acids solubilize phosphorus better in a lower pH range compared to a more neutral pH range. But even at a pH of 6, the cumulative amount of solubilized phosphorus showed an important impact of especially citric acid, which can be exuded by plant roots, on improving the phosphorus availability from tertiary phosphates. Since the dissolution mechanism also can make phosphorus available, which is more stable bound on structural reactive binding sites compared to better accessible surface binding sites (Gypser *et al.,* 2018; Wang *et al.,* 2013), the effectiveness is higher compared to anion or ligand exchange.

4.5.2 Kinetics of phosphorus release

The phosphorus mobilization from the Fe- and Ca-phosphates had a biphasic behavior with an initial fast stage within the first 48 h of reaction time and a slower second phase, which was also observed for phosphorus solubilization kinetics of soils or pedogenic hydroxides (Krumina *et al.,* 2016; Shariatmadari *et al.,* 2006; Smet *et al.,* 1998; Wang *et al.,* 2015). Previous studies

referred this biphasic kinetic to easily and immediately available as well as heavily and very slow exchangeable inorganic phosphorus pools (Barrow, 1983; Lookman *et al.,* 1995), which can be attributed to nonspecific adsorbed phosphorus from low-affinity sites and specific adsorbed phosphorus from high-affinity sites (Wang *et al.,* 2013) and a decreasing interaction of adsorbed phosphorus due to a decreasing surface charge (Fekri *et al.,* 2011; Islas-Espinoza *et al.,* 2014).

By using inorganic reaction solutions in batch experiments between 58 to 69 % of the totally released phosphorus was measured during the first 48 h for both minerals. Despite a slightly decrease of the extent of totally released phosphorus from vivianite by using organic acids within the first 48 h, approx. 45 % of the available phosphorus was mobilized in long-term. Certainly, for hydroxyapatite the application of organic acids clearly increased the phosphorus release up to 80 and 85 % during the first 48 h. This can be explained by a different structural accessibility of phosphorus binding sites of the minerals (Gypser *et al.,* 2018; Wang *et al.,* 2013). While anion exchange with $CaCl_2$ and $CaSO_4$ preferentially took part at easily available binding sites on the mineral surface, organic acids affect the more heavily available binding sites in addition, which can be embedded within the mineral structure. Thus, the cumulative release rate can be increased. However, it was detected that in short-term, citric and humic acid clearly increased the mobilization of phosphorus for hydroxyapatite, but not for vivianite. It can be reasoned that vivianite has a more stable structure at pH 6 compared to hydroxyapatite, affecting the phosphorus mobilization. In long-term, the dissolution of the minerals by citric acid increased the accessibility, and hence, the total available phosphorus (Basak, 2018; Taghipour and Jalali, 2013). This was supported by the time-dependent phosphorus release data, which revealed a higher initial phosphorus mobilization as well as release rate constant over time by using organic acids. The application of the used kinetic models displayed a lower amount of solubilized

phosphorus and hence, available binding sites for vivianite compared to hydroxyapatite and also for humic acid compared to citric acid.

4.5.3 Comparison of batch and FTR

The main benefit of the infinite sink approach by using FTR is the minimal alteration of the mineral-solution system (Frossard *et al.,* 2000) and the removal of mobilized phosphorus with the infinite sink without accumulation in the reaction solution, resulting in a new binding or precipitation in the solution or on the mineral surface (Kaupenjohann and Wilcke, 1995). In contrast, batch experiments are an inexpensive and simple approach (Kruse *et al.,* 2015) to determine the amount of long-term mobilized phosphorus.

The cumulative release rates of FTR after eight weeks of reaction time showed a 10- and 18-fold higher mobilization of phosphorus from hydroxyapatite and vivianite, respectively, compared to the batch setup by using $CaCl_2$. One possible explanation can be the enrichment of the solution in batch with phosphorus anions over time and hence, a competition for adsorption sites over a long-term residence time (Kruse *et al.,* 2015). Further, an impact of the residence time on the concentration gradient due to the flow-through setup affect the phosphorus release rates as well. At a given mean flow rate of 2.5 ml min^{-1} and with increasing reaction time, the porous flow rate was higher compared to the more static batch experiments. The batch experiments had a longer residence time to achieve an equilibrium concentration (Kruse *et al.,* 2015). But because of the continuous percolation and the infinite sink in the FTR setup, a short residence time and a concentration gradient were kept and hence, no chemical equilibrium was reached (Limousin *et al.,* 2007). Therefore, the capability of phosphorus mobilization can be overestimated compared to natural systems. On the other hand, the batch experimental setup had

a changing concentration gradient until sample taking. After refreshing of the solution, a new concentration gradient was created and a recent equilibrium can be reached.

Previous studies reported the Elovich (Basak, 2018; Fekri *et al.,* 2011; Hosseinpur and Pashamokhtari, 2008; Shariatmadari *et al.,* 2006) and the Parabolic function (Espinosa *et al.,* 2017; Shariatmadari *et al.,* 2006) as appropriate models to describe phosphorus release. The varying applicability of the Elovich equation for the batch experiments and the Exponential and Parabolic function for the FTR experimental setup can be explained by the porous flow rate during the reaction process for the FTR setup. Even after a longer reaction time, a continuing process of phosphorus release was measured. While the modelling of the phosphorus mobilization in batch can be described as a logarithmic process with decreasing reaction strength over time, FTR indicated an exponential P mobilization process with increasing reaction strength over time. Also the kinetic curves showed a continuing process of phosphorus release even after a longer reaction time (Espinosa *et al.,* 2017), which was more pronounced for vivianite. This indicated that after a continued reaction time, high amounts or nearly all of the bound phosphorus can be mobilized. According to McDowell and Sharpley (2003), dissolution will be the limiting step in phosphorus release over long-term, while desorption processes dominate in the short-term. It could be possible that the FTR method steadily affected heavily available phosphorus within the mineral structure by diffusion, which was provoked by the persistent concentration gradient. In comparison the batch method predominantly affected easily available phosphorus. The calculated diffusion rate constant k_P for vivianite and hydroxyapatite revealed a faster release rate of vivianite in $CaCl_2$, which is contradictory to the results of the batch experiments.

Due to the mentioned reasons, it is possible to either overestimate the phosphorus availability by using the FTR method, or underestimate the available phosphorus pools by using the batch method in long-term kinetic experiments (Miller *et al.,* 1989). A comparability of both

methods is not necessarily given because of the different amounts of reaction solution and its residence time for FTR. Also a comparison of both methods by using kinetic modelling is insufficient and allows merely a separate consideration of easily and heavily available phosphorus.

4.6 Conclusion

Long-term release experiments in batch and FTR were performed to characterize the kinetics and mechanism of phosphorus mobilization from the Fe- and Ca-phosphates vivianite and hydroxyapatite. The cumulative phosphorus release by organic acids was higher than by inorganic background solutions and followed the order $CaCl_2 \leq CaSO_4 <$ humic acid < citric acid. $CaCl_2$ and $CaSO_4$ showed a minor impact on phosphorus mobilization, while humic and especially citric acid increased the release of inorganic bound phosphorus. The better phosphorus release by citric acid compared to humic acid can possibly be explained by the more complex structure of humic acid, limiting desorption within the mineral structure. The decrease of C_{Total} and the formation of precipitate supported the accumulation of metal-organic complexes in the humic acid treatment, while citric acid seemed to induce the dissolution of the minerals at a pH of 6. The predominant amount of the totally released phosphorus was available during short-term, which indicated the presence of both easily and heavily accessible phosphorus binding sites. While anion exchange with $CaCl_2$ and $CaSO_4$ preferentially took part at easily available binding sites on the mineral surface, organic acids affect the more heavily available binding sites in addition, which can be embedded within the mineral structure.

The modeled time-dependent phosphorus release data revealed a higher initial phosphorus mobilization as well as release rate constant over time by using organic acids compared to

inorganic reaction solutions. At the same time, the applied kinetic models displayed a lower amount of released phosphorus for vivianite compared to hydroxyapatite, and also for the humic acid treatment compared to the citric acid treatment. While the kinetics of phosphorus release for the batch experiments fitted best with the Elovich equation with a decreasing reaction strength over time, the FTR experiments fitted best with the parabolic function with increasing reaction strength over time. The FTR-kinetic curves showed a continuing phosphorus release especially for vivianite, indicating the affection of heavily accessible phosphorus within the mineral structure by diffusion, which was provoked by the persistent concentration gradient. Also the clearly higher cumulative release rates of FTR compared to batch led to the assumption that the phosphorus availability was either overestimate by using the FTR method due to the impact of the residence time on the concentration gradient, or underestimated by using the batch method in long-term kinetic experiments.

The results indicate that phosphate, which is already fixed in soils or sediments by vivianite or hydroxyapatite, can be recovered by well-directed management strategies. This could be the use of catch crops such as *Lupinus alba* or *Medicago sativa* on agricultural soil, which substantially influence the phosphorus availability by increasing the organic acid secretion in the rhizosphere. However, further investigations are necessary, which are focused on the following: I) stability of these minerals (dissolution) under different conditions such as changing redox conditions in (wet) soils or sediments and the related release kinetics of phosphorus, and II) identification and verification of the specific phosphorus desorption mechanisms of Fe- and Ca-phosphates by various organic compounds.

5 General discussion

5.1 Phosphate adsorption mechanisms on iron- and aluminum hydroxides and its implications on desorption

The formation of Fe- and Al-hydroxides with specific properties such as crystallinity grade and the specific reactive surface is characteristic during soil alteration and affects transport and availability of phosphorus by adsorption, desorption and precipitation processes. Kinetics of adsorption and desorption, as well as FT-IR spectroscopy allowed conclusions about possible binding mechanisms on various mineral surfaces.

For gibbsite, several studies have described the generation of inner- and outer-sphere complexes between phosphate and the alumina surface (van Emmerik *et al.*, 2007; Zheng *et al.*, 2012). The increase and shift of the lateral Al-OH groups, observed with FT-IR, led to the conclusion of the formation of AlH_2PO_4 complexes during the initial phase of phosphorus adsorption. With continuing reaction time, the Al-OH peaks decreased displaying a reduced protonation and the formation of $AlHPO_4$ and Al_2HPO_4 surface complexes (Fig. 20A). The increase of adsorption during long-term adsorption led to the conclusion of precipitated $AlPO_4$ on the Al_2OH face sites or hydrogen-bonded outer-sphere complexes. A differentiation between surface complexation and precipitation could not be evaluated solely by the consideration of the P-O peak, and the absorption bands of the minerals themselves prevented an accurate description of the symmetry and protonation mode. The OH groups in the layers of gibbsite showed only minor and nonpermanent changes in intensity, and therefore, no phosphate was bound within the crystal structure. That was different compared to the suggested binding motifs on ferrihydrite,

which revealed the formation of a $FeHPO_4$ surface complex during the initial adsorption process, also described by Tejedor-Tejedor and Anderson (1990). With continuing adsorption time and increasing phosphorus concentration, the OH band intensity decreased, indicating the conversion of $FeHPO_4$ to Fe_2PO_4. The increasing intensity of the Fe-OH band indicated the liberation of reactive OH sites, which can be explained by the precipitation of $FePO_4$, as shown by Nanzyo (1988), and the migration of phosphate into the mineral particles (Willett *et al.*, 1988) (Fig. 20B).

The preferred development of Fe-phosphate precipitate was also suggested for the pure amorphous Fe-hydroxides, supporting the FT-IR findings of ferrihydrite. A shift of the OH vibrations to lower wavelength indicated a higher amount of hydrogen bonds compared to free OH groups (Al-Abadleh and Grassian, 2003) within Fe-hydroxide sample and hence, a main association of the FeO(OH) molecules by weak hydrogen bonds. Because of those weakly associated FeO(OH) molecules, $FePO_4$ precipitate was formed. This was bound by outer-sphere hydrogen bonds and enabled the binding of phosphate on already precipitated $FePO_4$ due to a reduced amount of available Fe-OH reaction sites (Fig. 21A). As a result, the extents of desorption from both the $CaCl_2$ and $CaSO_4$ treatments were close to zero. Ferrihydrite had a slightly higher extent of desorption than amorphous Fe-hydroxide, which can be explained by the more rigid structure of the former and a lower extent of precipitation. With increasing Al content, phosphorus desorption increased due to weaker both inner- and outer-sphere surface complexes (Fig. 21C). Amorphous aluminum hydroxide was mainly associated with more stable covalent OH bonds (Hass *et al.*, 2000). This stronger mineral structure of the Al-hydroxides led to a lower amount of precipitated Al-phosphate during the adsorption experiments at pH 6.

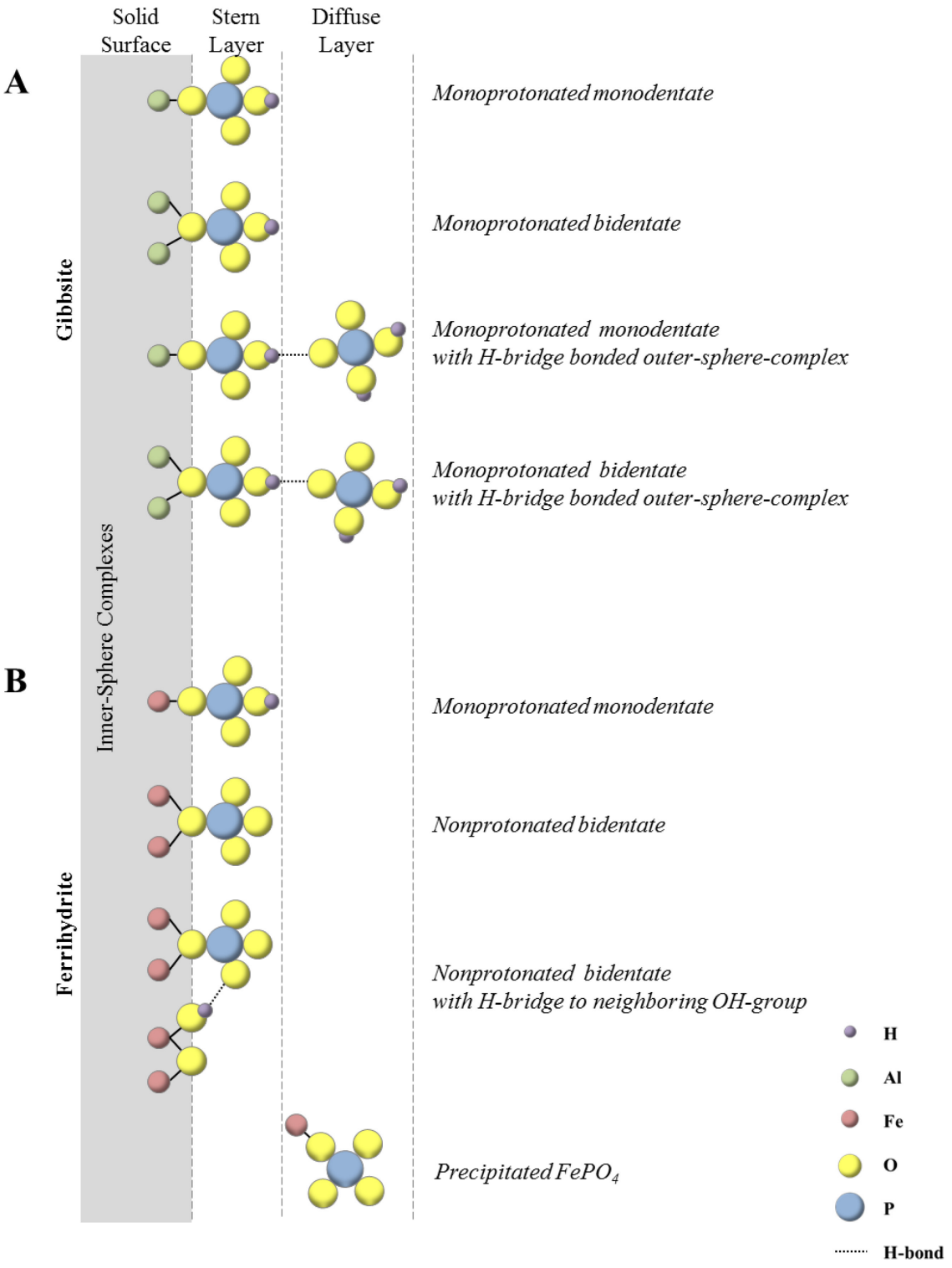

Fig. 20. Scheme of P adsorption on gibbsite and ferrihydrite (adapted from Antelo *et al.* 2010).

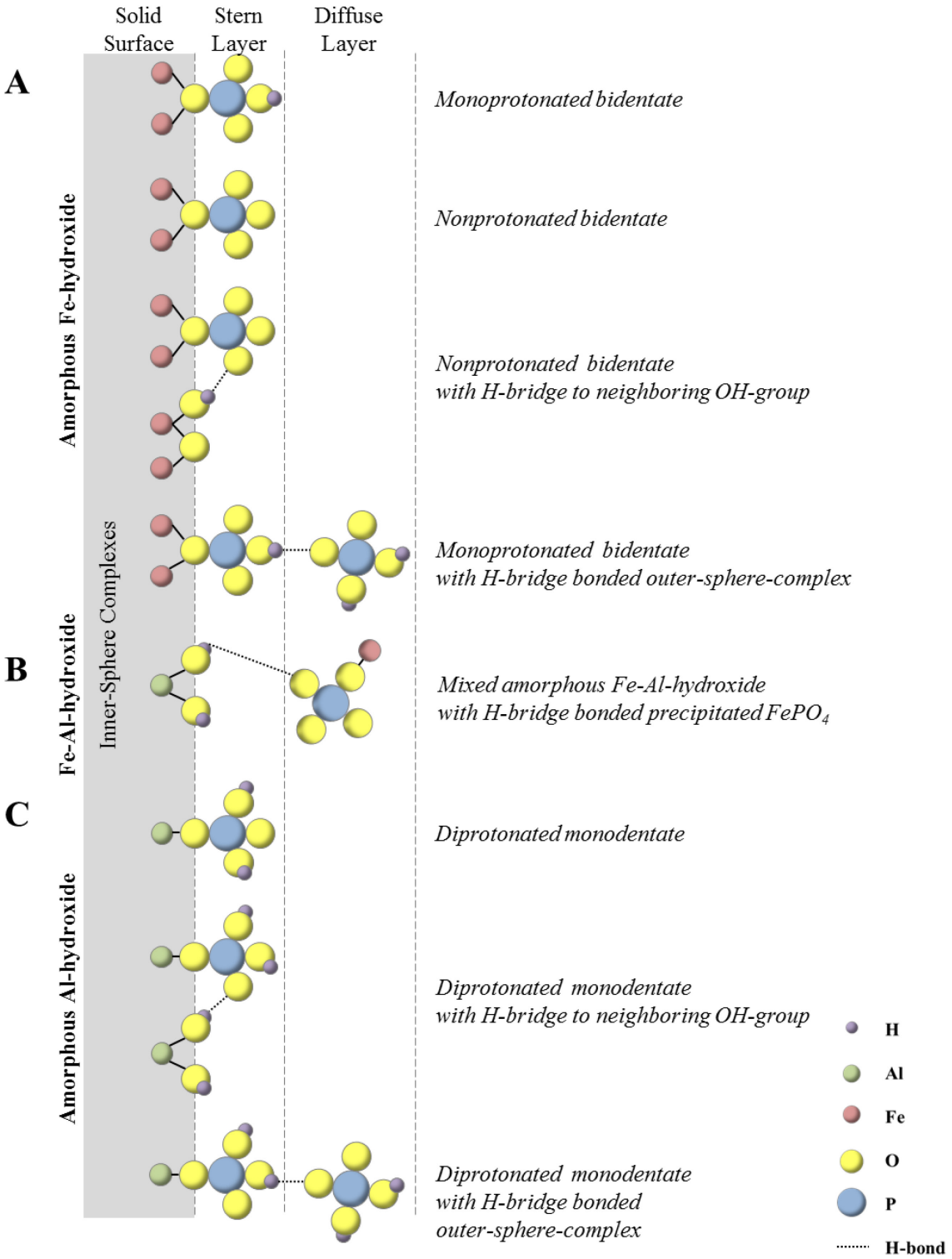

Fig. 21. Scheme of P adsorption on amorphous Fe- and Al-hydroxides (adapted from Antelo *et al.* 2010).

In general, a Fe_2HPO_4 or a Fe_2PO_4 surface complex was deduced for Fe-hydroxides, and an AlH_2PO_4 surface complex for Al-hydroxide and both revealed either hydrogen bonds to neighboring hydroxyl groups or hydrogen bonds to outer-sphere complexes (Fig. 21A to C). These different phosphate binding mechanisms, in particular, the predominant presence of monodentate and bidentate surface complexes rather than surface precipitation with increasing Al content, highly affect phosphorus desorption.

Especially the grade of crystallinity showed a major impact on the present binding motif. Gibbsite had a stable crystal structure, which led to a primary phosphate binding on the surface of the crystalline particles and a marginal formation of Al-phosphate precipitate, while the less-rigid amorphous structure of ferrihydrite and the Fe:Al-hydroxides enabled access to reactive sites within the particle structure. Hence, phosphate was bound both on the surface as well on structural binding sites as shown by Willett *et al.* (1988) and Parfitt (1989), affecting the extent of precipitation during phosphorus adsorption.

This fundamental understanding of phosphate binding motifs on contrasting mineral surfaces and possible binding changes over time enable a more detailed characterization of soils regarding their possible phosphorus fixation capacity as well as solubilization and mobilization in short- and long-term. Because of the weaker bound phosphate in surface complexes and the heavily bound phosphate in precipitates, respectively, fast as well as slow releasable phosphorus pools (Lookman *et al.*, 1997) were generated. According to this, it is recommended to determine the composition of pedogenic hydroxides in soils with regard to their Fe and Al content as well as crystalline and amorphous fractions in acidic and near-neutral soils.

5.2 Influence of organic and inorganic compounds on phosphorus desorption

Inorganic desorption solutions ($CaCl_2$ and $CaSO_4$) had only a remarkable effect on weaker bound and short-term releasable phosphorus. Especially precipitated phosphates were not affected and hence, unavailable for plants. Therefore, further specific measures are needed to mobilize heavily bound phosphorus and enhance the effective use of inorganic soil phosphorus pools. One possibility is the use of low- and high-molecular-weight organic acids, which occur in natural processes and do not have to be supplied artificially.

Citric acid is known for supporting phosphorus desorption from soil mineral particles (Harrold and Tabatabai, 2006; Lazo *et al.*, 2017; Wei *et al.*, 2010; Xu *et al.*, 2004), but also high-molecular-weight organic compounds such as humic acid play an important role in soil environment and phosphorus mobilization (Hua *et al.*, 2008; Jones, 1998). Relative to inorganic desorption solutions, organic compounds enhanced the release of phosphorus from Fe- and Al-hydroxides. The cumulative extent of desorption was higher for the organic ligand solutions, especially with the ligand citric acid, which exhibited two-fold higher desorption for goethite, gibbsite, and pure amorphous Al-hydroxide and even 36-fold higher desorption for 1 Fe : 10 Al than $CaCl_2$.

The extent of desorption varies strongly between both crystalline and amorphous hydroxides as well as the varying molar ratios of Fe to Al. Amorphous ferrihydrite and Fe:Al-hydroxides dominated by Fe had a low extent of desorption in the $CaCl_2$ solutions and a slightly higher release of phosphorus from $CaSO_4$. Since the predominant release mechanism during desorption with inorganic reaction solutions is the anion exchange (Fig. 22A and B), this could be explained by the higher adsorption affinity of SO_4^{2-} than Cl^-. Due to the higher valence and ionic radius of PO_4^{3-} and the higher affinity for binding on the hydroxide surface (Blume *et al.,* 2010;

Scheffer *et al.,* 2010), $CaCl_2$ and $CaSO_4$ were regarded as weak desorption solutions. The crystalline goethite, gibbsite, and the amorphous Fe:Al-hydroxides with a predominant Al content, on the other hand, had distinctively higher cumulative phosphorus desorption from $CaCl_2$ and $CaSO_4$. A less stable phosphorus binding was suggested on the crystalline hydroxides than on the amorphous hydroxides, and an influence of the Al content in Fe:Al-compounds.

The time-dependent desorption data, which were included in the Elovich, Exponential and Parabolic functions, suggested that phosphorus was desorbed from crystalline Fe- and Al-hydroxides by chemisorption reactions. For ferrihydrite and the Fe:Al-hydroxides with a predominant Fe content a delayed release and a diffusion-controlled process during phosphorus desorption was suggested. This is coincident with the results of the determination of phosphate binding mechanisms, which allowed the conclusion of phosphate migration to reactive sites within the particle structure. The presence of phosphate-hydroxide bindings of different stability is also supported by the biphasic desorption kinetics. Also the different extents of desorption, which were measured in the first (fast) or second (slow) phase, respectively, revealed desorption of nonspecifically adsorbed phosphorus from low-affinity sites and slower desorption of specifically adsorbed phosphorus from high-affinity sites (Wang *et al.* 2013).

Since the amount of carboxyl groups (-COOH) can increase phosphorus desorption (Xu *et al.*, 2004), citric acid seemed to be more effective than humic acid. This is also consistent with the kinetic data of this study. Othieno (1973) also described an adverse effect of humic acid on phosphorus availability. On the one hand, humic acid may also act as phosphorus adsorbing surface (Zhu *et al.,* 2018), on the other hand, could the more complex structure of humic acid act as a physical barrier and limiting desorption within the mineral surface (Rosa *et al.,* 2018; Wang *et al.,* 2016). Ligand exchange was concluded as the predominant release mechanism during desorption with humic acid due to a decrease of C_{Total} and the formation of organic precipitates in

the sample solution (Fig. 22C). For the citric acid treatment, a decrease of C_{Total} was not measured and, hence, a dissolution process suggested (Fig. 22D). This can be supported by findings of prior studies (Duputel *et al.,* 2013; Henintsoa *et al.,* 2017). These reaction mechanisms can additionally make specific and strongly bound phosphorus, such as precipitates, available. However, this study does not provide any concrete evidence about e.g. the type of ligand exchange of humic acid or proof of the dissolution of the hydroxides by citric acid. Additional measurements of the elemental concentrations in the reaction solutions as well as FT-IR spectroscopic analyses of the solid hydroxides are necessary for more precise conclusions. In this study, it was tried to analyze the hydroxides after desorption by using FT-IR spectroscopy, but the measured spectrum was overlaid by the silica sand on which the hydroxides were applied and the necessary peaks were not visible.

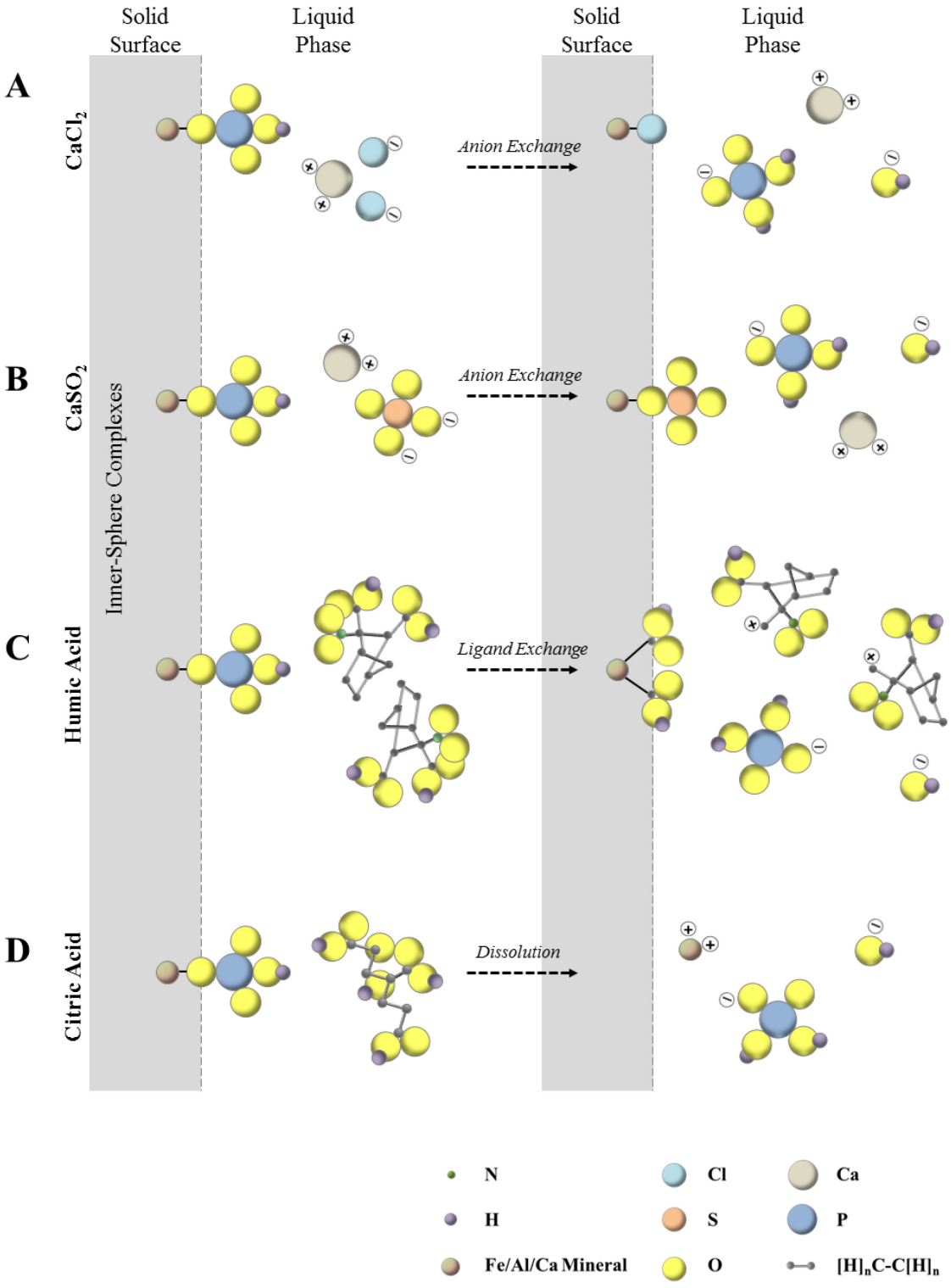

Fig. 22. Scheme of P desorption processes using the example of a monoprotonated monodentate inner-sphere surface complex.

5.3 Recovery of immobilized phosphorus from secondary resources

The mobility and availability of inorganic soil phosphorus are not only limited by ad- and desorption processes on Fe- and Al-hydroxides, also further pedogenic phosphate minerals generate a possible soil phosphorus storage, depending on the present soil pH conditions. In acidic soils, phosphorus can occur as the Fe-phosphate vivianite, while in neutral and calcareous soils the Ca-phosphate hydroxyapatite developed (Gustafsson *et al.*, 2012; Walker and Syers, 1976; Yadav and Verma, 2012). With regard of efficient use of already bound and stored phosphorus in soils as well as the global phosphorus reserves, the recovery from Fe- and Ca-phosphates is required. Relative to the desorption results with organic and inorganic compounds on Fe- and Al-hydroxides, similar results were observed for the Fe- and Ca-phosphates vivianite and hydroxyapatite. The cumulative phosphorus release with citric acid was substantially higher compared to humic acid. Only a minimal effect on phosphorus release was measured in the presented kinetic experiments with inorganic reaction solutions. Nevertheless, vivianite showed slightly higher phosphorus mobilization than hydroxyapatite. The use of organic solutions substantially increased the amount of solubilized phosphorus, but now hydroxyapatite had a stronger response than vivianite.

A possible explanation could be the varying different structural accessibility of phosphorus binding sites of both minerals (Gypser *et al.,* 2018; Wang *et al.,* 2013). Anion exchange with $CaCl_2$ and $CaSO_4$ preferentially took part at easily available binding sites on the mineral surface, organic acids affect the more heavily available binding sites in addition, which can be embedded within the mineral structure. The differences between vivianite and hydroxyapatite with respect to inorganic components may be due to the better accessibility of PO_4^{3-} ligands at the vivianite surface. It was presumed that OH ligands at the hydroxyapatite surface were better accessible than the PO_4^{3-} ligands (Fig. 23). With regard to the organic compounds, citric and humic acid

clearly increased the mobilization of phosphorus for hydroxyapatite. It can be reasoned that vivianite has a more stable structure at pH 6 compared to hydroxyapatite, affecting the phosphorus mobilization. In the long-term, the dissolution of the minerals by citric acid increased the accessibility, and hence, the total available phosphorus (Basak, 2018; Taghipour and Jalali, 2013).

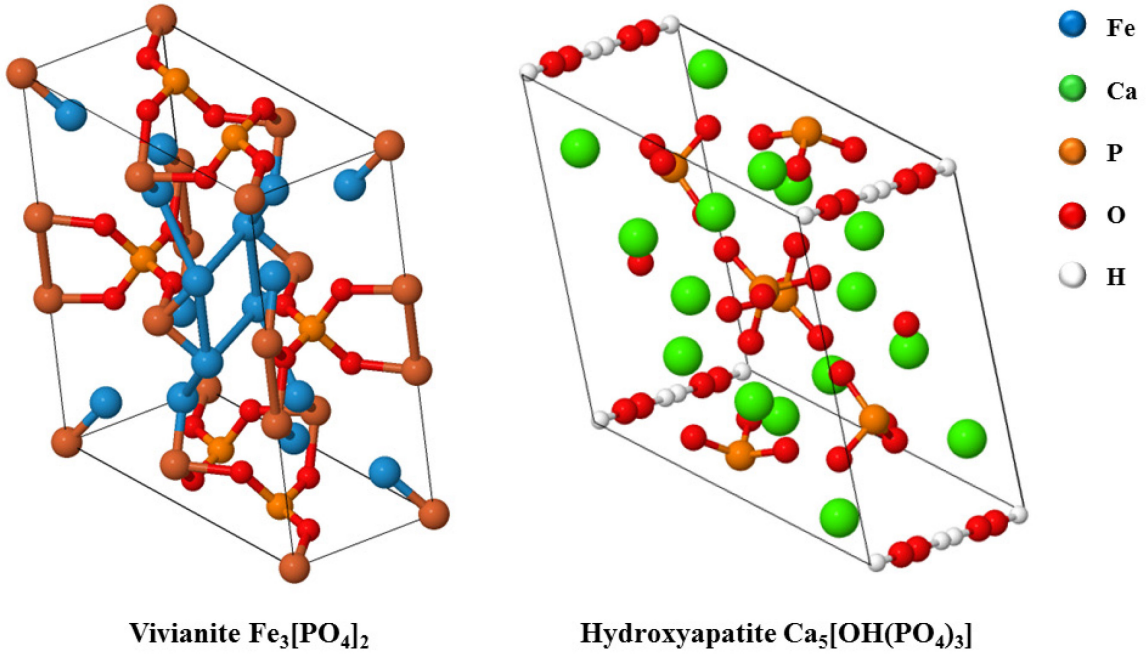

Fig. 23. Unit cells of vivianite and hydroxyapatite (RRUFF project (Lafuente *et al.,* 2015), according to Mori and Ito (1950) and Hughes *et al.* (1989)).

The amount of available inorganic phosphorus can be determined by long-term release kinetics, which includes both immediately as well as very slow available phosphorus (Frossard *et al.*, 2000; Hacker *et al.*, 2017). Release experiments on Fe- and Ca-phosphates were conducted both in batch and with an infinite sink approach. The main benefit of the infinite sink approach

by using a FTR setup is the minimal alteration of the mineral-solution system (Frossard *et al.*, 2000) and the removal of mobilized phosphorus without accumulation in the reaction solution, resulting in a new binding or precipitation in the solution or on the mineral surface (Kaupenjohann and Wilcke, 1995). On the contrary, batch experiments are an inexpensive and simple approach (Kruse *et al.*, 2015) to determine the amount of long-term mobilized phosphorus. Certainly, the cumulative release rates of FTR after eight weeks of reaction time showed a 10- and 18-fold higher mobilization of phosphorus compared to the batch setup. This can be explained by the enrichment of the solution in batch with phosphorus and a competition for adsorption sites over a long-term residence time (Kruse *et al.*, 2015). Also, the different residence times affect phosphorus release. The static batch experiment had a longer residence time achieve an equilibrium concentration while the continuous percolation FTR setup had a short residence time and a steady concentration gradient. Beside different extents of phosphorus release, also time-dependent kinetic modeling showed varying applicability, which contradicts to the results of the batch experiments. Hence, it is possible to either overestimate the phosphorus availability by using the FTR method or underestimate the available phosphorus pools by using the batch method in long-term kinetic experiments (Miller *et al.*, 1989). Also, a comparison of both methods by using kinetic modeling is insufficient and allows merely a separate consideration of easily and heavily purgeable phosphorus.

Both vivianite and hydroxyapatite are common sources of phosphorus in ecosystems worldwide (Scheffer *et al.*, 2010), where vivianite occures especially under anoxic conditions with low solubility. In the main phosphorus compounds containing Fe are sensitive to redox changes and can be dissolved under anoxic conditions. Fe-associated phosphorus, which was detected in anoxic soil and lake sediments and related to the stable Fe-phosphate vivianite, however, remained resistant to reductive dissolution (Hyacinthe and van Cappellen, 2004).

In a meta-analysis, Rothe *et al.* (2016) pointed out that the extraction of vivianite-bound phosphorus strongly depends on the crystallinity of the mineral. Phosphorus was not completely released from highly crystalline vivianite (sequential extraction method with citrate-dithionite-bicarbonate, bicarbonate-dithionite extraction), which further complicates the interpretation of phosphorus extractions. This shows that sequential phosphorus extractions, which are intended to determine the proportions of bioavailable or stable bound phosphorus, are only an approximate approach (Hupfer *et al.*, 1998; Lukkari *et al.*, 2007).

It was observed that either after 48 h of equilibration time, still, a measurable phosphorus release took place. Despite a high solubilization capacity of e.g. organic acids, desorption solutions can enhance the amount of available and strongly bound phosphorus in long-term. Whether conventional methods such as oxalate or dithionite extraction with short-term equilibration times can display the complete phosphorus content in soils is questionable in this consequence. Hence, it is possible to underestimate the actually available phosphorus pools in agricultural soils, and it can be summarized that accumulated phosphorus represents a high potential secondary phosphorus supplier that requires an accurate characterization of easily and heavily bound fractions and following a sustainable recovery.

6 Conclusions

I) Long-term adsorption experiments and FT-IR spectroscopic measurements indicated phosphate adsorption mainly on the surface of crystalline gibbsite while in-plane reaction sites were not affected. The formation of $AlHPO_4$ and Al_2HPO_4 was concluded. In long-term, limited extents of precipitated $AlPO_4$ on the Al_2OH face sites or hydrogen-bonded outer-sphere complexes were reasoned. For ferrihydrite, the initial appearance of a $FeHPO_4$ surface complex, conversion to a $FeHPO_4$ or Fe_2PO_4 complex and the precipitation of $FePO_4$ in long-term were described. Amorphous Fe-hydroxides have formed a Fe_2HPO_4 or a Fe_2PO_4 surface complex, while amorphous Al-hydroxides formed an AlH_2PO_4 surface complex. Both developed either hydrogen bonds to neighboring hydroxyl groups or hydrogen bonds to outer-sphere complexes. Fe:Al-hydroxide mixtures indicated the precipitation of $FePO_4$ due to a lower Fe amount, completely contributed to precipitation. The less-rigid structure of amorphous hydroxides led to higher accessibility of reactive sites within the particle structure and a higher amount of migrated and adsorbed phosphate relative to the reactive surface area.

II and III) The cumulative phosphorus desorption was higher for organic ligand solutions, especially for citric acid, relative to the inorganic solutions. The efficiency of the solutions differed between the crystalline and amorphous hydroxides. Phosphorus adsorbed on crystalline hydroxides can be more easily mobilized than phosphorus adsorbed on amorphous Fe- and Al-hydroxides. Anion exchange with $CaCl_2$ and $CaSO_4$ took part at easily available binding sites and, hence, easily bound phosphorus on the mineral surface, while naturally occurring organic acids additionally affect the more heavily available binding sites with stronger bound phosphorus, which can be embedded within the mineral structure.

During soil development, the passive phosphorus mobilization of humic acids changes phosphorus availability, but is less efficient for strongly bound phosphorous, as shown in the present experiment. The active strategy of plants to exude citric acid in the rhizosphere to enhance the phosphorus supply in case of demand is more effective to also solubilize strongly bound phosphorus. This positive effect could also be observed in the experiments with vivianite and hydroxyapatite.

These results showed that a better understanding of plant root-soil interactions and phosphorus acquisition root traits is necessary for increasing the efficiency of phosphorus uptake, especially in agricultural soils. This may include I) rhizosecretion, where, in addition to organic acids, proteoid roots and phytosiderophores are taken into account, II) plant-microbe interactions mediated by root exudates, and III) plant-mycorrhizal association. Different root trait strategies and an appropriate plant phosphorus utilization management need to be considered for enhancing an efficient phosphorus uptake. In this context, the role of cover crops, which are generally most effective in soil systems with low available phosphorus, is emphasized and needs to be related to adsorption and desorption processes. The combination of adapted crop rotation practices with included cover crops and intercropping can allow mobilizing phosphorus for plant growth and crop production, which is already fixed in soils.

Further investigations should deal with the questions I) how further inorganic and organic desorption solutions influence phosphate binding during desorption and if they affect the mobilization of already precipitated phosphate as well as from secondary phosphate resources such as biochars, II) stability and release kinetics of hydroxides and phosphates with changing soil parameters such as redox conditions, III) the influence of aggregate formation of Fe- and Al-hydroxides forced by organic compounds on phosphorus availability as well as the qualitative evaluation of organic and inorganic bound phosphorus, and IV) how can these findings be

implemented in the field for a better understanding of plant-soil interactions and their positive effect on phosphorus availability.

References

Aharoni, C., Sparks, D.L. (1991): Kinetics of soil chemical reactions: A theoretical treatment, In: Sparks, D.L., Suarez, D.L. (Eds.): Rates of soil chemical processes. Soil Science Society of America, Madison, Wi., pp. 1–18.

Al-Abadleh, H.A., Grassian, V.H. (2003): FT-IR study of water adsorption on aluminum oxide surfaces. Langmuir **19**, 341–347.

Anderson, P.R., Benjamin, M.M. (1990): Modeling adsorption in aluminum-iron binary oxide suspensions. Environ. Sci. Technol. **24**, 1586–1592.

Andersson, K.O., Tighe, M.K., Guppy, C.N., Milham, P.J., McLaren, T.I. (2015): Incremental acidification reveals phosphorus release dynamics in alkaline vertic soils. Geoderma **259-260**, 35–44.

Antelo, J., Avena, M., Fiol, S., Lopez, R., Arce, F. (2005): Effects of pH and ionic strength on the adsorption of phosphate and arsenate at the goethite-water interface. J. Colloid Interface Sci. **285**, 476–486.

Antelo, J., Fiol, S., Perez, C., Marino, S., Arce, F., Gondar, D., Lopez, R. (2010): Analysis of phosphate adsorption onto ferrihydrite using the CD-MUSIC model. J. Colloid Interface Sci. **347**, 112–119.

Arai, Y., Sparks, D.L. (2001): ATR–FTIR spectroscopic investigation on phosphate adsorption mechanisms at the ferrihydrite–water interface. J. Colloid Interf. Sci. **241**, 317–326.

Arai, Y., Sparks, D.L. (2007): Phosphate reaction dynamics in soils and soil components: A multiscale approach, In: Sparks, D.L. (Ed.): Advances in Agronomy, Vol. 94, Academic Press, San Diego, London, pp. 135–179.

Arlidge, E.Z., Farmer, V.C., Mitchell, B.D., Mitchell, W.A. (1963): Infra-red, X-ray and thermal analysis of some aluminium and ferric phosphates. J. Appl. Chem. **13**, 17–27.

Bais, H.P., Weir, T.L., Perry, L.G., Gilroy, S., Vivanco, J.M. (2006): The role of root exudates in rhizosphere interactions with plants and other organisms. Annu. Rev. Plant Biol. **57**, 233–266.

Barrow, N.J. (1983): A mechanistic model for describing the sorption and desorption of phosphate by soil. J. Soil. Sci., 733–750.

Basak, B.B. (2018): Phosphorus release by low molecular weight organic acids from low-grade Indian rock phosphate. Waste Biomass Valor. **11**, 1–9.

Basak, B.B. (2019): Evaluation of Indian rock phosphates for predicting agronomic potential through chemical and biological methods. Arch. Agron. Soil Sci. **24**, 1–11.

Behera, B.C., Singdevsachan, S.K., Mishra, R.R., Dutta, S.K., Thatoi, H.N. (2014): Diversity, mechanism and biotechnology of phosphate solubilising microorganism in mangrove: A review. Biocatal. Agric. Biotechnol. **3**, 97–110.

Blume, H.-P., Stahr, K., Leinweber, P. (2010): Bodenkundliches Praktikum. Spektrum Akademischer Verlag, Heidelberg.

Borggaard, O.K., Raben-Lange, B., Gimsing, A.L., Strobel, B.W. (2005): Influence of humic substances on phosphate adsorption by aluminium and iron oxides. Geoderma **127**, 270–279.

Brennicke, A., Schopfer, P. (2010): Pflanzenphysiologie. Spektrum Akademischer Verlag, Heidelberg.

Carpenter, S.R., Caraco, N.F., Correll, D.L., Howarth, R.W., Sharpley, A.N., Smith, V.H. (1998): Nonpoint pollution of surface waters with phosphorus and nitrogen. Ecol. Appl. **8**, 559–568.

Chen, C.R., Condron, L.M., Davis, M.R., Sherlock, R.R. (2004): Effects of plant species on microbial biomass phosphorus and phosphatase activity in a range of grassland soils. Biol. Fertil. Soils **40**, 313–322.

Chesti, M.-u.-H., Qadri, T.N., Hamid, A., Qadri, J., Azooz, M.M., Ahmad, P. (2013): Role of bio-fertilizers in crop improvement, In: Hakeem, K.R. (Ed.): Crop improvement. New approaches and modern techniques. Springer, New York, pp. 189–208.

Chitrakar, R., Tezuka, S., Sonoda, A., Sakane, K., Ooi, K., Hirotsu, T. (2006): Phosphate adsorption on synthetic goethite and akaganeite. J. Colloid Interf. Sci. **298**, 602–608.

Connor, P.A., McQuillan, A.J. (1999): Phosphate adsorption onto TiO_2 from aqueous solutions: An in situ internal reflection infrared spectroscopic study. Langmuir **15**, 2916–2921.

Cordell, D., Drangert, J.-O., White, S. (2009): The story of phosphorus: Global food security and food for thought. Global Environ. Chang. **19**, 292–305.

Cordell, D., White, S. (2010): Securing a sustainable phosphorus future for Australia. Farm Policy Journal **7**, 1–18.

Dai, L., Li, H., Tan, F., Zhu, N., He, M., Hu, G. (2016): Biochar: A potential route for recycling of phosphorus in agricultural residues. GCB Bioenergy **8**, 852–858.

Damon, P.M., Bowden, B., Rose, T., Rengel, Z. (2014): Crop residue contributions to phosphorus pools in agricultural soils: A review. Soil Biol. Biochem. **74**, 127–137.

Dean, L.A., Rubins, E.J. (1947): Anion exchange in soils: I. Exchangeable phosphorus and the anion-exchange capacity. Soil Sci **63**, 377–388.

Dodd, J., Large, D.J., Fortey, N.J., Kemp, S., Styles, M., Wetton, P., Milodowski, A. (2003): Geochemistry and petrography of phosphorus in urban canal bed sediment. Appl. Geochem. **18**, 259–267.

Dorozhkin, S.V. (2012): Dissolution mechanism of calcium apatites in acids: A review of literature. World J. Methodol. **2**, 1–17.

Dungait, J.A.J., Cardenas, L.M., Blackwell, M.S.A., Wu, L., Withers, P.J.A., Chadwick, D.R., Bol, R., Murray, P.J., Macdonald, A.J., Whitmore, A.P., Goulding, K.W.T. (2012): Advances in the understanding of nutrient dynamics and management in UK agriculture. Sci. Total Environ. **434**, 39–50.

Duputel, M., van Hoye, F., Toucet, J., Gérard, F. (2013): Citrate adsorption can decrease soluble phosphate concentration in soil: Experimental and modeling evidence. Appl. Geochem. **39**, 85–92.

Edixhoven, J.D., Gupta, J., Savenije, H.H.G. (2014): Recent revisions of phosphate rock reserves and resources: A critique. Earth Syst. Dynam. **5**, 491–507.

Egorova, S.R., Lamberov, A.A. (2015): Formation and distribution of phases during the dehydration of large hydrargillite floccules. Inorg. Mater. **51**, 331–339.

Elser, J.J., Bracken, M.E.S., Cleland, E.E., Gruner, D.S., Harpole, W.S., Hillebrand, H., Ngai, J.T., Seabloom, E.W., Shurin, J.B., Smith, J.E. (2007): Global analysis of nitrogen and phosphorus limitation of primary producers in freshwater, marine and terrestrial ecosystems. Ecol. Lett. **10**, 1135–1142.

Espinosa, D., Sale, P., Tang, C. (2017): Effect of soil phosphorus availability and residue quality on phosphorus transfer from crop residues to the following wheat. Plant Soil **416**, 361–375.

Eynard, A., del Campillo, M.C., Barrón, V., Torrent, J. (1992): Use of vivianite ($Fe_3(PO_4)_2 \cdot 8H_2O$) to prevent iron chlorosis in calcareous soils. Fert. Res. **31**, 61–67.

Fadaeerayeni, S., Sohrabi, M., Royaee, S.J. (2015): Kinetic modeling of MTO process applying ZSM-5 zeolite modified with phosphorus as the reaction catalyst. Petrol. Sci. Technol. **33**, 1093–1100.

Fekri, M., Gorgin, N., Sadegh, L. (2011): Phosphorus desorption kinetics in two calcareous soils amended with P fertilizer and organic matter. Environ. Earth Sci. **64**, 721–729.

Föllmi, K.B., Hosein, R., Arn, K., Steinmann, P. (2009): Weathering and the mobility of phosphorus in the catchments and forefields of the Rhône and Oberaar glaciers, central Switzerland: Implications for the global phosphorus cycle on glacial–interglacial timescales. Geochimica et Cosmochimica Acta **73**, 2252–2282.

Freese, D., Weidler, P.G., Grolimund, D., Sticher, H. (1999): A Flow-Through Reactor with an Infinite Sink for Monitoring Desorption Processes. J. Environ. Qual. **28**, 537–543.

Frossard, E., Bauer, J.P., Lothe, F. (1997): Evidence of vivianite in $FeSO_4$-flocculated sludges. Water Res. **31**, 2449–2454.

Frossard, E., Condron, L.M., Oberson, A., Sinaj, S., Fardeau, J.C. (2000): Processes governing phosphorus availability in temperate soils. J. Environ. Qual. **29**, 15–23.

Frost, R.L. (1998): Hydroxyl deformation in kaolins. Clay Clay Miner. **46**, 280–289.

García-Domínguez, M.T., García-Domínguez, J.C., López, F., Diego, C.M. de, Díaz, M.J. (2015): Maximizing furfural concentration from wheat straw and Eucalyptus globulus by nonisothermal autohydrolysis. Environ. Prog. Sustain. **34**, 1236–1242.

Gérard, F. (2016): Clay minerals, iron/aluminum oxides, and their contribution to phosphate sorption in soils: A myth revisited. Geoderma **262**, 213–226.

Gerke, J. (1994): Kinetics of soil phosphate desorption as affected by citric acid. Z. Pflanzenernaehr. Bodenk. **157**, 17–22.

Gerke, J., Römer, W., Jungk, A. (1994): The excretion of citric and malic acid by proteoid roots of Lupinus albus L; effects on soil solution concentrations of phosphate, iron, and aluminum in the proteoid rhizosphere in samples of an oxisol and a luvisol. Z. Pflanzenernaehr. Bodenk. **157**, 289–294.

Gharabaghi, M., Noaparast, M., Irannajad, M. (2009): Selective leaching kinetics of low-grade calcareous phosphate ore in acetic acid. Hydrometallurgy **95**, 341–345.

Ghassemi, M., Recht, H.L. (1971): Phosphate precipitation with ferrous iron. Water Pollution Control Research Series **9**, 1–64.

Giroto, A.S., Fidélis, S.C., Ribeiro, C. (2015): Controlled release from hydroxyapatite nanoparticles incorporated into biodegradable, soluble host matrixes. RSC Adv. **5**, 104179–104186.

Goldberg, S., Sposito, G. (2008): On the mechanism of specific phosphate adsorption by hydroxylated mineral surfaces: A review. Commun. Soil Sci. Plan. **16**, 801–821.

Goyne, K.W., Brantley, S.L., Chorover, J. (2006): Effects of organic acids and dissolved oxygen on apatite and chalcopyrite dissolution: Implications for using elements as organomarkers and oxymarkers. Chem. Geol. **234**, 28–45.

Grolimund, D., Borkovec, M., Federer, P., Sticher, H. (1995): Measurement of sorption isotherms with flow-through reactors. Environ. Sci. Technol. **29**, 2317–2321.

Guppy, C.N., Menzies, N.W., Moody, P.W., Blamey, F.P.C. (2005): Competitive sorption reactions between phosphorus and organic matter in soil: A review. Aust. J. Soil Res. **43**, 189.

Gustafsson, J.P., Mwamila, L.B., Kergoat, K. (2012): The pH dependence of phosphate sorption and desorption in Swedish agricultural soils. Geoderma **189-190**, 304–311.

Gypser, S., Hirsch, F., Schleicher, A.M., Freese, D. (2018): Impact of crystalline and amorphous iron- and aluminum hydroxides on mechanisms of phosphate adsorption and desorption. J. Environ. Sci. **70**, 175-189.

Hacker, N., Gleixner, G., Lange, M., Wilcke, W., Oelmann, Y. (2017): Phosphorus release from mineral soil by acid hydrolysis: Method development, kinetics, and plant community composition effects. Soil Sci. Soc. Am. J. **81**, 1389–1400.

Harouiya, N., Chaïrat, C., Köhler, S.J., Gout, R., Oelkers, E.H. (2007): The dissolution kinetics and apparent solubility of natural apatite in closed reactors at temperatures from 5 to 50 °C and pH from 1 to 6. Chem. Geol. **244**, 554–568.

Harrold, S.A., Tabatabai, M.A. (2006): Release of inorganic phosphorus from soils by low-molecular-weight organic acids. Commun. Soil Sci. Plan. Anal. **37**, 1233–1245.

Hass, K.C., Schneider, W.F., Curioni, A., Andreoni, W. (2000): First-principles molecular dynamics simulations of H_2O on α-Al_2O_3 (0001). J. Phys. Chem. B. **104**, 5527–5540.

Heindel, R.C., Lyons, W.B., Welch, S.A., Spickard, A.M., Virginia, R.A. (2018): Biogeochemical weathering of soil apatite grains in the McMurdo Dry Valleys, Antarctica. Geoderma **320**, 136–145.

Henintsoa, M., Becquer, T., Rabeharisoa, L., Gerard, F. (2017): Geochemical and microbial controls of the effect of citrate on phosphorus availability in a ferralsol. Geoderma **291**, 33–39.

Hinsinger, P. (2001): Bioavailability of soil inorganic P in the rhizosphere as affected by root-induced chemical changes: A review. Plant Soil **237**, 173–195.

Hosseinpur, A., Pashamokhtari, H. (2008): Impact of treated sewage sludge application on phosphorus release kinetics in some calcareous soils. Environ. Geol. **55**, 1015–1021.

Hou, E., Tang, S., Chen, C., Kuang, Y., Lu, X., Heenan, M., Wen, D. (2018): Solubility of phosphorus in subtropical forest soils as influenced by low-molecular organic acids and key soil properties. Geoderma **313**, 172–180.

Hua, Q.X., Li, J.Y., Zhou, J.M., Wang, H.Y., Du, C.W., Chen, X.Q. (2008): Enhancement of phosphorus solubility by humic substances in ferrosols. Pedosphere **18**, 533–538.

Hughes, J.M., Cameron, M., Crowley, K.D. (1989): Structural variations in natural F, OH, and Cl apatites. Am. Mineral. **74**, 870–876.

Hupfer, M., Fischer, P., Friese, K. (1998): Phosphorus retention mechanisms in the sediment of an eutrophic mining lake. Water Air Soil Pollut. **108**, 341–352.

Hyacinthe, C., van Cappellen, P. (2004): An authigenic iron phosphate phase in estuarine sediments: Composition, formation and chemical reactivity. Mar. Chem. **91**, 227–251.

Islas-Espinoza, M., Solís-Mejía, L., Esteller, M.V. (2014): Phosphorus release kinetics in a soil amended with biosolids and vermicompost. Environ. Earth Sci. **71**, 1441–1451.

Javid, S., Rowell, D.L. (2002): A laboratory study of the effect of time and temperature on the decline in Olsen P following phosphate addition to calcareous soils. Soil Use Manage. **18**, 127–134.

Ji, B., Hu, H., Zhao, Y., Mu, X., Liu, K., Li, C. (2014): Effects of deep tillage and straw returning on soil microorganism and enzyme activities. Sci. World J. **2014**, 451493.

Johnson, B.B., Ivanov, A.V., Antzutkin, O.N., Forsling, W. (2002): ^{31}P Nuclear magnetic resonance study of the adsorption of phosphate and phenyl phosphates on γ-Al_2O_3. Langmuir **18**, 1104–1111.

Johnson, S.E., Loeppert, R.H. (2006): Role of organic acids in phosphate mobilization from iron oxide. Soil Sci. Soc. Am. J. **70**, 222.

Johnston, H.W. (1952): The solubilization of phosphate. I. The action of various organic compounds on dicalcium and tricalcium phosphates. N. Z. J. Sci. Technol. **33**, 436–446.

Johnston, H.W., Miller, R.B. (1959): The solubilization of "insoluble" phosphate. IV. The reaction between organic acids and tricalcium phosphate. N. Z. J. Sci. Technol. **2**, 109–120.

Jones, D.L. (1998): Organic acids in the rhizosphere: A critical review. Plant Soil **205**, 25–44.

Kalsi, H.K., Singh, R., Dhaliwal, H.S., Kumar, V. (2016): Phytases from Enterobacter and Serratia species with desirable characteristics for food and feed applications. 3 Biotech **6:64**, 1–13.

Kaupenjohann, M., Wilcke, W. (1995): Heavy metal release from a serpentine soil using a pH-stat technique. Soil Sci. Soc. Am. J. **59**, 1027.

Khan, M.S., Zaidi, A., Ahmad, E. (2014): Mechanism of Phosphate Solubilization and Physiological Functions of Phosphate-Solubilizing Microorganisms, In: Khan, M.S., Zaidi, A., Musarrat, J. (Eds.): Phosphate Solubilizing Microorganisms. Springer International Publishing, Cham, pp. 31–62.

Khare, N., Martin, J.D., Hesterberg, D. (2007): Phosphate bonding configuration on ferrihydrite based on molecular orbital calculations and XANES fingerprinting. Geochim. Cosmochim. Ac. **71**, 4405–4415.

Kloprogge, J.T., Ruan, H.D., Frost, R.L. (2002): Thermal decomposition of bauxite minerals: infrared emission spectroscopy of gibbsite, boehmite and diaspore. J. Mater. Sci. **37**, 1121–1129.

Kolesova, V.A., Ryskin, Y.I. (1959): Infrared absorption spectrum of hydrargillite $Al(OH)_3$. Opt. Spectrosc. **7**, 165.

Kpomblekou-A, K., Tabatabai, M.A. (2003): Effect of low-molecular weight organic acids on phosphorus release and phytoavailabilty of phosphorus in phosphate rocks added to soils. Agric. Ecosyst. Environ. **100**, 275–284.

Krumina, L., Kenney, J.P.L., Loring, J.S., Persson, P. (2016): Desorption mechanisms of phosphate from ferrihydrite and goethite surfaces. Chem. Geol. **427**, 54–64.

Kruse, J., Abraham, M., Amelung, W., Baum, C., Bol, R., Kühn, O., Lewandowski, H., Niederberger, J., Oelmann, Y., Rüger, C., Santner, J., Siebers, M., Siebers, N., Spohn, M., Vestergren, J., Vogts, A., Leinweber, P. (2015): Innovative methods in soil phosphorus research: A review. J. Plant Nutr. Soil. Sci. **178**, 43–88.

Kubicki, J.D., Paul, K.W., Kabalan, L., Zhu, Q., Mrozik, M.K., Aryanpour, M., Pierre-Louis, A.M., Strongin, D.R. (2012): ATR-FTIR and density functional theory study of the structures, energetics, and vibrational spectra of phosphate adsorbed onto goethite. Langmuir **28**, 14573–14587.

Lafuente, B., Downs, R.T., Yang, H., Stone, N. (2015): The power of database: The RRUFF project, In: Danisi, R.M., Armbruster, T. (Eds.): Highlights in mineralogical crystallography. De Gruyter, Berlin, Boston, pp. 1–29.

Laiti, E., Persson, P., Öhman, L.-O. (1996): Surface complexation and precipitation at the H^+−orthophosphate−aged γ-Al_2O_3 /water Interface. Langmuir **12**, 2969–2975.

Lan, M., Comerford, N.B., Fox, T.R. (1995): Organic anions' effect on phosphorus release from spodic horizons. Soil Sci. Soc. Am. J. **59**, 1745.

Lazo, D.E., Dyer, L.G., Alorro, R.D. (2017): Silicate, phosphate and carbonate mineral dissolution behaviour in the presence of organic acids: A review. Miner. Eng. **100**, 115–123.

Li, W., Pierre-Louis, A.-M., Kwon, K.D., Kubicki, J.D., Strongin, D.R., Phillips, B.L. (2013): Molecular level investigations of phosphate sorption on corundum (α-Al_2O_3) by ^{31}P solid state NMR, ATR-FTIR and quantum chemical calculation. Geochim. Cosmochim. Ac. **107**, 252–266.

Li, X., Luo, L., Yang, J., Li, B., Yuan, H. (2015): Mechanisms for solubilization of various insoluble phosphates and activation of immobilized phosphates in different soils by an efficient and salinity-tolerant Aspergillus niger strain An2. Appl. Biochem. Biotech. **175**, 2755–2768.

Lijklema, L. (1980): Interaction of orthophosphate with iron(III) and aluminum hydroxides. Environ. Sci. Technol. **14**, 537–541.

Limousin, G., Gaudet, J.-P., Charlet, L., Szenknect, S., Barthès, V., Krimissa, M. (2007): Sorption isotherms: A review on physical bases, modeling and measurement. Appl. Geochem. **22**, 249–275.

Liu, R., Zhao, D. (2007): In situ immobilization of Cu(II) in soils using a new class of iron phosphate nanoparticles. Chemosphere **68**, 1867–1876.

Liu, W., Zhang, Y., Jiang, S., Deng, Y., Christie, P., Murray, P.J., Li, X., Zhang, J. (2016): Arbuscular mycorrhizal fungi in soil and roots respond differently to phosphorus inputs in an intensively managed calcareous agricultural soil. Scientific reports **6**, 24902.

Lookman, R. (1995): Phosphate Chemistry in Excessively Fertilised Soils. Dissertation. Faculteit Landbouwkkundige en Toegepaste Biologische Westenschappen, Leuven.

Lookman, R., Freese, D., Merckx, R., Vlassak, K., van Riemsdijk, W.H. (1995): Long-term kinetics of phosphate release from soil. Environ. Sci. Technol. **29**, 1569–1575.

Lookman, R., Grobet, P., Merckx, R., van Riemsdijk, W.H. (1997): Application of ^{31}P and ^{27}Al MAS NMR for phosphate speciation studies in soil and aluminium hydroxides: promises and constraints. Geoderma **80**, 369–388.

Loring, J.S., Sandstrom, M.H., Noren, K., Persson, P. (2009): Rethinking arsenate coordination at the surface of goethite. Chem. Europ. J. **15**, 5063–5072.

Luengo, C., Brigante, M., Antelo, J., Avena, M. (2006): Kinetics of phosphate adsorption on goethite: comparing batch adsorption and ATR-IR measurements. J. Colloid Interface Sci. **300**, 511–518.

Lukkari, K., Hartikainen, H., Leivuori, M. (2007): Fractionation of sediment phosphorus revisited. I: Fractionation steps and their biogeochemical basis. Limnol. Oceanogr. Methods **5**, 433–444.

Masset, S., Monteil-Rivera, F., Dupont, L., Dumonceau, J., Aplincourt, M. (2000): Influence of humic acid on sorption of Co(II), Sr(II), and Se(IV) on goethite. Agronomie **20**, 525–535.

McDowell, R.W., Sharpley, A.N. (2003): Phosphorus solubility and release kinetics as a function of soil test P concentration. Geoderma **112**, 143–154.

McLaughlin, J.R., Ryden, J.C., Syers, J.K. (1977): Development and evaluation of a kinetic model to describe phosphate sorption by hydrous ferric oxide gel. Geoderma **18**, 295–307.

Mehmood, A., Akhtar, M.S., Imran, M., Rukh, S. (2018): Soil apatite loss rate across different parent materials. Geoderma **310**, 218–229.

Miller, D.M., Sumner, M.E., Miller, W.P. (1989): A comparison of batch- and flow-generated anion adsorption isotherms. Soil Sci. Soc. Am. J. **53**, 373.

Mori, H., Ito, T. (1950): The structure of vivianite and symplesite. Acta Cryst. **3**, 1–6.

Mukherjee, S., Sen, S.K. (2015): Exploration of novel rhizospheric yeast isolate as fertilizing soil inoculant for improvement of maize cultivation. J. Sci. Food Agr. **95**, 1491–1499.

Murphy, J., Riley, J.P. (1962): A modified single solution method for the determination of phosphate in natural waters. Anal. Chim. Acta **27**, 31–36.

Myronyuk, I.F., Mandzyuk, V.I., Sachko, V.M., Gun'ko, V.M. (2016): Structural and morphological features of disperse alumina synthesized using aluminum nitrate nonahydrate. Nanoscale Res. Lett. **11**, 153.

Nanzyo, M. (1986): Infrared spectra of phosphate sorbed on iron hydroxide gel and the sorption products. Soil Sci. Plant Nutr. **32**, 51–58.

Nanzyo, M. (1988): Phosphate sorption on the clay fraction of Kanuma pumice. Clay Science **7**, 89–96.

Novák, C., Pokol, G., Izvekov, V., Gál, T. (1990): Studies on the reactions of aluminium oxides and hydroxides. J. Therm. Anal. **36**, 1895–1909.

Othieno, C.O. (1973): The effect of organic mulches on yields and phosphorus utilization by plants in acid soils. Plant Soil **38**, 17–32.

Othman, R., Panhwar, Q.A. (2014): Phosphate-Solubilizing Bacteria Improves Nutrient Uptake in Aerobic Rice, In: Khan, M.S., Zaidi, A., Musarrat, J. (Eds.): Phosphate Solubilizing Microorganisms. Springer International Publishing, Cham, pp. 207–224.

Owen, D., Williams, A.P., Griffith, G.W., Withers, P.J.A. (2015): Use of commercial bio-inoculants to increase agricultural production through improved phosphrous acquisition. Appl. Soil Ecol. **86**, 41–54.

Parab, N., Sinha, S., Mishra, S. (2015): Coal fly ash amendment in acidic field: Effect on soil microbial activity and onion yield. Appl. Soil Ecol. **96**, 211–216.

Parfitt, R.L. (1979): Anion adsorption by soils and soil materials, In: Brady, N.C. (Ed.): Advances in Agronomy, Vol. 30, Academic Press, New York, San Francisco, London, pp. 1–50.

Parfitt, R.L. (1989): Phosphate reactions with natural allophane, ferrihydrite and goethite. J. Soil. Sci. **40**, 359–369.

Parfitt, R.L., Atkinson, R.J., Smart, R.S.C. (1975): The mechanism of phosphate fixation by iron oxides. Soil Sci. Soc. Am. Pro. **39**, 837-841.

Parfitt, R.L., Fraser, A.R., Russell, J.D., Farmer, V.C. (1977): Adsorption on hydrous oxides: II. Oxalate, benzoate and phosphate on gibbsite. J. Soil. Sci. **28**, 40–47.

Persson, P., Nilsson, N., Sjöberg, S. (1996): Structure and bonding of orthophosphate ions at the iron oxide-aqueous interface. J. Colloid Interface Sci. **177**, 263–275.

Phambu, N., Humbert, B., Burneau, A. (2000): Relation between the infrared spectra and the lateral specific surface areas of gibbsite samples. Langmuir **16**, 6200–6207.

Rahnemaie, R., Hiemstra, T., van Riemsdijk, W.H. (2007): Geometry, charge distribution, and surface speciation of phosphate on goethite. Langmuir **23**, 3680–3689.

Reddy, K.R., Kadlec, R.H., Flaig, E., Gale, P.M. (1999): Phosphorus retention in streams and wetlands: A review. Crit. Rev. Env. Sci. Tec. **29**, 83–146.

Reijnders, L. (2014): Phosphorus resources, their depletion and conservation: A review. Resour. Conserv. Recycl. **93**, 32–49.

Roldán, R., v. Barrón, Torrent, J. (2002): Experimental alteration of vivianite to lepidocrocite in a calcareous medium. Clay Miner. **37**, 709–718.

Rombolà, A.D., Toselli, M., Carpintero, J., Ammari, T., Quartieri, M., Torrent, J., Marangoni, B. (2003): Prevention of iron-deficiency induced chlorosis in kiwifruit (Actinidia deliciosa) through soil application of synthetic vivianite in a calcareous soil. J. Plant Nutr. Soil Sci. **26**, 2031–2041.

Rosa, S.D., Silva, C.A., Maluf, H.J.G.M. (2018): Humic acid-phosphate fertilizer interaction and extractable phosphorus in soils of contrasting texture. Rev Cienc. Agron. **49**, 32–42.

Rothe, M., Kleeberg, A., Hupfer, M. (2016): The occurrence, identification and environmental relevance of vivianite in waterlogged soils and aquatic sediments. Earth-Science Reviews **158**, 51–64.

Rout, K., Mohapatra, M., Anand, S. (2012): 2-line ferrihydrite: synthesis, characterization and its adsorption behaviour for removal of Pb(II), Cd(II), Cu(II) and Zn(II) from aqueous solutions. Dalton T. **41**, 3302–3312.

RRUFF project online: Database of Raman spectrsocopy, X-ray diffraction and chemistry of minerals. http://rruff.geo.arizona.edu [access on 20.06.2019].

Ruan, H.D., Frost, R.L., Kloprogge, J.T. (2001a): Comparison of raman spectra in characterizing gibbsite, bayerite, diaspore and boehmite. J. Raman Spectrosc. **32**, 745–750.

Ruan, H.D., Frost, R.L., Kloprogge, J.T. (2001b): The behavior of hydroxyl units of synthetic goethite and its dehydroxylated product hematite. Spectrochim. Acta A **57**, 2575–2586.

Russell, J.D. (1979): Infrared spectroscopy of ferrihydrite: Evidence for the presence of structural hydroxyl groups. Clay Miner. **14**, 109–114.

Sample, E.J., Soper, R.J., Racz, G.J. (1980): Reactions of phosphate fertilizers in soils, In: Khasawneh, F.E., Sample, E.C., Kamprath, E.J. (Eds.): The role of phosphorus in agriculture. Am. Soc. Agron., Madison, Wisconsin, 263–310.

Sattari, S.Z., Bouwman, A.F., Giller, K.E., van Ittersum, M.K. (2012): Residual soil phosphorus as the missing piece in the global phosphorus crisis puzzle. P. Natl. A. Sci. **109**, 6348–6353.

Scheffer, F., Schachtschabel, P., Blume, H.-P., Brümmer, G. W., Horn, R., Kandeler, E., Kögel-Knabner, I., Kretzschmar, R., Stahr, K., Thiele-Bruhn, S., Welp, G., Wilke, B.-M. (2010): Lehrbuch der Bodenkunde, 16th ed. Spektrum Akademischer Verlag, Heidelberg.

Scheidegger, A., Borkovec, M., Sticher, H. (1993): Coating of silica sand with goethite: Preparation and analytical identification. Geoderma **58**, 43–65.

Scholz, R.W., Wellmer, F.W. (2013): Approaching a dynamic view on the availability of mineral resources: What we may learn from the case of phosphorus? Global Environ. Chang. **23**, 11–27.

Schwertmann, U., Fischer, W.R. (1973): Natural "amorphous" ferric hydroxide. Geoderma **10**, 237–247.

Schwertmann, U., Cornell, R. M. (2008): Iron oxides in the laboratory: Preparation and characterization. Wiley-VCH, Hoboken, pp. 209.

Seitz, M.A., Riedner, R.J., Malhotra, S.K., Kipp, R.J. (1973): Iron-phosphate compound identification in sewage sludge residue. Environ. Sci. Technol. **7**, 354–357.

Shang, C., Stewart, J.W.B., Huang, P.M. (1992): pH effect on kinetics of adsorption of organic and inorganic phosphates by short-range ordered aluminum and iron precipitates. Geoderma **53**, 1–14.

Shariatmadari, H., Shirvani, M., Jafari, A. (2006): Phosphorus release kinetics and availability in calcareous soils of selected arid and semiarid toposequences. Geoderma **132**, 261–272.

Sharma, S.B., Sayyed, R.Z., Trivedi, M.H., Gobi, T.A. (2013): Phosphate solubilizing microbes: sustainable approach for managing phosphorus deficiency in agricultural soils. SpringerPlus **2:587**, 1–14.

Shirodkar, S., Hutchinson, R.L., Perry, D.L., White, J.L., Hem, S.L. (1990): Aluminum compounds used as adjuvants in vaccines. Pharm. Res. **7**, 1282–1288.

Simpson, R.J., Oberson, A., Culvenor, R.A., Ryan, M.H., Veneklaas, E.J., Lambers, H., Lynch, J.P., Ryan, P.R., Delhaize, E., Smith, F.A., Smith, S.E., Harvey, P.R., Richardson, A.E.

(2011): Strategies and agronomic interventions to improve the phosphorus-use efficiency of farming systems. Plant Soil **349**, 89–120.

Sims, J.T., Pierzynski, G.M. (2005): Chemistry of phosphorus in soils, In: Tabatabai, M.A., Sparks, D.L. (Eds.): Chemical processes in soils, Vol. 8, Soil Science Society of America Book Series, Madison, pp. 151–192.

Smet, J.D., Vanderdeelen, J., Hofman, G. (1998): Effect of soil properties on the kinetics of phosphate release. Commun. Soil Sci. Plan. Anal. **29**, 2135–2147.

Steffens, D. (1994): Phosphorus release kinetics and extractable phosphorus after long-term fertilization. Soil Sci. Soc. Am. J. **58**, 1702–1708.

Strauss, R., Brümmer, G.W., Barrow, N.J. (1997): Effects of crystallinity of goethite: II. Rates of sorption and desorption of phosphate. Eur. J. Soil Sci. **48**, 101–114.

Strobel, B.W. (2001): Influence of vegetation on low-molecular-weight carboxylic acids in soil solution. A review. Geoderma **99**, 169–198.

Ström, L., Olsson, T., Tyler, G. (1994): Differences between calcifuge and acidifuge plants in root exudation of low-molecular organic acids. Plant Soil **167**, 239–245.

Sujana, M.G., Soma, G., Vasumathi, N., Anand, S. (2009): Studies on fluoride adsorption capacities of amorphous Fe/Al mixed hydroxides from aqueous solutions. J. Fluorine Chem. **130**, 749–754.

Sun, C., Xue, D. (2013): In situ ATR-IR observation of nucleation and crystal growth of KH_2PO_4 in aqueous solution. Cryst. Eng. Comm. **15**, 10445.

Syers, J. K., Johnston, A. E., Curtin, D. (2008): Efficiency of soil and fertilizer phosphorus use: Reconciling changing concepts of soil phosphorus behaviour with agronomic information. Food and Agricultural Organization of the United Nations, Rome, pp. 108.

Taghipour, M., Jalali, M. (2013): Effect of low-molecular-weight organic acids on kinetics release and fractionation of phosphorus in some calcareous soils of western Iran. Environ. Monit. Assess. **185**, 5471–5482.

Talebi Atouei, M., Rahnemaie, R., Goli Kalanpa, E., Davoodi, M.H. (2016): Competitive adsorption of magnesium and calcium with phosphate at the goethite water interface: Kinetics, equilibrium and CD-MUSIC modeling. Chem. Geol. **437**, 19–29.

Taşkın, M.B., Şahin, Ö., Taskin, H., Atakol, O., Inal, A., Gunes, A. (2018): Effect of synthetic nano-hydroxyapatite as an alternative phosphorus source on growth and phosphorus nutrition of lettuce (Lactuca sativa L.) plant. J. Plant Nutr. **41**, 1148–1154.

Taylor, K.G., Hudson-Edwards, K.A., Bennett, A.J., Vishnyakov, V. (2008): Early diagenetic vivianite [$Fe_3(PO_4)_2 \cdot 8H_2O$] in a contaminated freshwater sediment and insights into zinc uptake: A μ-EXAFS, μ-XANES and Raman study. Appl. Geochem. **23**, 1623–1633.

Tejedor-Tejedor, M.I., Anderson, M.A. (1990): The protonation of phosphate on the surface of goethite as studied by CIR-FTIR and electrophoretic mobility. Langmuir **6**, 602–611.

Torrent, J. (1997): Interactions between phosphate and iron oxide. Adv. Geoecol. **30**, 321–344.

Torrent, J., Schwertmann, U., Barron, V. (1992): Fast and slow phosphate sorption by goethite-rich natural materials. Clay Clay Miner. **40**, 14–21.

Tressardi, R. (2000): Vivianite from the Iceman of the Tisenjoch (Tyrol, Austria): Mineralogical-chemical data, In: Bortenschlager, S., Oeggl, K. (Eds.): The Iceman and his natural environment. Palaeobotanical Results. Springer Vienna, Vienna, pp. 137–141.

Tüysüz, H., Salabaş, E.L., Weidenthaler, C., Schüth, F. (2008): Synthesis and magnetic investigation of ordered mesoporous two-line ferrihydrite. J. Am. Chem. Soc. **130**, 280–287.

van Emmerik, T.J., Sandstrom, D.E., Antzutkin, O.N., Angove, M.J., Johnson, B.B. (2007): ^{31}P solid-state nuclear magnetic resonance study of the sorption of phosphate onto gibbsite and kaolinite. Langmuir **23**, 3205–3213.

van Riemsdijk, W.H., Lyklema, J. (1980): Reaction of phosphate with gibbsite ($AI(OH)_3$) beyond the adsorption maximum. J. Colloid Interface Sci. **76**, 55–66.

van Vuuren, D.P., Bouwman, A.F., Beusen, A.H.W. (2010): Phosphorus demand for the 1970–2100 period: A scenario analysis of resource depletion. Global Environ. Chang. **20**, 428–439.

Walker, T.W., Syers, J.K. (1976): The fate of phosphorus during pedogenesis. Geoderma **15**, 1–19.

Wang, H., Zhu, J., Fu, Q., Hong, C., Hu, H., Violante, A. (2016): Phosphate adsorption on uncoated and humic acid-coated iron oxides. J. Soils Sediments **16**, 1911–1920.

Wang, X., Li, Q., Hu, H., Zhang, T., Zhou, Y. (2005): Dissolution of kaolinite induced by citric, oxalic, and malic acids. J. Colloid Interf. Sci. **290**, 481–488.

Wang, X., Liu, F., Tan, W., Li, W., Feng, X., Sparks, D.L. (2013): Characteristics of phosphate adsorption-desorption onto ferrihydrite. Soil Sci. **178**, 1–11.

Wang, Y., Chen, X., Whalen, J.K., Cao, Y., Quan, Z.Q., Lu, C., Shi, Y. (2015): Kinetics of inorganic and organic phosphorus release influenced by low molecular weight organic acids in clacareous, neutral and acidic soils. J. Plant Nutr. Soil Sci. **178**, 555–566.

Wei, L., Chen, C., Xu, Z. (2010): Citric acid enhances the mobilization of organic phosphorus in subtropical and tropical forest soils. Biol. Fertil. Soils **46**, 765–769.

Weng, L., Vega, F.A., van Riemsdijk, W.H. (2011): Competitive and synergistic effects in pH dependent phosphate adsorption in soils: LCD modeling. Environ. Sci. Technol. **45**, 8420–8428.

Wilfert, P., Dugulan, A.I., Goubitz, K., Korving, L., Witkamp, G.J., van Loosdrecht, M.C.M. (2018): Vivianite as the main phosphate mineral in digested sewage sludge and its role for phosphate recovery. Water Res. **144**, 312–321.

Wilfert, P., Mandalidis, A., Dugulan, A.I., Goubitz, K., Korving, L., Temmink, H., Witkamp, G.J., van Loosdrecht, M.C.M. (2016): Vivianite as an important iron phosphate precipitate in sewage treatment plants. Water Res. **104**, 449–460.

Willett, I.R., Chartres, C.J., Nguyen, T.T. (1988): Migration of phosphate into aggregated particles of ferrihydrite. J. Soil. Sci. **39**, 275–282.

Wyngaard, N., Cabrera, M.L., Jarosch, K.A., Bünemann, E.K. (2016): Phosphorus in the coarse soil fraction is related to soil organic phosphorus mineralization measured by isotopic dilution. Soil Biol. Biochem. **96**, 107–118.

Xiong, L., Wang, P., Hunter, M.N., Kopittke, P.M. (2018): Bioavailability and movement of hydroxyapatite nanoparticles (HA-NPs) applied as a phosphorus fertiliser in soils. Environ Sci. Nano **5**, 2888–2898.

Xu, R., Zhu, Y., Chittleborough, D. (2004): Phosphorous release from phosphate rock and iron phosphate by low-molecular-weight organic acids. J. Environ. Sci. **16**, 5–8.

Yadav, B., Verma, A. (2012): Phosphate solubilization and mobilization in soil through microorganisms under arid ecosystems, In: Ali, M. (Ed.): The functioning of ecosystems. InTechOpen, pp. 93–108.

Yang, M., Lin, J., Zhan, Y., Zhu, Z., Zhang, H. (2015): Immobilization of phosphorus from water and sediment using zirconium-modified zeolites. Environ. Sci. Pollut. Res. Int. **22**, 3606–3619.

Yuan, H.M., Blackwell, M., McGrath, S., George, T.S., Granger, S.H., Hawkins, J.M.B., Dunham, S., Shen, J.B. (2016): Morphological responses of wheat (Triticum aestivum L.) roots to phosphorus supply in two contrasting soils. J. Agric. Sci. **154**, 98–108.

Zheng, T.-T., Sun, Z.-X., Yang, X.-F., Holmgren, A. (2012): Sorption of phosphate onto mesoporous gamma-alumina studied with in-situ ATR-FTIR spectroscopy. Chem. Cent. J. **6**, 26.

Zhu, J., Li, M., Whelan, M. (2018): Phosphorus activators contribute to legacy phosphorus availability in agricultural soils: A review. Sci. Total Environ. **612**, 522–537.

Acknowledgements

At this point I would like to thank apl- Prof. Dr. Dirk Freese for the involvement into the working group, the very interesting topic and for his confidence.

Many thanks to all members of the Chair of Soil Protection and Recultivation for a great and productive working atmosphere.

In particular, I would like to thank Gabriele Franke, Regina Müller, Denis Henning and Anita Maletzki for their technical assistance during the laboratory work and the huge amount of analyzed samples.

Furthermore, I would like to appreciate Dr. Katja Boldt-Burisch, Petra Klammer and Dr. Maik Veste for their continuous support, constructive criticism and understanding.